The University of Nottingham

Faculty of Engineering

Department of Electrical and Electronic Engineering

Research and Implementation on Optical Wireless Communication technologies

Name: Xing Chen

Student ID: 10278096

Supervisor: Dr. Nafizah Khan

Thesis submitted in partial fulfilment of the requirements for the Degree of Master of Philosophy

Abstract

Continuous global growth and increasing demand for wireless communication cause a shortage of radio frequency (RF) spectrum. Optical wireless communication (OWC) is expected to alleviate this looming spectrum crisis. Among OWC technologies, free space optic (FSO) and visible light communication (VLC) have rapidly become a research hot spot because of significant development and application prospects.

This study aims to investigate the characteristics of OWC technologies and offer theoretical support for enhancing the transmission performance. To achieve this goal, simulation models are set up, and better system parameters and modulation schemes are selected.

In the FSO model, an established modulation, absolute added correlative coding (AACC), is compared with four-level pulse amplitude modulation (4-PAM) in terms of transmission distance, eye diagram and bitrate. The results indicate that AACC transmits longer distance and at a higher bitrate than 4-PAM.Using the bit error rate (BER) with an estimation of 10^{-9}, the transmission distance achieved by AACC is 1.12 km, compared to 1.09 km for 4-PAM. And the bitrate of AACC is 18.7 Gbit/s, while it of 4-PAM is 16.7 Gbit/s. From the above results, the AACC modulation gives an improvement of 3% in the distance and 12% in the bitrate compared to 4-PAM modulation. In indoor VLC model, simulation results like illumination distribution, received power, signal-to-noise ratio (SNR) and root-mean-square (RMS) delay are evaluated. The illumination distribution between one light emitting diode (LED) array and four LED arrays is compared. It shows that four LED displays provide more uniform illumination. And the received power in LOS channel and NLOS channel are analysed. It shows that the contribution of LOS channel is decisive for the received power, and the assistance of NLOS channel is concentrated near the walls. In addition to these simulation results, measure algorithms of indoor positioning system (IPS) based on the same model are also investigated. It provides an experimental foundation for the construction of a robust and high data rate light fidelity (Li-Fi) system as well as a more accurate IPS. With the continuous

improvement of OWC technologies, a more efficient and secure wireless communication network will be widely used.

Acknowledgements

At first, I would like to thank Prof. Amin took me into the field of optical wireless communications. As lead the way, he gave me great inspiration.

Then I would like to express my sincere gratitude to Dr. Nafizah who helped with this research. I was deeply influenced by her rigorous scientific research attitude, rigorous logical thinking ability and strict project work requirements.

Next I am grateful to the internal Dr. Gnanam for her valuable time and useful advice. I thank her from the bottom of my heart.

In addition, Ms. Munawwarah and all other working teachers gave me daily care and help. I would also like to thank my seniors, Nguyen Dong-Nhat, Festou and Amrita. Their heartful discussion and helpful suggestion gave me a lot of support.

At last, I would like to thank my parents for their support, understanding, patient and being helpful behind my back, which is my greatest motivation throughout my study. I give my deepest gratitude and sincerest love to them for their love and support through my life.

Table of Contents

List of Figures

List of Tables

List of Abbreviations

AACC	Absolute Added Correlative Coding
AI	Artificial Intelligence
AM	Amplifier
AMD	Adaptive Minimum-voltage Detector
APD	Avalanche Photodiode
APT	Acquisition Pointing and Tracking
AWG	Arbitrary Waveform Generator
BER	Bit Error Rate
BS	Base Station
CCD	Charge Coupled Device
CDMA	Code Division Multiple Access
CIDF	Component Iteration Data Flow
CIM	Colour Intensity Modulation
CMOS	Complementary Metal Oxide Semiconductor
CSK	Colour Shift Keying
CW	Continuous Wave
DA	Differential Amplifier
DC	Direct Current
DPPM	Differential Pulse Position Modulation
DPSK	Differentially Phase Shift Keying
DSP	Digital Signal Processor
D2D	Device-to-Device
ESA	European Space Agency
EMI	Electromagnetic Interference
FDM	Frequency Division Multiplexing
FDMA	Frequency Division Multiple Access
FFT	Fast Fourier Transform
FIR	Far Infrared
FOV	Field of View
FSO	Free Space Optical
GG	Gamma-Gamma
GPS	Global Positioning System
ICI	Interchannel Interference
IFFT	Inverse Fast Fourier Transform
IM/DD	Intensity Modulation / Direct Detection
IoT	Internet of Thing
IPS	IndoorPositioning System
IR	Infrared
IrDA	Infrared Data Association
IS	Image Sensor
ISI	Intersymbol Interference

ISO	International Organization for Standardization
LD	Laser Diode
LED	Light Emitting Diode
LiDAR	Light Detection and Ranging
Li-Fi	Light Fidelity
LOS	Line-of-sight
LPF	Low-Pass Filter
LS	Level-Shift
MAC	Medium Access Control
MCM	Multi-Carrier Modulation
MD	Mobile Device
MIMO	Multiple Input Multiple Output
MOS	Metal Oxide Semiconductor
MZM	Mach-Zehnder Modulator
M2M	Machine-to-Machine
M-PAM	M-aryPulse Amplitude Modulation
NA	Numerical aperture
NASA	National Aeronautics and Space Administration
NE	Negative Exponential
NIR	Near Infrared
NLOS	Non-Line-of-Sight
NRZ	Non-Return-to-Zero
OCC	Optical Camera Communication
OCI	Optical Communication Image
OFDM	Orthogonal Frequency Division Multiplexing
OFDMA	Orthogonal Frequency Division Multiple Access
OLED	Organic Light Emitting Diode
OOK	On-Off Keying
OWC	Optical Wireless Communication
PAM	Pulse Amplitude Modulation
PD	Photodiode
PDF	Probability Density Function
PIN	Positive-Intrinsic-Negative
PLC	Power Line Communication
PPM	Pulse Position Modulation
PSK	Phase Shift Keying
PWM	Pulse Width Modulation
QAM	Quadrature Amplitude Modulation
RADAR	Radio Detection and Ranging
RF	Radio Frequency
RMS	Root-Mean-Square
RZ	Return-to-Zero
SCM	Single-Carrier Modulation
SNR	Signal-to-Noise Ratio
SWIR	Short-wavelength Infrared
TDD	Time Division Duplexing
TDMA	Time Division Multiple Access
TIA	Transimpedance Amplifier

TIR	Thermal Infrared
UOWC	Underwater Optical Wireless Communication
UV	Ultraviolet
VCSEL	Vertical-Cavity Surface-Emitting Laser
VL	Visible Light
VLC	Visible Light Communication
VLCC	Visible Light Communications Consortium
VPPM	Variable Pulse Position Modulation
V2X	Vehicle-to-Everything
WBAN	Wireless Body Area Networks
WDD	Wavelength Division Duplexing
WDM	Wavelength Division Multiplexing
WDMA	Wavelength division multiple access
Wi-Fi	Wireless Fidelity
WLAN	Wireless Local Area Networks
WMAN	Wireless Metropolitan Area Networks
WPAN	Wireless Personal Area Networks
4G	Fourth-generation
4-PAM	Four-level Pulse Amplitude Modulation
5G	Fifth-generation

1. Introduction

1. 1. Background

In recent decades, social and technological development has been driven to a large extent by innovations in wireless communication technologies. Wireless communication has become closely integrated into people's daily lives. According to a related study, nearly two-thirds of the global population will have Internet access by 2023. Therefore, Internet users are predicted to increase from 3.9 billion in 2018 to 5.3 billion by 2023. During the same period, the number of wireless devices connected to the networks, such as smartphones, tablets and smart electrical appliances, will also grow from 18.4 billion in 2018 to 29.3 billion by 2023 [1].

At the same time, mobile networks are upgraded from fourth-generation (4G) to fifth-generation (5G), requiring better network performance. Figure 1.1 shows that the peak data rate requirement for wireless communication will reach 20 Gbit/s in some applications, while the spectrum efficiency will be three times higher than before. Highly reliable communications at high mobility of up to 500 km/h and very low latency requirements of 1 ms will also be required. 5G is also envisaged to support connection densities of up to $10^6/km^2$ for large-scale communications. It is foreseeable that more new requirements will emerge as emerging technologies, such as the Internet of Things (IoT), cloud services and edge services, continue to evolve.

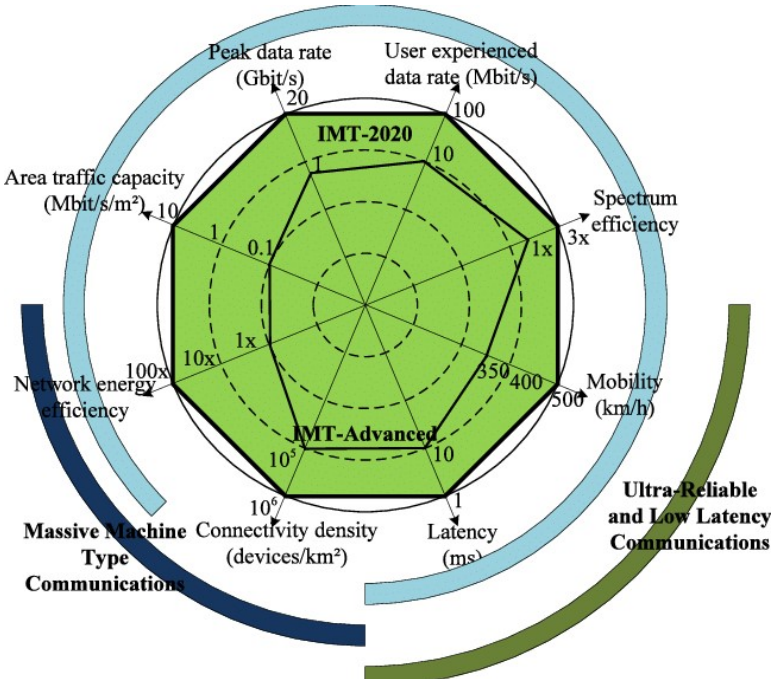

Figure 1.1 Key performance of 5G in IMT-2020. [2]

Despite technological advances over the last decade, the spectrum utilisation for wireless communication systems has reached saturation with less available radio frequency (RF) spectrum resources to distribute. Along with this trend, the shortage of RF spectrum is becoming a looming issue. Driven by this crisis, the optical spectrum has been extensively researched as a potential solution for developing alternatives since the optical spectrum can provide 10,000 times of unlicensed frequency bandwidth [3].

Although optical fibre transmission can address bandwidth issues, it has limitations, such as low mobility and relatively expensive construction costs. Alternatively, OWC system, which uses air to transmit information, is therefore seen as a potential solution to overcome these limitations. OWC offers many advantages, such as high bandwidth, no need for spectrum licenses and immunity to electromagnetic interference. There are two leading technologies for OWC systems: FSO communication system and VLC system. FSO communication system is a point-to-point system that typically uses lasers to transmit information and can provide a cost-effective protocol-transparent link with high data rates. VLC system operates in the visible light range and utilizes light-emitting diodes (LED), which can be pulsed at a very high frequency without any noticeable impact on the lighting output and the human eye.

FSO can be used as a powerful ultra-long connectivity solution for terrestrial-to-satellite communications, satellite-to-satellite communications, and intra-planetary communications. One of the significant milestones in this field occurred in 2001 when a 50 Mbit/s FSO system was successfully established between the ARTEMIS geostationary satellite and the SPOT-4 French Earth observation satellite in the sun-synchronous low earth orbit [4]. In October 2013, NASA's "Lunar Laser Communications Demonstration" was established between the Moon and the Earth. This FSO system can achieve an impressive data rate of 622 Mbit/s over a distance of 384,600 km [5]. It is expected that FSO will be the primary enabling technology in space and satellite links. Besides, FSO can also be used for short-distance transmissions, such as building-to-building links, vehicle-to-vehicle links, and even inter-chip links. Nowadays, FSO technology has been applied to products by some companies [6]. A high-performance FSO system is expected to be adopted as part of a next-generation heterogeneous wireless network in the backhaul to offer an uninterrupted connection with its fibre optic counterpart. In addition, because the FSO system is easy to install and redeploy, it is especially useful in catastrophic situations where the local infrastructure is damaged. A case of the FSO deployment efficiency as a backup system was witnessed after the 9/11 terrorist attacks in New York City, where landlines were damaged, and financial corporations promptly arranged the FSO system in the Wall Street region [7].

Light fidelity (Li-Fi) and IPS can be seen as the subsets of indoor VLC systems, simultaneously offering illumination, communication and positioning. Li-Fi is regarded as part of the international 5G mobile communications standard. It uses LEDs as a transmitter and offers communication and illumination at the same time. Also, reusing existing lighting infrastructure for communication saves costs. Some companies have started exploring the commercialisation of these Li-Fi technologies. For example, Haas's company offers an initial product that promises a data rate of 5 Mbit/s for both the visible light downlink and the infrared uplink [8]. Besides, Li-Fi can be applied in places with electromagnetic interference. One potential application area is in the medical industry, where hospitals have long banned mobile phones and Wireless Fidelity (Wi-Fi) hotspots that may interfere with sensitive medical equipment. Li-Fi can provide communication for patients and visitors, while lower data rate light-based

systems can track the position of mobile devices from wheelchairs and gurneys to emergency rooms. In other examples, short-range Li-Fi signals in galleries and museums provide spectators with introductions about each piece of art in the vicinity. Mobile robots can navigate to the factory floor by obtaining positional data from overhead luminaires with resolutions of up to a few centimetres. Additionally, Li-Fi is a potential candidate for many other applications. Some former Boston University students have developed a system that sends information about special offers to shoppers' existing smartphone cameras based on the shopper's location [9]. With the continuous improvement and enhancement of LED lighting systems in automobiles, researchers from the Optical Wireless Communication Technology Laboratory at the University of Ozyegin in Turkey have developed intelligent communication systems based on Li-Fi communication [10]. IPS is a complementary technology to Global Positioning System (GPS).GPS accuracy deteriorates because walls or tall buildings block GPS satellites' signal, and GPS cannot be implemented in an indoor environment. In turn, IPS can use an indoor VLC model to determine the physical location in an indoor environment.

1. 2. Problem Statement

With the increasing demand for wireless communication, OWC technologies need to be improved to meet the higher requirement. FSO communication utilizes optical spectrum to transmit information through free space. In FSO system, the current modulation format is not effective to support higher data rate. The recent established modulation format, AACC could be applied in FSO system, and provides a better transmission performance in terms of transmission distance, eye diagram and bitrate compared with current modulation format. Indoor VLC system is recognized as an advanced and promising technology, which combines lighting, communication and location at once. Li-Fi system and IPS are two subsets of it. The transmission performance of indoor VLC system is influenced by its channel characteristics. Currently the transmission channel in simulation model is line-of-sight (LOS) channel which is not accurate enough for design and implantation of indoor VLC system. Therefore, a simulation model of LOS channel and non-line-of-sight (NLOS) channel is proposed in this project. The project aims to analyse the simulation of Li-Fi system in terms of illumination distribution, received power, signal-to-noise ratio (SNR) and root-mean-square (RMS) delay. Also, the study in the measurement algorithms of IPS is considered to improve the accuracy of indoor location by using the same simulation model.

1. 3. Research Aim and Objectives

The primary aim of this research is to investigate the characteristics of OWC technologies and enhance the transmission performance by setting up simulation models specifically on FSO and VLC systems.

To achieve this aim, the following are the specific objectives of the study.

A. FSO-related research:

   i. Investigate the performance of AACC in the FSO system over 4-PAMusing mathematical analysis and the bit error rate (BER) development.

   ii. Evaluate the performance comparison of AACC in the FSO system with 4-PAM in terms of transmission distance and bit rate.

B. VLC-related research:

   i. Develop an indoor VLC model using LOS channel and NLOS channel and investigate the characteristics of Li-Fi system.

   ii. Investigate the transmission performance of Li-Fi system in terms of received power, SNR and RMS delay.

   iii. Analyse the measurement algorithms of IPS that used the same indoor VLC model.

1. 4. Scope of the Research

This research primarily studies the characteristics of OWC technology, focusing on FSO and VLC systems. Figure 1.2 provides a hierarchical overview of the research's scope and performance evaluation. Figure 1.3 provides the performance evaluation of FSO system and VLC system that includes Li-Fi and IPS. The shaded boxes of Figure 1.2 and Figure 1.3 are the related OWC system study and performance evaluation of OWC technologies that were researched in this thesis.

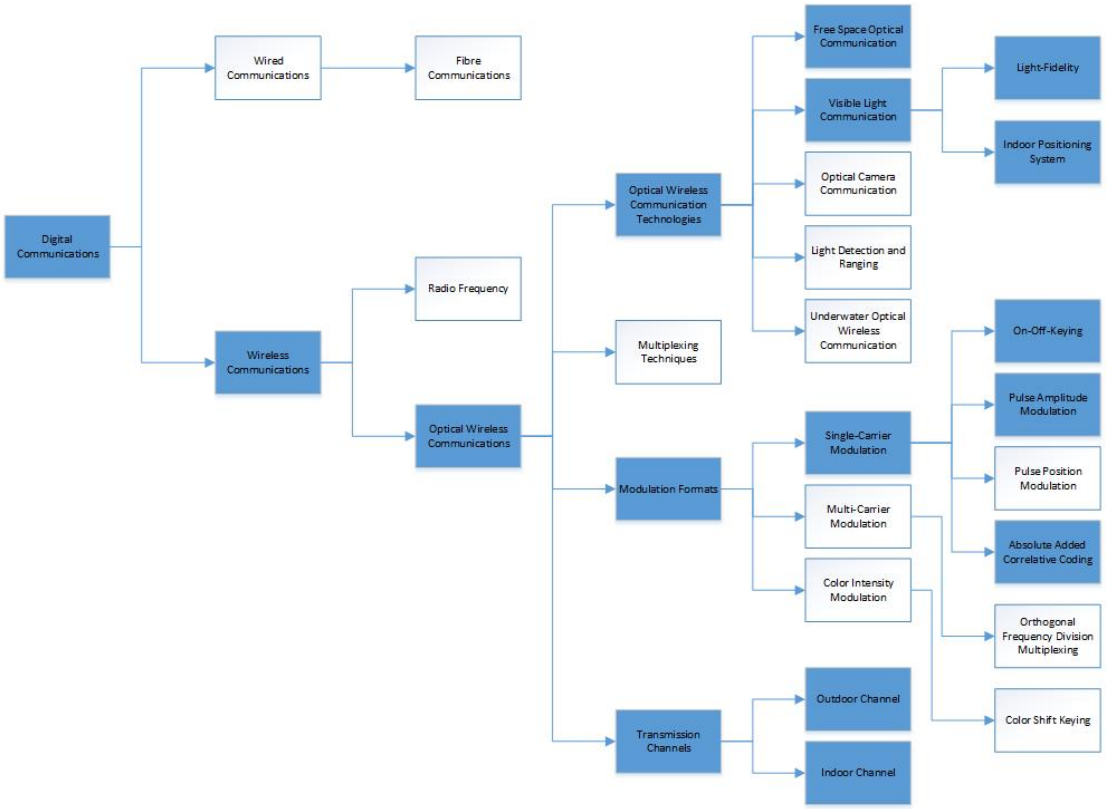

Figure 1.2 The scope of research.

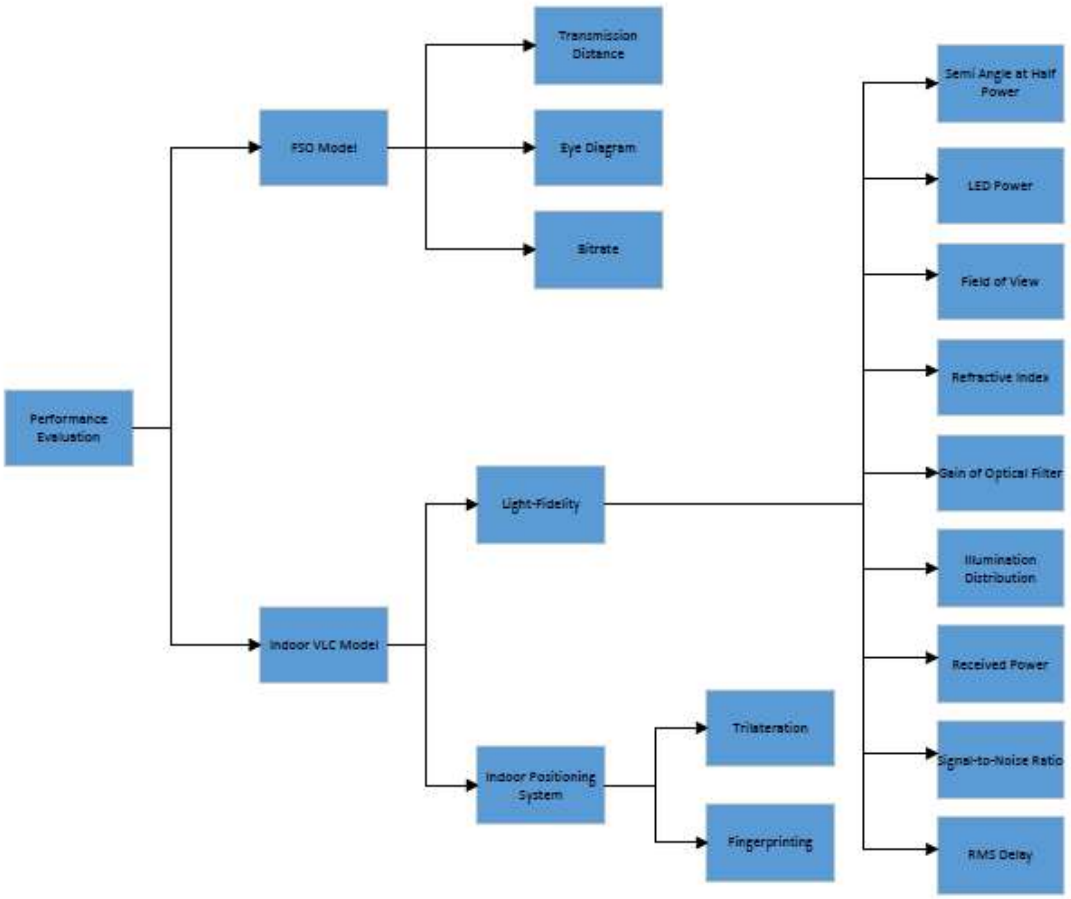

Figure 1.3 The performance evaluation of the research.

The FSO system is analysed using the outdoor channels that uses performance comparison to develop models on AACC and 4-PAM. This is achieved as stated on specific objective i and ii. The VLC system is analysed using the indoor channels based on the performance development on Li-Fi and IPS. This is achieved as stated on specific objective iii and iv.

The FSO system's different transmission performance between multi-level modulation formats 4-PAM and AACC is studied. This FSO system is modeled and simulated by using OptiSystem. And the FSO system is a model for high data rate and short-haul communication. Besides, the research does not consider the mobility and alignment of the FSO system. In the same circumstance, attention is given to the difference between 4-PAM and AACC.

The VLC system investigates the transmission performance in the LOS channel and NLOS channel, and the model is simulated by MATLAB. This VLC system is only suited for the indoor environment and cannot be used for the outdoor environment. Besides, this work does not take random orientation into consideration. Based on this, for the indoor VLC model, both the Li-Fi system and IPS are studied. The Li-Fi researched the parameter characteristics and transmission performance by adopting this VLC system. Besides, the measurement algorithms of IPS are studied by utilizing the same model.

1.5. Contribution of the Research

This thesis presents an extensive overview of emerging OWC technologies and focuses on FSO and VLC systems, including Li-Fi and IPS. The research results accomplished from the research are:

i. Comparison of transmission performance between two multi-level modulation formats applied in the FSO system.
ii. Evaluation of test performance from a LOS channel and NLOS channel in the Li-Fi system.
iii. Investigation of measurement algorithms from IPS based on the VLC system.

1.6. Software

Two simulation softwares applied to set up the model of OWC technologies are:

i. OptiSystem: a simulation software that is used to design, test and optimize optical communication links
ii. MATLAB: a computer language for technical computing and data visualization

1. 7. Thesis Organisation

The thesis is divided into five chapters. Chapter 1 gives an introduction of research, including research aim, objectives, scope and contribution. Chapter 2 provides a literature review about the OWC and proposes background knowledge of OWC technologies. Chapter 3 describes the research methodology, including the setup of FSO and indoor VLC experiments. Chapter 4 illustrates the research results, including the investigation of different modulations performance in the FSO model, analysis of the transmission performance in the Li-Fi model and comparison of different approaches in IPS. Finally, Chapter 5 contains the research's conclusion and future works.

2. Literature Review

2. 1. Introduction

In this chapter, the main characteristics of OWC are introduced and reviewed from various aspects, including an overview of OWC technology, current research development and reports on relevant findings, as well as different technologies under the OWC umbrella. Additionally, to provide a clear technical understanding of OWC theory, this chapter introduces some fundamental concepts of the OWC system, such as system schematic blocks, modulation formats and transmitting channel features. These concepts support the set-up and investigation of the performance of the models adopted in the research work. Moreover, the benefits, drawbacks and prospects of OWC are also discussed.

2. 2. An Overview of OWC

OWC encompasses a range of technologies that utilize light to transmit data through free space, diverging from traditional radio frequency (RF) systems. Key OWC technologies include FSO and VLC, each exhibiting unique characteristics and advantages suitable for specific applications. The development of wireless communication can be described as a continuous evolution from low-frequency to high-frequency transmission methods. Initially, long-wave communication was significant due to its ability to travel long distances without obstruction. Subsequently, short-wave communication was developed, which include ground wave and sky wave propagation and could cover thousands of kilometers. This was followed by the adoption of ultra-short waves and microwaves, including millimeter waves, which became predominant in wireless communication. Eventually, the optical spectrum, with higher frequency, emerged as the new medium of wireless transmission. Figure

2.1 illustrates the electromagnetic spectrum, highlighting the transition from radio communication in the lower frequency bands to optical wireless communication in the higher frequency bands.

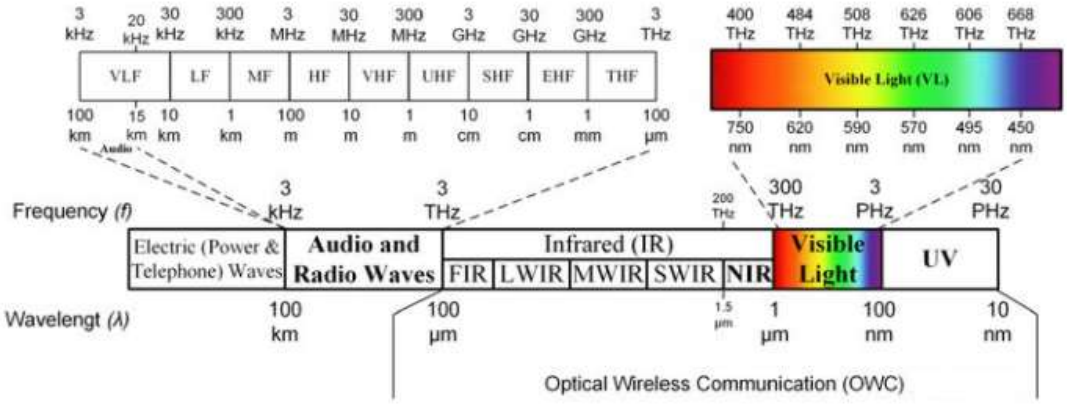

Figure 2.1. Electromagnetic spectrum. [11]

In optical wireless communication, “optical” refers to the use of the optical spectrum as the signal transmission medium, and “wireless” indicates that no wires, such as optical fibres, are needed to propagate the signal. The term OWC encompasses the optical transmission using propagation medium such as infrared (IR), visible light (VL) and ultraviolet (UV) spectra. For instance, IR is an electromagnetic wave with a wavelength between microwave and visible light. It can be further categorized into near-infrared (NIR), short-wavelength infrared (SWIR), thermal infrared (TIR) and far infrared (FIR). VL refers to the portion of the optical spectrum visible to the human eye, with wavelength between 360nm and 760nm. UV is a general term for the electromagnetic spectrum between visible light and X-rays, which is not perceivable by the human eye.

2. 2. 1. Research of OWC Technology

As an emerging communication technology, OWC technologies have attracted the interest of many research institutes and have achieved a series of research results. The following sections focus on some of them in FSO, Li-Fi and IPS.

FSO technology, a line-of-sight communication method, offers substantial bandwidth and immunity to electromagnetic interference. However, its performance is heavily influenced by atmospheric conditions, which can significantly impact the system's

reliability and transmission distance. Al-Gailani et al. provided a comprehensive survey on FSO communication systems, highlighting the technical challenges and potential future developments [12]. This aligns with the research objective of conducting a mathematical analysis and developing a BER model for FSO systems, as understanding these challenges is crucial for accurate BER modeling. Kaushal and Kaddoum specifically introduced the various challenges of FSO terrestrial and space links and techniques to mitigate the impact of atmospheric and improve the availability and reliability of FSO systems at physical and network levels, for instance, diversity, adaptive optics, error control codes, modulation, hybrid RF/FSO and modification in application, transport and link layer [13]. Jahid et al. explored atmospheric mitigation techniques, such as diversity and adaptive optics, which are vital for enhancing the reliability and availability of FSO systems [14]. These techniques are directly related to the research objective of evaluating the BER model's performance in comparison with other modulation formats, as they provide a framework for mitigating errors caused by atmospheric disturbances. Chatzidiamantis et al. investigated adaptive subcarrier Phase Shift Keying (PSK) intensity modulation, which improves system adaptability to varying channel conditions [15]. This is particularly relevant to the research goal of proposing solutions to enhance FSO performance in terms of transmission distance and bitrate. By understanding how modulation formats like PSK can be optimized, the research can suggest effective strategies for improving FSO system performance. Levidala et al. focused on Multiple Input Multiple Output (MIMO) configurations in dual-hop underwater and FSO communication systems, highlighting the importance of addressing turbulence and pointing errors to enhance overall system performance [16]. The research objectives of comparing BER models across modulation formats and proposing enhancements are supported by these findings, as MIMO configurations offer a pathway to mitigate common issues in FSO systems. Magidi and Jabeena reviewed hybrid modulation schemes in FSO, demonstrating how combining different modulation formats can significantly improve system robustness and performance [17]. This supports the objective of evaluating the BER model's effectiveness, as hybrid modulation schemes may provide a benchmark for assessing the performance of the developed BER model. Naveenkumar et al. experimentally demonstrated Optical 4-PAM generation for short-reach optical communications, showcasing how 4-PAM

can double the bit rate with fewer propagation penalties compared to OOK [18]. This aligns with the objective of proposing solutions to enhance FSO performance, as 4-PAM modulation could be considered for improving transmission distance and bitrate in FSO systems. Szczerba et al. compared the modulation formats 4-PAM and OOK in a high-data-rate short-distance fibre link. It is shown that 4-PAM can double the bit rate while having fewer propagation penalties than OOK [19]. Chowdhury and Choyon designed a novel hybrid OFDM FSO communication system, analyzing its performance under diverse weather conditions [20]. Their work highlights the need for robust modulation techniques that can withstand environmental variability, which is crucial for achieving the research objective of enhancing FSO performance based on the findings from BER analysis and modulation format comparison.

Li-Fi, a critical subset of VLC technology, leverages visible light for high-speed data transmission, particularly in indoor environments where secure and high-speed wireless communication is essential. This section aligns with the research objectives focusing on developing indoor VLC models and evaluating Li-Fi systems' performance in both LOS and NLOS channels. Siddique et al. discussed the future potential of VLC technology, particularly the role of Li-Fi in next-generation OWC networks, emphasizing the importance of bandwidth optimization and efficient modulation schemes[21]. This aligns with the objective of evaluating the transmission performance of the Li-Fi system in terms of received power, SNR, and RMS delay, as these factors are directly influenced by the modulation techniques employed. Jenila and Jeyachitra reviewed green indoor optical wireless communication systems, highlighting pathways toward widespread deployment of Li-Fi technology [22]. Their insights are valuable for analyzing the measurement algorithms of IPS using the same indoor VLC model, ensuring that it is both sustainable and efficient. Wu et al. demonstrated a high-speed 4-PAM VLC system with polarization-multiplexing injection-locked VCSELs, achieving impressive data rates and system performance [23]. The findings from this study support the evaluation of the VLC system's transmission performance, particularly in terms of SNR and RMS delay, by showcasing the potential of advanced modulation techniques to improve system performance. Karunatilaka et al. provided an extensive overview of LED-based indoor VLC, discussing key aspects such as modulation schemes, channel characteristics, and

system performance [3]. This foundational work underpins the objective of developing an indoor VLC model using both LOS and NLOS channels, as it highlights the critical factors affecting indoor VLC performance. Rahman et al. reviewed advanced techniques to achieve multi-gigabit transmission rates in VLC systems, emphasizing the importance of bandwidth optimization and efficient modulation schemes [24]. This aligns with the research goal of investigating the performance of the Li-Fi system under various parameters, as bandwidth optimization directly influences data rates and system efficiency. Wang et al. demonstrated the use of GaN-based micro-LEDs, which are pivotal for achieving high bandwidths and multi-gigabit data rates in Li-Fi systems [25]. This directly supports the research objective of investigating the characteristics and transmission performance of the Li-Fi system under various parameters. Particularly in terms of received power, SNR, and RMS delay, as the use of advanced LEDs is crucial for optimizing these metrics. Lian and Brandt-Pearce explored the use of Orthogonal Frequency Division Multiple Access (OFDMA) in multiuser VLC systems, showing significant improvements in spectral efficiency and data rates [26]. This study is relevant to the objective of investigating Li-Fi system performance, as OFDMA could be incorporated into the developed VLC model to enhance spectral efficiency.Hu et al. presented a visible light communication system utilizing a compact tricolor laser transmitter, which achieved remarkable data rates and system efficiency [27]. This aligns with the objective of enhancing the VLC model to reflect advanced modulation techniques, ensuring that the model accurately represents the potential of high-efficiency Li-Fi systems. Geng et al. explored the latest advances in VLC technologies and their applications, providing critical insights into the future trends of Li-Fi systems [28]. These developments directly inform the research objective of investigating Li-Fi system performance under various conditions, ensuring that the research remains aligned with the latest technological advancements. Loureiro et al. conducted a survey on recent high-capacity demonstrations and digital modulation techniques in VLC, emphasizing the potential for further developments in Li-Fi technology [29]. These findings align with the research goal of proposing enhancements to the Li-Fi system based on the performance evaluations conducted using the VLC model. Miramirkhani and Uysal provided channel modeling for indoor VLC, stressing the importance of accurate channel models for system performance [30].

This directly supports the objective of developing and refining the VLC model, ensuring it accurately reflects the complexities of indoor environments and enhances system performance.

IPS utilizing VLC technology, has emerged as effective solutions for achieving precise indoor localization. This aligns with the research objectives focused on analyzing IPS measurement algorithms using the developed VLC model. Do and Yoo wrote a comprehensive introduction to IPS, including classification, techniques and comparison among existing techniques and research prospects [31]. Sheikh et al. proposed a Time Difference of Arrival (TDOA) based IPS using VLC, achieving high localization accuracy by leveraging the unique properties of light [32]. This study is relevant to the research objective of evaluating IPS performance, as it provides a basis for developing algorithms that enhance localization accuracy within the VLC model. Rahman et al. reviewed advancements in indoor localization via visible lights, emphasizing the integration of various techniques to improve accuracy and robustness [33]. This supports the objective of analyzing IPS measurement algorithms, as it highlights the importance of incorporating multiple techniques into the VLC model to achieve high accuracy and robustness. Yang et al. introduced a 3D localization scheme based on BLE signal fingerprinting and convolutional neural networks, demonstrating significant improvements in localization accuracy and computational efficiency [34]. These advancements are critical for refining the VLC model to ensure it accurately represents IPS performance, particularly in complex indoor environments. Maheepala et al. reviewed various light-based IPS technologies, highlighting the potential of visible light propagation models and attitude identification in achieving high-precision indoor positioning [35]. This study informs the research objective of analyzing IPS algorithms, as it underscores the importance of precise propagation modeling in the VLC system. El-Ganiny et al. proposed a preamble channel estimation scheme for filter bank multi-carrier-based indoor VLC systems, showing superior performance in terms of accuracy and bit error rate [36]. This study is relevant to the objective of evaluating IPS performance, as it provides a framework for integrating advanced channel estimation techniques into the VLC model. Zhu et al. introduced an indoor visible light positioning algorithm combining ellipse-based asymmetrically clipped optical OFDM, mitigating the effect of multipath distortion and achieving high positioning accuracy

[37]. This study supports the objective of refining the VLC model, particularly in terms of its ability to handle multipath distortion and maintain high positioning accuracy. Dawood et al. performed a comparative analysis of localization algorithms for visible light communication, contributing to the understanding of different techniques for improving IPS performance [38]. This analysis aligns with the research objective of analyzing IPS algorithms within the VLC model, ensuring that the model incorporates the most effective techniques for accurate indoor positioning. Hosseini et al. improved multi-floor WiFi-based indoor positioning systems by fingerprint grouping, enhancing localization accuracy without the need for additional devices [39]. Their findings are relevant to the objective of analyzing IPS algorithms, as they offer insights into techniques that can be adapted for use within the VLC model to enhance accuracy. Tiku and Pasricha provided an overview of indoor localization techniques, highlighting the various methods and their effectiveness in different environments [40]. This overview is critical for ensuring that the VLC model is versatile and effective across various indoor environments, supporting the research objective of analyzing IPS performance.

2. 2. 2. Benefits and Drawbacks

OWC systems present numerous advantages. First, they can achieve very high data transmission speeds due to signal transmission at the speed of light. Second, they are immune to electromagnetic interference, which is a significant advantage in environments where electromagnetic noise is prevalent. Additionally, OWC systems do not require spectrum licenses, as they operate in the optical spectrum, which is more secure than traditional radio frequencies, reducing the risk of information interception. Moreover, OWC systems boast a low bit error rate and high bandwidth. However, despite these apparentadvantages, OWC systems are also subject to several limitations. Their performance is highly susceptible to environmental factors, as air, the transmission medium, can be affected by physical obstructions and atmospheric conditions. For instance, the presence of fog, rain, or even heavy clouds can degrade the signal quality. Additionally, the ambient light interference, such as from the sun or other light sources, can also negatively impact the system's performance. Table 2.1 summarises the advantages and disadvantages of the OWC system.

Table 2.1. The advantages and disadvantages of the OWC system.

Advantages	Disadvantages
Speed of light	Physical obstructions
High data transmission rate	Atmospheric effects
Immunity to electromagnetic interference	Light pollution
No spectrum license required	
Secure and private	
Low bit error rate	

2. 2. 3. Prospects

It is clear that OWC not only encompasses a wide range of specific research fields but also leads to a variety of applications. In general, these applications can be grouped into the following broad categories.

The first category is outdoor wireless applications, such as inter-satellite connection, vehicular networks, intelligent transport systems, networks in catastrophic situations, broadcasting, etc.

The second category is indoor wireless applications, for example, wireless indoor local area networks, sensitive areas, smart homes, smart supermarkets, etc.

The final category comprises other applications, including image sensing systems, navigation, underwater networks, wireless body area networks, machine-to-machine communications, secure communications, etc.

2. 3. OWC Technologies

In theoretical terms, OWC technologies employ light to modulate signals into high-speed optical carrier waves, with the original information being demodulated and retrieved by the receiver. The fundamental operation principle of an OWC system is illustrated in the general block diagram in Figure 2.2. Initially, the input electrical data

is processed by a modulator and subsequently converted into an optical signal by a transmitter. The transmitter typically comprises a driver circuit, an optical source and transmitter optics. The optical signal is then transmitted through the atmospheric channel. Upon reaching the receiver, the optical signal is received by an optical detector, converted back into an electrical signal, and forwarded to a demodulator. Following demodulation, the original electrical input is deciphered. The specific components, including transmitter, receiver, transmission media and modulation technique, can vary depending on the OWC technology employed. Generally, LEDs or LDs are utilized as transmitters, while photodiodes (PD) or cameras function as receivers. The transmission media can encompass IR, VL or UV spectra.

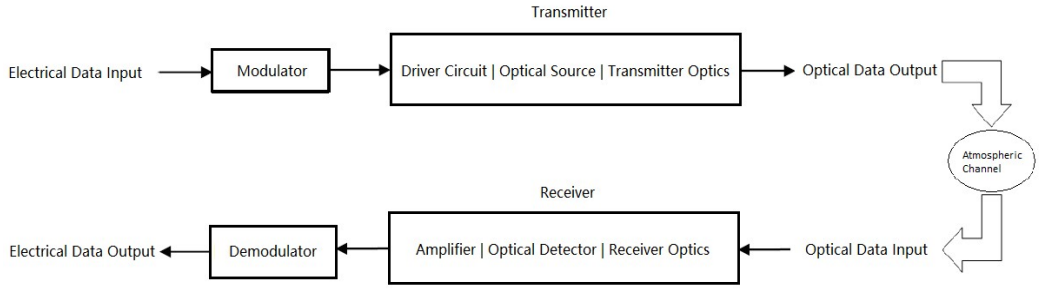

Figure 2.2. The basic blocks of the OWC system.

2. 3. 1. Free Space Optical Communication

FSO communication is an OWC technology that utilizes modulated IR or VL beams to transmit information through the air, free space or vacuum. The basic operation principle of FSO is similar to that of optical fibre, except that the modulated beams travel through the air instead of optical fibre. FSO technology involves transmitting these modulated optical beams through the atmosphere to provide point-to-point communication links.

FSO systems offer high bandwidth and data rates, leveraging the vast unlicensed spectrum of optical frequencies, making them suitable for high-capacity backhaul links in telecommunications networks. However, FSO requires a clear LOS link between the transmitter and receiver, which can limit deployment in environments with physical obstructions or severe atmospheric conditions. The direct propagation of light in FSO systems results in minimal latency, which is beneficial for real-time applications.

Additionally, the narrow beam width of FSO links reduces the risk of interception and eavesdropping, providing inherent physical layer security. FSO systems are relatively easy to deploy and can be quickly reconfigured, making them suitable for temporary or emergency communication setups.

As a significant advancement over copper cable communication, fibre optic communication is becoming the primary wired communication method for achieving high data rates, gradually superseding cable communication. However, it has some notable drawbacks. The civil works required for laying fibre optic cables are time-consuming and expensive. In comparison, FSO technology is easier to install and redeploy,, and the implementation cost of FSO communication is lower than that of fibre optics. These benefits make FSO a popular research topic. However, FSO communication is highly affected by the diversity of outdoor transmission channels. Weather condition and atmospheric turbulence can lead to poor communication performance. Moreover, FSO communication requires a strict LOS propagation between the transmitter and receiver. Additionally, factors such as thermal expansion and contraction, or building swaying caused by wind, can affect the alignment and maintenance of the laser between the two endpoints. A potential solution is to widen the laser divergence angle or to adopt Acquisition, Pointing and Tracking (APT) techniques.

The transmission performance of FSO systems is influenced by various factors, including atmospheric conditions, alignment precision, and beam divergence. Simulation models are instrumental in understanding and optimizing these factors to enhance system performance. Atmospheric effects such as attenuation, caused by absorption and scattering due to fog, rain, and dust, can significantly reduce signal strength. Simulation studies often model these effects using empirical and theoretical models to predict link availability and reliability. Atmospheric turbulence induces random fluctuations in the refractive index, leading to scintillation and beam wandering. This effect is modeled using statistical methods, such as the log-normal or Gamma-Gamma distributions, to analyze its impact on BER and signal quality.

Precise alignment of the transmitter and receiver is crucial for maintaining a strong FSO link. Misalignment can result from thermal expansion, wind, and mechanical

vibrations. Simulation models incorporate alignment error probabilities to assess system robustness. The natural divergence of the optical beam over distance affects the received power. Gaussian beam propagation models are used to simulate the beam spread and optimize the transmitter optics to minimize divergence.

2. 3. 2. Visible Light Communication

VLC uses visible light, typically from LEDs, for data transmission. VLC systems can provide both illumination and data communication simultaneously, leveraging the widespread adoption of LED lighting. With advanced modulation schemes, these systems can achieve high data rates, comparable to traditional RF systems. While VLC generally requires LOS for optimal performance, it can also operate in diffuse link configurations where light reflections off surfaces enable communication. VLC systems are immune to electromagnetic interference, making them suitable for environments where RF communication is problematic, such as hospitals and aircraft. Similar to FSO, the confined coverage area of VLC links enhances security. Additionally, visible light is safe for human exposure, unlike certain RF frequencies.

VLC has many advantages over RF communication, including better confidentiality, higher security, and no electromagnetic interference, due to the transmission medium of light. The abundant optical spectrum extends the communication bandwidth to visible light frequencies, alleviating the RF spectrum shortage crisis. Thus, VLC is a valuable supplement to existing RF communication systems.

Speaking of IR communication, although it emerged earlier, its limitations cannot be overlooked. IR may harm the human eye, and its transmission power is limited, resulting in shorter transmission distances and lower data rates. Furthermore, IR is highly directional and can only be transmitted point-to-point, making it unsuitable for mobile equipment. IR communication requires separate light sources and receiving equipment. In comparison, VLC integrates both lighting and communication, emits light that is not harmful to the human eye, allowing for higher emission power. Moreover, the scattered light used in VLC requires less directionality, and the communication link is less likely to be blocked.

The performance of VLC systems is characterized by factors such as modulation techniques, receiver design, and ambient light interference. Simulation models provide insights into optimizing these parameters for enhanced performance. On-Off Keying (OOK) is a simple and widely used modulation scheme in VLC, which modulates the LED intensity to represent binary data. Simulation models evaluate its performance under different lighting conditions and data rates. Orthogonal Frequency Division Multiplexing (OFDM) enhances VLC data rates by multiplexing multiple carrier signals, with simulations assessing its effectiveness in mitigating inter-symbol interference and maximizing spectral efficiency. The choice of photodetectors, such as photodiodes or avalanche photodiodes, impacts the sensitivity and bandwidth of the VLC system. Simulation models analyze the trade-offs between these parameters to optimize receiver performance. Optical filters reduce ambient light noise, while concentrators enhance the received signal strength. Simulation studies explore the design and placement of these components to improve the SNR. Ambient light sources, such as sunlight and artificial lighting, introduce noise in VLC systems. Simulation models incorporate scenarios with varying ambient light levels to develop algorithms for interference mitigation, such as adaptive filtering and error correction codes.

2.3.3. Light-Fidelity

Li-Fi is an OWC technology, utilizing visible light from LED lamps for high-speed data transmission. Unlike traditional Wi-Fi, which utilizes radio waves, Li-Fi leverages the light spectrum, offering several distinctive characteristics and advantages.

Li-Fi systems can achieve significantly higher data rates compared to conventional Wi-Fi, with laboratory experiments demonstrating speeds exceeding 10 Gbps. This is facilitated by the large bandwidth available in the visible light spectrum, which is approximately 10,000 times larger than the RF spectrum. Li-Fi utilizes advanced modulation techniques to enhance data transmission rates and improve spectral efficiency.

The use of VL provides Li-Fi systems with a high level of security. Since light waves cannot penetrate opaque objects like walls, Li-Fi communication is inherently secure from external eavesdropping, which is a common concern in RF-based systems.

Additionally, the confined coverage area of Li-Fi allows for precise control over the communication environment, further enhancing its security.

Another key characteristic of Li-Fi is its dual functionality. LED lights, already ubiquitous in indoor environments, are used simultaneously for illumination and data transmission. This dual-use capability not only reduces the need for additional infrastructure but also makes Li-Fi a cost-effective solution for integrating lighting and communication.

Li-Fi systems are also immune to electromagnetic interference (EMI), making them suitable for use in environments where RF communication is problematic, such as hospitals, aircraft, and industrial settings. The absence of EMI ensures that Li-Fi does not interfere with sensitive electronic equipment, providing a safer communication alternative.

The transmission performance of Li-Fi systems is a critical area of study, with key metrics including received power, SNR, and RMS delay spread. These parameters are essential for evaluating the efficiency and reliability of Li-Fi communication.

Received power in Li-Fi systems is influenced by several factors, including the distance between the transmitter and receiver, the angle of incidence, and the presence of obstacles or reflective surfaces. The power received by the photodetector decreases with increasing distance from the light source, following the inverse square law. Additionally, the orientation of the LED and the photodetector plays an important role in determining the received power. The use of reflectors and optical concentrators can help mitigate power loss by focusing the light more effectively onto the photodetector.

Simulation models and experimental setups often analyze received power under various conditions to optimize the placement and orientation of Li-Fi components. These studies aim to maximize received power while minimizing energy consumption, ensuring efficient and sustainable operation of Li-Fi systems.

The SNR is an important metric that determines the quality of the received signal in Li-Fi systems. It is influenced by the intensity of the transmitted light, ambient light interference, and the sensitivity of the photodetector. High SNR values indicate clear

and reliable communication, while low SNR values suggest potential issues with data transmission accuracy.

Ambient light sources, such as sunlight and artificial lighting, introduce noise into Li-Fi systems. To mitigate this, optical filters and advanced signal processing techniques are employed to enhance SNR. Simulation models evaluate SNR under different ambient light conditions, providing insights into the effectiveness of these mitigation strategies.

Moreover, the use of adaptive modulation schemes can dynamically adjust the transmission parameters based on the SNR, optimizing the data rate and ensuring robust communication. For instance, in high SNR scenarios, higher-order modulation schemes can be employed to increase data throughput, while in low SNR conditions, more robust modulation schemes can be used to maintain communication reliability.

RMS delay spread is a measure of signal dispersion in time due to multipath propagation, which occurs when transmitted light reflects off surfaces before reaching the receiver. This can cause inter-symbol interference (ISI), degrading the quality of communication.

In indoor environments, where Li-Fi is predominantly used, multipath effects can be significant due to the presence of walls, ceilings, and furniture. Simulation models and experimental studies assess the impact of multipath propagation on RMS delay spread, using techniques such as ray tracing to model the behavior of light in complex environments.

To mitigate the adverse effects of RMS delay spread, Li-Fi systems can employ equalization techniques and error correction codes. These methods help to reconstruct the original signal by compensating for the delays introduced by multipath propagation. Additionally, the use of diffuse link configurations, where light reflections are intentionally utilized, can help to minimize ISI and improve overall system performance.

Li-Fi is an OWC system that uses LED as the light source for short-range transmission. Compared to conventional light sources, such as incandescent and fluorescent lamps, LED has the advantage of long service life, low power consumption, and low heat generation. In addition, LED is an electric driver with variable brightness in response to

modulated current. In general, LED is applied for illuminating through a constant current. The optical output could also be changed at a very high speed through prompt and subtle current changes.

The Li-Fi operating principle is relatively simple. When the LED is on, a binary digit "1" is transmitted, and a binary digit "0" is transmitted when the LED is off. Data can be coded in light when the rate at which the LEDs flicker on and off is changed to provide strings of 1s and 0s. It needs to note that with quick modulation in the LED intensity, the output seems constant to people as human eyes could not detect the changes.

In comparison to the widespread use of Wi-Fi, Li-Fi offers several distinct advantages, including higher data rates, lower cost, greater spectrum availability, and enhanced security. These attributes make Li-Fi particularly suitable for use in the electromagnetic-sensitive environments, such as aircraft cabins, hospitals and nuclear plants, where RF-based technologies might pose risks or face restrictions. However, Li-Fi technology has limitations, particularly in outdoor applications. Due to its reliance on visible light, Li-Fi cannot penetrate physical obstructions and is less effective over long distances. This restriction limits Li-Fi's practicality for outdoor or long-distance applications[41]. Table 2.2summarizes the key differences between Li-Fi and Wi-Fi, highlighting the unique characteristics and applications of Li-Fi that distinguish it from traditional RF-based wireless communication systems.

Table 2.2. The characteristic comparison between Li-Fi and Wi-Fi. [41]

Features	**Li-Fi**	**Wi-Fi**
Transmission Media	VL for downlink and VL or IR or UV or RF for uplink	RF for downlink and uplink
Maximum Data Rate	10 Gbit/s using LED and 100 Gbit/s using LD (combined with optical diffuser)	6 Gbit/s using IEEE 802.11 ad
Transmission Distance	10 m	100 m
Electromagnetic Interference Level	Low	High
Transmission	Directional	Omnidirectional
Cost	Low	High
Modulation Technique	IM/DD	AM
Power Consumption	Low	High
Risk and Safety Issues to Human	No	Yes

2. 3. 4. Indoor Positioning System

With lightweight mobile devices (MD) becoming an essential part of daily life in recent years, location estimation has emerged as a topic of increasing interest.According to a new report by the Pew Research Center's Internet Project, 74 % of adult MD owners use positioning systems to obtain directions or other information about their current location [42].

In the field of positioning, GPS stands unparalleled in terms of coverage area and cost. As a satellite-based positioning system, GPS has been extensively utilized in various outdoor environments, including military, healthcare, manufacturing, marketing, logistics, and car navigation. However, the inevitable drawback of GPS is that it requires a LOS connection between GPS receivers and satellites to determine a person's or object's location. When GPS is used indoors, its accuracy significantly deteriorates because walls or tall buildings block the signal from GPS satellites. Additionally, GPS generally comes with higher power consumption, high latency, and low efficiency. These limitations have prompted many researchers to develop alternative techniques and methods to provide indoor location services. VLC-based IPS are a promising alternative approach. VLC-based IPS refers to the tracking and monitoring of people or objects inside buildings. It is a network of devices that can communicate with internal sensors in MDs and uses a light propagation model to determine the physical location of an MD in a closed environment.

In terms of performance metrics, the accuracy of location information is of great importance. There is usually an error between the actual mobile location and the estimated location. The precision of location refers to the confidence interval or the percentage of successful location detection. Other performance metrics include coverage, capacity, scalability, and delay of the positioning system. The coverage metric refers to the space boundary for estimating location information. The capacity metric refers to how many location estimations are processed by every unit of time. The scalability metric shows the system's performance in the face of significantly increasing location requests and wider coverage. The delay metric represents the time spent between location awareness and information reporting. All of these performance metrics are determined by the adoption of sensing technology, radio channel and

environmental characteristics, the bandwidth of sensing signals, infrastructure capability of the system, location algorithm, and complexity of signal processing techniques used in the estimation of location information.

Similar to all other emerging technologies, there are always concerns about protecting users' privacy data from abuse. There is a need to have security protocols in the location system to protect location information.

2. 3. 4. 1. Sensing Technologies of IPS

Based on the sensing technologies, there are both advances and limitations in the positioning systems due to the different sensor signal types. The types of signals are determined by various factors, such as reflection, diffraction, scattering and propagation delay. Some technologies commonly use wireless signals for IPS, such as ultrasound, VL, and RF. Technological limitations include effective range, regulatory constraints, available bandwidth, power constraints, cost, security, and interference [42].

Walls or obstructions block VL signals. As a result, VL signals have a minimal range in an indoor context but feature a high transmission speed. In general, a VL signal has a range of about five meters. Compared with ultrasound devices, the size of these devices is usually smaller [43]. In an indoor environment, this type of signal can be interfered resulting in the problem of accurate sensing.

As the RF signal can penetrate most indoor building materials, it features an excellent range in an indoor context, offering a significant transmission speed. Frequencies could be used free of charge, even without authorization. The RF signal has the most extended range compared with infrared and ultrasound.

Ultrasound is generally operated at lower frequency bands compared with the other two types of signals. However, ultrasound is characterized by excellent location sensing precision in slow sound transmission speed. Regarding the advantage, ultrasound devices are simple in design and low cost. Nonetheless, ultrasound could not penetrate walls but reflect off most obstructions indoors. Ultrasound has a short range, about 3 m

to10 m, and has a 1 cm distance measurement resolution. The performance of ultrasound is affected by the working temperature.

2. 3. 4. 2. Measurement Algorithms of IPS

Usually, the algorithms in VLC-based indoor positioning consist of proximity, triangulation, fingerprinting and vision analysis. Proximity is the most straightforward approach to VLC-based indoor positioning. With the adoption of proximity, the absolute or relative location could not be obtained, and just proximity location information is available. Therefore, the determination of the proximity location of MD is based on signals from one LED base station. Triangular geometric properties which include the information of lateration and angulation could be used for position determination. The distance from the MD to LED base stations could be determined by using lateration. The position of MD is decided by angulation based on the measured angles relative to multiple base stations. With matching online measured data and pre-measured position-related data, the relative position could be estimated using fingerprinting. With different data characteristics obtained in measure points, these differences are used to estimate the position for identifying fingerprinting. Vision analysis refers to geometric relations between the 2D positions in the projections on the image sensor and the 3D object positions in the actual world. The pinhole camera model references geometric relationships in vision analyses[32].

One measurement algorithms of VLC-based IPS adopting trilateration is as follows. The signal is decoded to separate the information from each LED by wavelength. After the receiver receives the power from light sources, the data is used to calculate the distance between each LED and the receiver. The estimated location of the receiver is able to be determined.

According to LOS channel transfer function, the distance can be calculated in Eq.(2.1)

$$d = \sqrt{\frac{P_t(m+1)A_{det}\cos^m\phi T_s(\psi)g(\psi)\cos\psi}{2\pi P_r}} \qquad \text{Eq.(2.1)}$$

Because the four LED arrays are placed on the underside of the ceiling and the receiver is put on the ground, the height between them is fixed. The length between the receiver and origin point in the plane can then be given in Eq.(2.2)

$$l = \sqrt{d^2 - h^2} \quad \text{Eq.(2.2)}$$

And the position of the receiver can be obtained by Eq.(2.3) to Eq.(2.6)

$$(x - x_1)^2 + (y - y_1)^2 = {l_1}^2 \quad \text{Eq.(2.3)}$$

$$(x - x_2)^2 + (y - y_2)^2 = {l_2}^2 \quad \text{Eq.(2.4)}$$

$$(x - x_3)^2 + (y - y_3)^2 = {l_3}^2 \quad \text{Eq.(2.5)}$$

$$(x - x_4)^2 + (y - y_4)^2 = {l_4}^2 \quad \text{Eq.(2.6)}$$

where (x_i, y_i) are the coordinates of ith LED array, l_i are the distance between the projection of ith transmitter and the receiver in one plane.

By using substitution and subtraction, the quadratic equations can be rearranged to linear equations and expressed in matrix form, which is given in Eq.(2.7)

$$AX = B \quad \text{Eq.(2.7)}$$

where A, X and B are given in Eq.(2.8) to Eq.(2.10)

$$A = \begin{bmatrix} x_2 - x_1 & y_2 - y_1 \\ x_3 - x_1 & y_3 - y_1 \\ x_4 - x_1 & y_4 - y_1 \end{bmatrix} \quad \text{Eq.(2.8)}$$

$$X = \begin{bmatrix} x \\ y \end{bmatrix} \quad \text{Eq.(2.9)}$$

$$B = \frac{1}{2}\begin{bmatrix} ({x_2}^2 + {y_2}^2 - {l_2}^2) - ({x_1}^2 + {y_1}^2 - {l_1}^2) \\ ({x_3}^2 + {y_3}^2 - {l_3}^2) - ({x_1}^2 + {y_1}^2 - {l_1}^2) \\ ({x_4}^2 + {y_4}^2 - {l_4}^2) - ({x_1}^2 + {y_1}^2 - {l_1}^2) \end{bmatrix} \quad \text{Eq.(2.10)}$$

The solution can then be calculated using the matrix inverse, which is given in Eq.(2.11)

$$X = (A^T A)^{-1} A^T B \quad \text{Eq.(2.11)}$$

Alternatively, Cramer's Rule can be used to solve Eq.(2.3) to Eq.(2.6), and the coordinate of receiver is given in Eq.(2.12) and Eq.(2.13)

$$x = \frac{\begin{vmatrix} \alpha & 2\Delta y_2 \\ \beta & 2\Delta y_3 \\ \gamma & 2\Delta y_4 \end{vmatrix}}{\begin{vmatrix} 2\Delta x_2 & 2\Delta y_2 \\ 2\Delta x_3 & 2\Delta y_3 \\ 2\Delta x_4 & 2\Delta y_4 \end{vmatrix}} \quad \text{Eq.(2.12)}$$

$$y = \frac{\begin{vmatrix} 2\Delta x_2 & \alpha \\ 2\Delta x_3 & \beta \\ 2\Delta x_4 & \gamma \end{vmatrix}}{\begin{vmatrix} 2\Delta x_2 & 2\Delta y_2 \\ 2\Delta x_3 & 2\Delta y_3 \\ 2\Delta x_4 & 2\Delta y_4 \end{vmatrix}} \quad \text{Eq.(2.13)}$$

where the parameter α, β, γ, Δx_i and Δy_i are given in Eq.(2.14) to Eq.(2.18)

$$\alpha = \left({l_1}^2 - {l_2}^2\right) - \left({x_1}^2 - {x_2}^2\right) - \left({y_1}^2 - {y_2}^2\right) \quad \text{Eq.(2.14)}$$

$$\beta = \left({l_1}^2 - {l_3}^2\right) - \left({x_1}^2 - {x_3}^2\right) - \left({y_1}^2 - {y_3}^2\right) \quad \text{Eq.(2.15)}$$

$$\gamma = \left({l_1}^2 - {l_4}^2\right) - \left({x_1}^2 - {x_4}^2\right) - \left({y_1}^2 - {y_4}^2\right) \quad \text{Eq.(2.16)}$$

$$\Delta x_i = x_i - x_1 \quad \text{Eq.(2.17)}$$

$$\Delta y_i = y_i - y_1 \quad \text{Eq.(2.18)}$$

2. 3. 5. Optical Camera Communication

Currently, smart devices are frequently used in daily life and commonly feature front and rear cameras with LED flashes. Consequently, there are initiatives to implement OWC technologies using the device's flash and camera as the transmitter and receiver, respectively, to minimize hardware modifications. Greater attention is given to utilizing LEDs and other light sources as transmitters and image sensors (IS) as receiving modules and displays.

Optical Camera Communication (OCC) differs from VLC in several key aspects. Firstly, OCC systems use both IR and VL, while VLC systems use only VL as a transmission medium. Secondly, OCC systems exclusively utilize LEDs, whereas VLC systems employ both LEDs and LDs as transmitters. Thirdly, OCC systems use only cameras as receivers, while VLC systems use both PDs and cameras.

Therefore, when LEDs and cameras are used as the transmitter and receiver, respectively, a VLC system could be regarded as an OCC system. Conversely, when

VL is adopted as the transmission medium, an OCC system could be regarded as a VLC system. The receiver in OCC is an optical IS or a camera composed of PD arrays. Within the camera's field of view (FOV), the projection effect onto multiple positions on an IS achieved by light from various sources in different directions, which is then sampled using different pixels with the application of the imaging lens in front of the IS. A two-dimension PD array model can be used in a camera, typically comprising over 10 million pixels, with each pixel measuring 1-10 μm in size [43], [44]. Consequently, in a camera equipped with superior spatial resolution, light originating from diverse directions is directed onto disparate sensor positions through a lens and is subsequently sampled by distinct pixels. This differentiation facilitates the segregation of light from multiple sources and orientations, which is paramount for imaging MIMO systems and spatial-division multiplexing in VLC. Utilizing IS, data transmitted from two discrete LED sources were efficiently captured and discerned.

Pixels associated with extraneous noise sources, such as sunlight, digital displays, and ambient lighting, can be isolated and excluded. This segregation ensures secure, non-interfering, and dependable communication in both indoor and outdoor environments through the application of IS.

2.3.6. Light Detection and Ranging

Light Detection and Ranging (LiDAR) represents a sophisticated optical remote sensing technology that measures the distance to, and gathers data on, distant objects through the emission of laser pulses[45]–[50]. NIR and VL are usually transmission mediums in LiDAR for image objects. There are various materials to be targeted by LiDAR, such as rain, chemical compounds, aerosols, dust, clouds, and individual molecules. Physical features can be mapped out at high resolution using a narrow laser beam. For example, the terrain could be detected at a resolution of 30 cm by using LiDAR from an aircraft [46]. Utilizing laser beams, LiDAR technology enables the measurement of scattered light properties and the creation of 3D maps. The LiDAR system comprises four principal components: a laser, a photodetector, a scanner, and a positioning system. Data acquisition via LiDAR occurs across three primary platforms: aerial, space-based, and terrestrial, with aerial platforms being the most commonly

employed. Terrestrial LiDAR data, in particular, is extensively utilized in the development of autonomous vehicle technologies. LiDAR finds a broad spectrum of applications across various fields, including transportation, meteorology, autonomous navigation, architectural surveying, military operations, space exploration, robotic vision, precision guidance, and vehicle anti-collision systems [48][49].

In practical application, significant parallels exist between LiDAR and radio detection and ranging (RADAR). Both technologies leverage related concepts for monitoring the movements and positions of objects. However, their operational methodologies and optimal application contexts differ markedly. The fundamental operating principle of both technologies involves the detection of characteristics through the reflection of energy from target objects. LiDAR utilizes optical light as the transmission medium, whereas RADAR employs microwaves. In both systems, energy is emitted as signals from a transmitter, and upon striking an object, a portion of the signal's energy is reflected back. The receiver captures this reflected energy to ascertain the object's size, distance, and other relevant attributes. Additionally, there are also distinctions in the nature and dimensions of the objects that each technology is capable of detecting and measuring with precision[41]. Table 2.3 summarizes the fundamental differences between LiDAR and RADAR.

Table 2.3. The characteristic comparison between LiDAR and RADAR. [41]

Feature	LiDAR	RADAR
Transmission Media	NIR or VL	Radio wave
Transmitter	Laser	Antennae
Receiver	CCD	Antennae
Target Size	Small	Large
Atmospheric Impact	High	Low

2. 3. 7. Underwater Optical Wireless Communication

In comparison to underwater fibre optic and copper communication systems, underwater wireless communication offers superior services for mobile platforms. Table 2.4 outlines the differences among the three primary underwater wireless communication technologies: low-frequency RF communication, underwater acoustic communication and underwater optical wireless communication (UOWC).

Table 2.4. The characteristic comparison among underwater wireless communication.

Features	Low-frequency RF Communication	Underwater Acoustic Communication	UOWC
Transmission Distance	10 m	10 km	100 m
Transmission Media	radio waves	sound wave	VL
Speed	2.3×10^8 m/s	1500 m/s	2.3×10^8 m/s
Attenuation	high	low	high
Data Rate	Mbps	kbps	Gbps
Band	30 – 300 MHz	10 – 15 kHz	5×10^{14} Hz
Delay	medium	high	low
Cost	high	high	low

Underwater RF communication employs low-frequency electromagnetic waves as the transmission medium. Despite the widespread use of electromagnetic waves for terrestrial communication, their propagation in seawater is significantly attenuated due to the skin effect, with attenuation increasing at higher frequencies. Consequently, only low-frequency bands are viable for practical underwater communication. Additionally, the long wavelength characteristic of RF communication necessitates larger receiving equipment, posing challenges for communication between small devices.

Underwater acoustic communication, on the other hand, utilizes sound waves as the transmission medium. This technology is relatively mature and widely adopted. Unlike electromagnetic waves, sound waves experience minimal attenuation in water, approximately 0.4 dB/km. Consequently, underwater acoustic communication can achieve transmission distances up to 10 km or more [51]. However, underwater acoustic communication has inherent limitations. Firstly, the available bandwidth for underwater acoustic communication is extremely narrow, approximately 100 kHz. As a result, the data transmission rate achievable with this technology is less than megabits per second, which falls short of the requirements for high-speed, high-capacity data transmission [51]. Moreover, sound waves travel at approximately 1500 m/s in water, which is significantly slower than the speed of light. Consequently, transmitted signals experience a time delay of several seconds over distances of a few kilometers, resulting in a relatively large communication delay for underwater acoustic communication.

Additionally, environmental factors greatly influence the transmission of sound waves, leading to reflections and multipath effects, which limit both the communication range and data rate.

Another significant concern, particularly in the military domain, is the security of the transmission. Underwater acoustic communication is non-directional; the signal disperses in all directions, akin to a broadcast transmission. This dispersion allows eavesdroppers to intercept sound signals over distances of several kilometers without detection, rendering underwater acoustic communication unsuitable for confidential communications. Lastly, similar to low-frequency RF communication, the receiving equipment used in underwater acoustic communication is relatively large, posing challenges for deployment in compact systems.

In comparison to its predecessors, UOWC offers several advantages. Firstly, UOWC boasts a significantly higher transmission rate, capable of reaching data rates in the gigabits per second range, far surpassing the capabilities of underwater acoustic and low-frequency electromagnetic wave communication. This is due to UOWC's larger available bandwidth compared to acoustic communication and its relatively lower channel attenuation than underwater radio communications. As a result, UOWC provides an effective compromise, delivering gigabit communication links over distances up to 100 meters. Secondly, UOWC features low energy consumption. The highly directional nature of light enables UOWC systems to operate with lower transmitting power than underwater acoustic communication, resulting in reduced power loss and lower energy requirements for data transmission. Additionally, UOWC offers enhanced confidentiality. The signal transmitted by a UOWC system propagates only in the intended direction, minimizing the risk of eavesdropping. Interception is only possible within the receiver's range, enhancing the security of communication. Finally, UOWC systems are compact, facilitating easier integration compared to other communication devices. Advances in semiconductor technology have enabled the integration of UOWC transceivers into semiconductor devices. The increasing miniaturization of optoelectronic components supports the high degree of integration necessary for UOWC systems, making them a viable option for modern, space-constrained applications.

2. 3. 8. Summary of OWC Technologies

This section presents a comprehensive review of various OWC technologies, identifying their technological differences in terms of standards, transmitters, receivers, transmission media, modulation techniques, operational principles, security levels, and attenuation characteristics. Table 2.5 summarizes key differences across these technologies, focusing on their architectures, applications, fundamental principles, advantages, and limitations.

Table 2.5. The characteristic comparison among wireless communication technologies. [41]

Features	VLC	Li-Fi	IPS	OCC	FSO	LiDAR	UOWC	RF
Transmitter	LED/LD	LED/LD (combined LDs with optical diffuser)	LED/LD (combined LDs with optical diffuser)	LED	LD	laser	LED/LD	antenna
Receiver	PD/ camera	PD	PD	camera	PD	CCD	PD	antenna
Transmission Distance	20 m	10 m	10 m	200 m	10,000 km	8,000 km	100 m	100 km
Interference Level	low	low	low	zero	low	low	low	high
Noise	sun plus ambient light sources	sun plus ambient light sources	sun plus ambient light sources	sun plus ambient light sources	sun plus ambient light sources	sun plus ambient light sources	ambient light sources	electrical and electronic appliances
Environmental Impact	yes	yes	yes	no	yes	yes	yes	yes
Data Rate	10 Gbit/s using LED and 100 Gbit/s using LD	10 Gbit/s using LED and 100 Gbit/s using LD	10 Gbit/s using LED and 100 Gbit/s using LD	54 Mbit/s	40 Mbit/s		Gbit/s	6 Gbit/s (IEE 802.11ad at frequencies around 60 GHz)
Security	high	high	high	high	high	high	high	low
Transmission Media	VL	IR/VL/UV	IR/VL/UV	IR/VL	IR/VL/UV	IR/VL	VL	radio waves
Spectrum License	no	no	no	no	no	no	no	yes
Path Loss	medium (very high for NLOS)	medium (very high for NLOS)	medium (very high for NLOS)	low	medium	medium	medium	high

Indoor VLC is typically employed as the transmission model for both Li-Fi and IPS. Li-Fi is commonly utilized for communication and illumination, whereas IPS is primarily used for localization and illumination. While indoor VLC can facilitate high-data-rate communication, its effectiveness is limited in outdoor environments

due to interference from natural light and other sources, and it is not suitable for long-distance communication. The OCC system can be used for communication, positioning and imaging, demonstrating effectiveness for long-distance communication both indoors and outdoors. However, the OCC system has a low data rate because conventional cameras have low frame rates. FSO can provide high-data-rate and ultra-long-range communication, but its performance is significantly impacted by outdoor conditions. As a specialized sensing technology, LiDAR is typically used for high-resolution 3D mapping. Despite its high cost and susceptibility to environmental factors, LiDAR remains a critical tool for precise mapping applications. UOWC is specifically employed for underwater communication.

These OWC technologies are utilized in various scenarios for distinct purposes, ensuring their effective use. OWC can achieve data rates up to 100 Gbit/s, whereas RF-based communication peaks at 6 Gbit/s. In terms of communication distance, RF-based technology outperforms OWC. However, RF-based communication is more susceptible to interference and has a lower security level compared to OWC. Additionally, OWC systems are sensitive to obstruction by obstacles. In summary, both OWC and RF technologies are poised for effective utilization in future wireless communication systems.

The BER model developed in this research for FSO communication shows significant improvements in bit error rate and transmission distance when compared to standard FSO systems. This enhancement is critical for long-distance, high-bandwidth applications where minimizing errors is essential. The VLC model, focusing on indoor environments with both LOS and NLOS channels, demonstrates improved performance in terms of bit error rate and received power, especially under controlled LOS conditions. However, NLOS scenarios exhibit a moderate increase in RMS delay and a corresponding decrease in SNR, highlighting areas for further optimization.

These findings align with the research objectives, particularly in enhancing transmission performance and exploring the comparative advantages of different modulation formats and channel conditions within OWC technologies. By focusing on these key metrics, the research contributes to the broader understanding and

development of more efficient and reliable OWC systems, particularly in challenging communication environments.

There has been profound research conducted on a variety of OWC technologies. The technological differences are identified in terms of different standards, transmitters, receivers, transmission media, modulation techniques, operation principles, levels of security, attenuation characteristics, and other key performance metrics. Table 2.6summarizes the comparison of the FSO model and VLC model developed in this research with other similar systems.

Table 2.6. The comparison of FSO model and VLC model.

Model/System	**FSO Model**	**VLC Model (Developed)**	**FSO (Standard)**	**Li-Fi (Standard)**	**OCC**	**RF-Based Communication**
Transmission Distance	Up to 10 km	20 m (LOS), 10 m (NLOS)	Up to 5 km	10 m	200 m	Up to 100 km
BER	10−9 to 10−6	10-7 to 10-4	10-6	10-5	10-3	10-2
Received Power	high	moderate	high	moderate	low	variable
SNR	high	moderate to high	high	moderate	low	low
RMS Delay	low	moderate	low	low	high	high

2. 4. Transmitter and Receiver System

The transmitter and receiver are two essential components in the OWC system. The transmitter is used to modulate the data into the signal which is suitable for transmission in channel by the light. At the receiver, the photodetector converts the optical carrier wave into electrical signal using Intensity Modulation / Direct Detection (IM/DD) techniques. This section provides a thorough review of the transceiver system, including the mechanism of the transmitter and receiver blocks, modulation and demodulation formats.

2. 4. 1. Transmitter Block

The optical transmitter block is responsible for modulating the original data and converting the electrical signal into an optical signal. This optical signal is then emitted into the transmission channel. The optical transmitter block primarily consists of two main components: the light source and the modulator.

2. 4. 1. 1. Light Source

Common light sources in OWC systems include LEDs and LDs.

LEDs are semiconductor-based light-emitting devices characterized by several advantageous properties: low heat generation, high power efficiency, long service life, compact size, straightforward light source design, rapid response speed, high vibration resistance, and environmental friendliness. These attributes position LEDs as a promising option for next-generation lighting solutions.

LDs, similar to the LEDs, are semiconductor devices that feature a PN junction. However, LDs differ by incorporating a resonant cavity that selectively resonates and amplifies photons at specific frequencies, resulting in coherent light with a narrow spectral width. This process, known as stimulated emission, distinguishes LDs from LEDs. Table 2.7 summarizes the key differences between these two light sources.

Table 2.7. The difference between LED and LD.

Features	LED	LD
Transmission Distance	short	long
Directionality	divergent	concentrated
Power	low	high
Service Life	long	short
Cost	low	high
OWC Technologies	VLC, Li-Fi, IPS, OCC, UOWC	FSO, VLC, Li-Fi, IPS, UOWC

Generally, LDs are suitable for OWC technologies that require high data rates and long distance communication. Conversely, LEDs are more appropriate for OWC technologies that also serve illumination purposes, making them ideal for indoor environments.

2.4.1.2. Modulator

The modulator controls the parameters of a carrier in accordance with electrical signals of the original data. There are two different types of modulation applied for OWC systems. One is direct modulation and the other is external modulation. In terms of direct modulation, the signal modulation is carried out simultaneously with the light source, and the modulation is achieved by changing the input drive current of the light. The advantage is cheap and straightforward, while the disadvantage is that the transmission speed is slow and suitable under 3 GHz. Therefore, direct modulation is utilized in low data rate and medium data rate OWC systems. External modulation means that the modulator is set up outside the light source and the modulating signal is loaded on after the light wave has been formed, changing the characteristics of the output optical signal. The advantage is that it can be used in high power light source at high speed, while the disadvantage is that it is relatively expensive and complex.

The modulator widely used in external modulation is Mach-Zehnder modulator (MZM). The operating principle of MZM is based on the Mach-Zehnder interference principle, which uses the electro-optic effect to control the laser. Figure 2.3 shows the structure of MZM. There are two paths for incoming light at the input coupler where the input optical signal is divided into two beams with identical parameters. The magnitude of the external voltage affects the refractive index of the paths, resulting in a different

phase delay between the two optical signals. Due to this interference, the coupled optical signal will have two possibilities at the output coupler. When the range between the two optical beams is an integer multiple of the wavelength, the coupling of the two beams will be coherently enhanced. On the contrary, when the range between the two optical beams is half an integer multiple of the wavelength, the destructive interference of the two beams will result in a very weak output signal. Therefore, the input optical beam can be modulated by properly controlling the applied voltage of both arms.

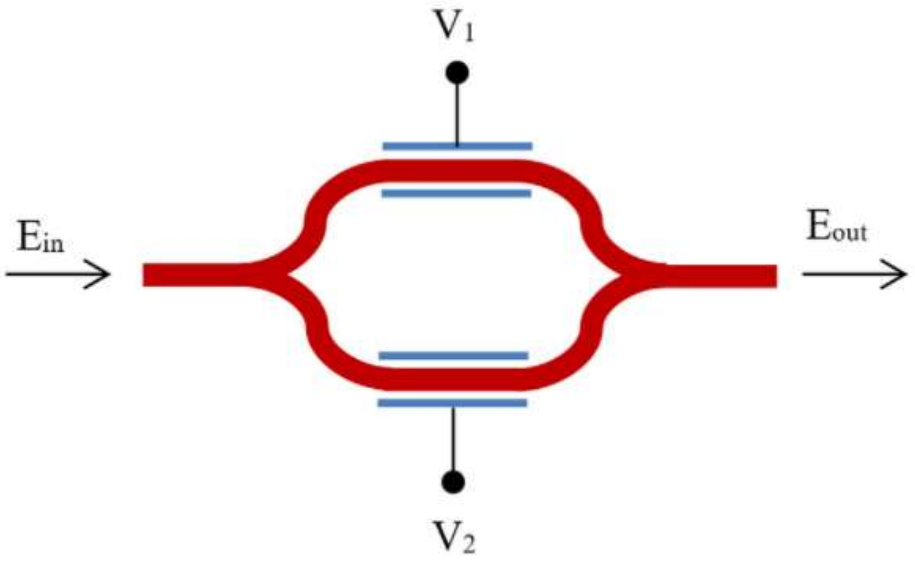

Figure 2.3. The structure of MZM.

A large number of advanced optical modulation formats are based on using these MZMs, due to the better modulation performance, the independently modulating intensity and phase of the optical field. Therefore, various important modulation formats can be generated in an easy and convenient way.

2. 4. 2. **Receiver Block**

The optical receiver block is designed to efficiently receive the optical signal and convert it into the electrical signal. After demodulation, the corresponding original data can be extracted. The optical receiver block primarily consists of a photodetector, a demodulator and a filter.

2.4.2.1. **Photodiode**

The common photodiodes applied in OWC systems are Positive-Intrinsic-Negative (PIN) photodiode and Avalanche Photodiode (APD).

PIN photodiode uses the photoelectric effect. Under certain conditions, the semiconductor device is exposed to light and generates a photocurrent, which converts the light signal into an electrical signal. The advantages of PIN photodiode are low noise performance and temperature stability. The output noise is lower than that of APD and the response varies less with temperature. However, the disadvantage is that the low responsiveness leads to poor receiver sensitivity and limited system transmission distance.

An APD is an optoelectronic device known for its high gain and high detection sensitivity. Compared to a PIN photodiode, an APD can detect lower energy light signals, making it ideal for communication systems requiring high detection sensitivity. This high sensitivity is attributed to the internal avalanche amplification effect. In an APD, electron-hole pairs are generated through the photoelectric effect. When a voltage is applied, electrons drift towards the N-pole while holes drift towards the P-pole. The rate of carrier drift depends on the strength of the inverse bias. As the inverse bias increases, the carriers gain sufficient energy to impact the lattice with significant force, creating additional electron-hole pairs. This chain reaction, known as the avalanche amplification effect, results in enhanced signal detection [52]. However, the APD has some drawbacks. It produces higher noise levels compared to the PIN photodiode and requires higher precision in bias control and tracking. Table 2.8 summarizes the differences between PIN photodiodes and APDs.

Table 2.8. The difference between PIN and APD.

Features	PIN	APD
Transmission Distance	short	long
Receiver Sensitivity	low	high
Noise	low	high
Date Rate	slow	fast
Response Time	fast	slow
Operating Voltage	low	high
Cost	low	high
OWC Technologies	FSO, VLC, Li-Fi, IPS, UOWC	FSO, VLC, Li-Fi, IPS, UOWC

Overall, APDs are suitable for OWC technologies requiring high receiver sensitivity and long-distance communication. Conversely, PIN photodiodes, which are relatively simple and convenient, are suitable for communication systems with low receiver sensitivity requirements and short-distance transmission.

2. 4. 2. 2. Image Sensor

In addition to photodiodes, image sensors can also serve as detectors, recovering signals through digital image processing. The primary image sensors available on the market today are Semiconductor Charge Coupled Devices (CCD) and Complementary Metal Oxide Semiconductors (CMOS).

CCD image sensors technology is based on metal oxide semiconductor (MOS) capacitors. These sensors can operate across a wide range, from far-infrared to X-ray. A CCD image sensor comprises an array of capacitors, each storing an electrical charge proportional to the light intensity of the corresponding pixel. Control circuitry transfers the charge sequentially from one capacitor to the next, with the final capacitor dumping its charge into a charge amplifier. The main advantage of CCD sensors is their ability to detect multiple optical signals simultaneously. They also offer a good field of view with an optical lens, facilitating easier capture and tracking of light sources. However, CCD sensors require complex high-speed digital signal processing software and hardware, which can limit image processing speed.

CMOS image sensors feature photodiodes and CMOS transistor switches for each pixel, allowing individual amplification of the pixel signals. By operating the switch matrix,

pixel signals can be accessed directly and sequentially, enabling faster operation than CCD image sensors. The presence of an amplifier for each pixel reduces noise generated during the reading of electrical signals converted from captured light. Additionally, CMOS image sensors are more cost-effective to produce. Table 2.9 summarizes the differences between these two types of image sensors.

Table 2.9. The difference between CCD and CMOS.

Features	CCD	CMOS
Optical Imaging Quality	high	low
Noise	high	low
Speed	slow	fast
Cost	high	low
OWC Technologies	OCC, LiDAR	OCC

2.4.2.3. Filter

The input sinusoidal signals of different frequencies are used for analysis of electrical low pass filter. There is the same amplitude in the input and output signals at the frequencies below the break frequency. With the increase of the input frequency, it is more than the break frequency, and then the output signal amplitude drops sharply. Based on the theoretical analysis, the magnitude response is similar to the one in the experiments. According to the experimental results, the theoretical formula is valid for a first-order, low-pass filter based on single resistors and capacitors. As a result, LPF can be effectively used for testing performance.

2.4.3. Modulation and Demodulation Formats

In a communication architecture, an analog or digital signal must first to be modulated before being transmitted through a specific channel. Modulation involves converting data into a wireless spectrum by embedding information into an electronic or optical carrier signal. When the receiver obtains the message from the transmission channel, it uses reverse engineering to restore the original signal, a process known as demodulation.

In OWC systems, IM/DD is predominantly used. At the transmitter, the signal waveform modulates the immediate energy of the transmitted power at the desired

wavelength. This technique, known as intensity modulation (IM), is one of the most common modulation methods. Here, the electrical data signals serve as input to the transmitter driver. At the receiver, a photodetector generates electrical signals based on the immediate energy of the received optical signals. This process is called direct detection (DD). In IM/DD modulation, the input energy of the receiver must always be positive.

The most common modulations techniques in OWC systems include single-carrier modulation (SCM), multi-carrier modulation (MCM) and colour intensity modulation (CIM). SCM schemes encompass OOK, pulse position modulation (PPM) and pulse amplitude modulation (PAM). SCM provides a straightforward solution for frequency-flat channel and is widely used to achieve data rates of up to 100 Mbit/s. However, with increasing data rates, SCM is susceptible to non-linear signal distortion and ambient interference. MCM, particularly OFDM, performs better in high data rate transmission. OFDM transmits parallel data streams through a collection of orthogonal subcarriers, enhancing performance in challenging conditions. CIM is a specialized modulation scheme for VLC that adds an additional degree of freedom. It leverages time, frequency, space, colour, and their combinations to provide high-speed communication suitable for most illumination regimes [53]. Some modulation formats applied in OWC systems are mentioned in Figure 2.4.

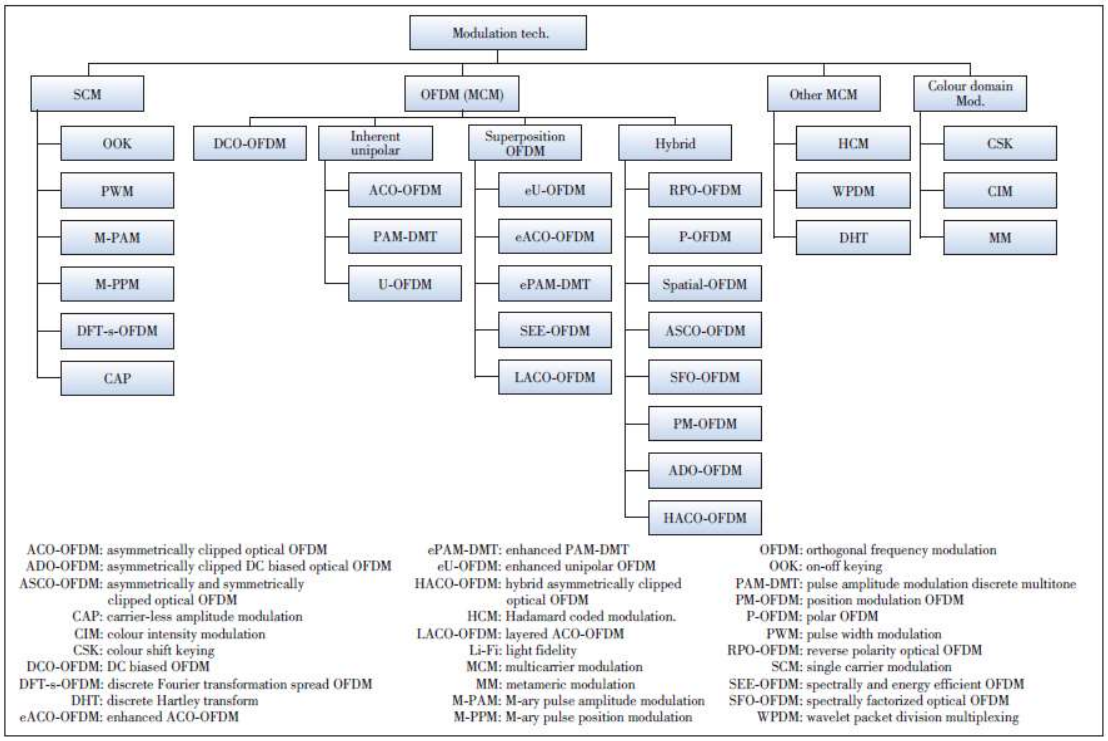

Figure 2.4. The modulation techniques of OWC. [53]

2. 4. 3. 1. **On-Off-Keying**

OOK is a modulation format that controls the light source to pulse on or off at each bit interval to deliver the basic bits. This simplicity makes OOK modulation the most prevalent in OWC systems. It is straightforward to design and implement, but the modulation system is susceptible to ambient noise in the transmission channel [54]. OOK modulation can be further subdivided into Non-Return-to-Zero On-Off Keying (NRZ-OOK) modulation format and Return-to-Zero On-Off Keying (RZ-OOK) modulation format, based on the control methods of the signal pulse. Figure 2.5 illustrates their distinct modulation waveforms. NRZ-OOK represents a binary digit "1" by the presence of a carrier for a given duration, and a binary digit "0"by the absence of a carrier for the same duration. In contrast, RZ-OOK requires the signal to return to zero at the end of each pulse, leading to a higher bandwidth requirement compare to NRZ-OOK.

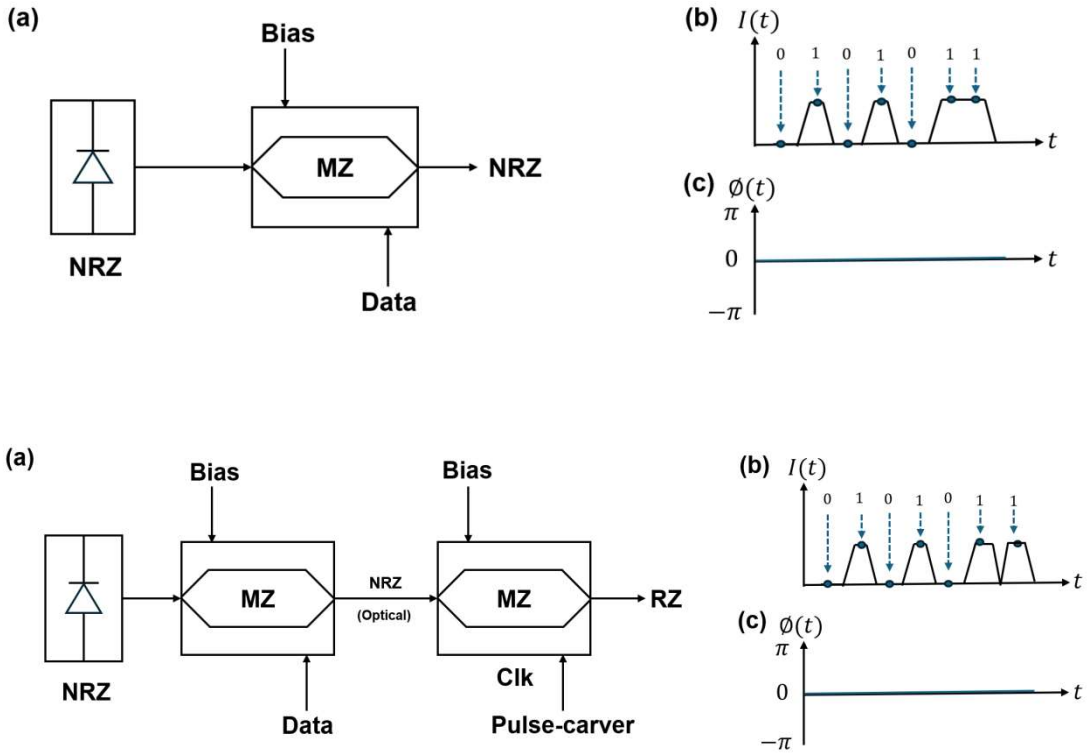

Figure 2.5. The waveform of NRZ-OOK and RZ-OOK.

2. 4. 3. 2. Pulse Position Modulation

As shown in Figure 2.6, the PPM modulation format maps x original digital data bits into 2^x time slots, with the receiver obtaining the carried information by determining the position of the pulse within the time slot. The duty cycle of 2^x-PPM can be expressed as 2^{-x}. When x is large, the duty cycle becomes very low, making PPM modulation less suitable for VLC systems. Additionally, the PPM transceiver is more complicate than the OOK transceiver due to the requirement for slot synchronization and symbol synchronization.

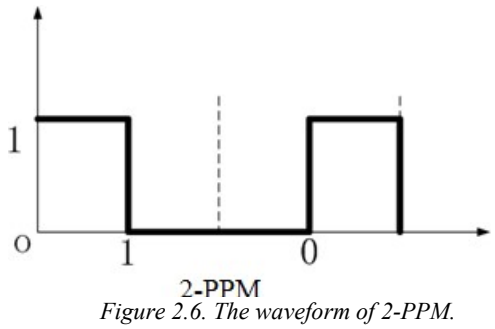

Figure 2.6. The waveform of 2-PPM.

2. 4. 3. 3. Differential Pulse Position Modulation

As illustrated in Figure 2.7, the Differential Pulse Position Modulation (DPPM) modulation format achieves higher bandwidth efficiency compare to PPM by eliminating redundant time slots from the PPM modulation waveform. However, it is still constrained by the system's modulation bandwidth. Since each modulated waveform in DPPM ends with a pulse, symbol synchronization is not required. Consequently, the transceiver architecture of DPPM is simpler than that of PPM.

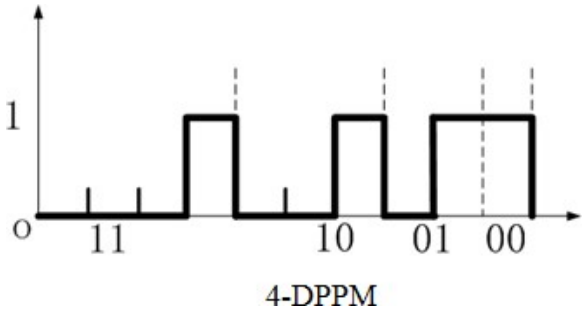

Figure 2.7. The waveform of 4-DPPM.

2. 4. 3. 4. Pulse Amplitude Modulation

The PAM modulation format is a multi-level modulation scheme where the transmitted signal is mapped to different pulse amplitudes. Compare to OOK modulation, each PAM signal can represent more bits of information, thereby achieving higher spectrum efficiency. For instance, each signal of 4-PAM can carry two bits of information. However, as PAM is a multi-level modulation technique, it is more sensitive to system noise and requires a higher SNR for optimal performance in OWC systems. Figure 2.8 illustrates the modulation waveform of 4-PAM.

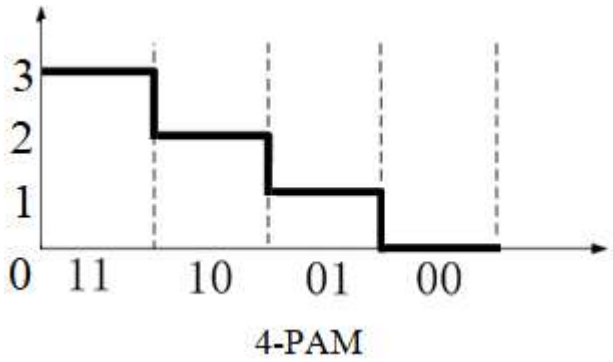

Figure 2.8. The waveform of 4-PAM.

2. 4. 3. 5. Absolute Added Correlative Coding

AACC is a modulation format based on partial-response signaling [55]. In comparison to other modulation formats, it has several benefits. Firstly, in terms of spectral efficiency, the AACC format can utilize spectral resources more effectively and increase transmission capacity. Secondly, in terms of dispersion tolerance and receiver sensitivity, the AACC format is significantly better than traditional modulation formats. In addition, in the process of signal coding and decoding, the AACC format also shows higher efficiency and accuracy. However, the AACC format also has some drawbacks in practical applications, such as higher implementation complexity and higher costs.

This modulation format has the potential to replace 4-PAM and is well-suited for short-haul, direct-detection based optical systems. Figure 2.9 shows the signal constellation diagrams of NRZ, 4-PAM and AACC. The electrical AACC signal constellation diagram resembles that of 4-PAM. Traditional binary signals, such as NRZ, transmit only 1 bit per symbol, whereas multi-level signals, like those used in AACC and 4-PAM, transmit 2 bits per symbol. Consequently, multi-level signals offer more efficient transmission speeds and are more suitable for future OWC systems.

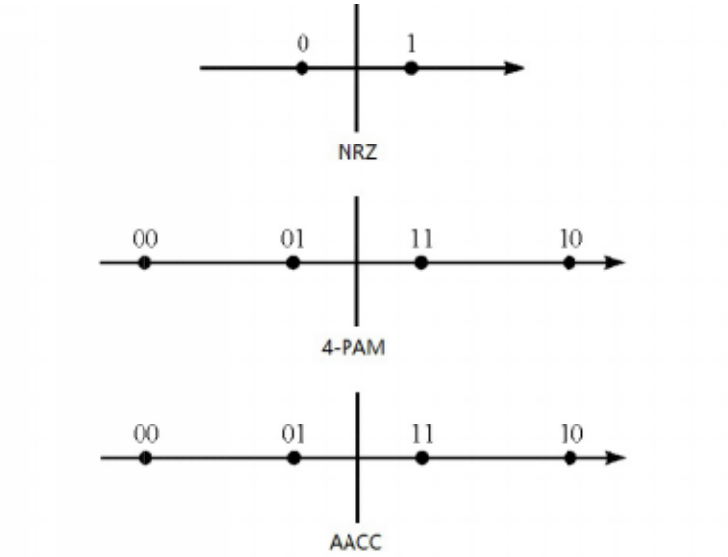

Figure 2.9. Signal constellation diagram among NRZ, 4-PAM and AACC.

Figure 2.10 illustrates the schematic diagram of the electrical AACC signal. The electrical AACC signal with 2 bits per symbol is generated by combining two duobinary signals of unequal amplitude through an electrical adder to form a multi-level bipolar signal. This signal is symmetrical with reference to zero amplitude. The process concludes by taking the absolute value of the generated multi-level bipolar signal using an electronic absolute value device, yielding a unique positive polarity symbol in each case. With this method to generating AACC multi-level-intensity signaling, a data recovery rule can be employed to recover the original data at the receiver [56].

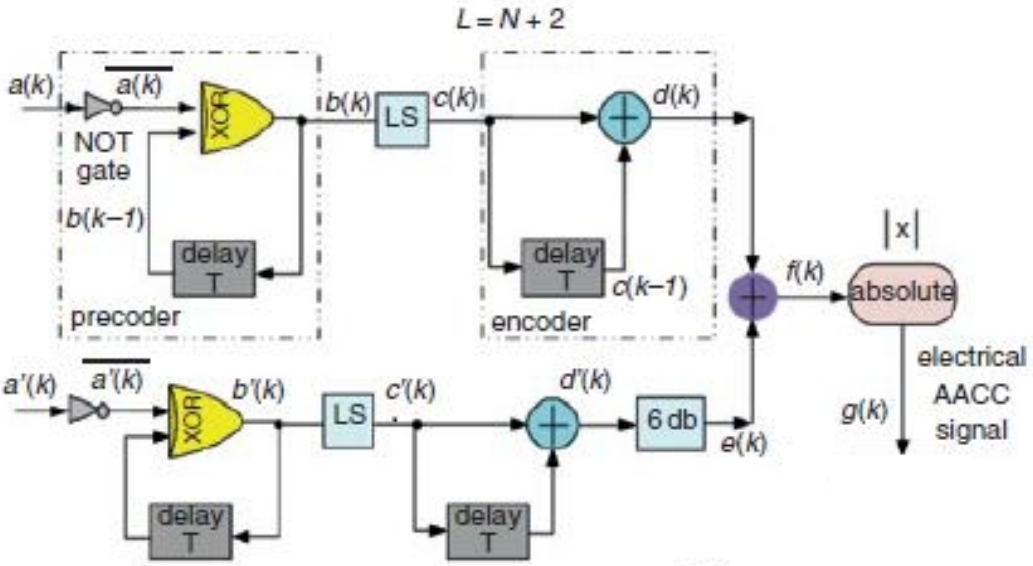

Figure 2.10. Electrical AACC signal. [57]

The transmitter consists of two lanes, each processing an input binary data stream. The first one includes a pre-coder, a Level-Shift (LS) component and an encoder. The pre-coder is composed of a logic NOT gate and a logic XOR gate with a one-bit delay-and-add loop. It functions as a correlative coding mechanism to avoid recursive decoding at the receiver, thereby preventing error propagation and reducing hardware complexity. The encoder performs an electrical one-bit delay-and-add operation to convert a random binary signal into a normalized three-level electrical signal. This conversion is achieved by adding the current bit to the previous bit, leading to an electrical ternary voltage signal. A similar process can be carried out for the second one, except that a 6 dB electrical attenuator component is added to divide the amplitude to half of its value. The relation between the number of generated levels (L) and the number of lanes (N) right after the electrical adder and the absolute circuit, can be simplified and presented in Eq.(2.19)

$$L = N + 2 \qquad \text{Eq.(2.19)}$$

Table 2.10 depicts the transmitted and received bit stream for AACC modulation format. In fact, the procedure by which a binary sequence {0,1} is converted to ternary-levels {-2,0,2} and {-1,0,1} and then to quaternary-level signals {0,1,2,3}. The intensity levels are equidistant and nonnegative, which is advantageous in IM/DD channel. For differential precoding and encoding, a reference bit is crucial to initiate the

progress. This reference bit can be arbitrarily set to logic “1” or logic “0”. In Table 2.10, the reference bit b(k) and b’(k) at time instant k = -1 were set to logic “0”.

Table 2.10. Transmitted and received bit stream for AACC modulation.

k	-1	0	1	2	3	4	5	6	7
$a(k)$		1	0	1	1	0	1	0	0
$\overline{a(k)}$		0	1	0	0	1	0	1	1
$b(k)$	0	0	1	1	1	0	0	1	0
$c(k)$	-1	-1	1	1	1	-1	-1	1	-1
$d(k)$		-2	0	2	2	0	-2	0	0
$a'(k)$		1	1	0	0	1	0	1	0
$\overline{a'(k)}$		0	0	1	1	0	1	0	1
$b'(k)$	0	0	0	1	0	0	1	1	0
$c'(k)$	-1	-1	-1	1	-1	-1	1	1	-1
$d'(k)$		-2	-2	0	0	-2	0	2	0
$e(k)$		-1	-1	0	0	-1	0	1	0
$f(k)$		-3	-1	2	2	-1	-2	1	0
$g(k)$		3	1	2	2	1	2	1	0

Figure 2.11 shows a waveform representation of the output signal for each block of the AACC transmitter [56]. AACC is a recent discovered modulation based on partial-response signaling which can become a replace to 4-PAM and suited for short-haul in direct-detection based optical system.

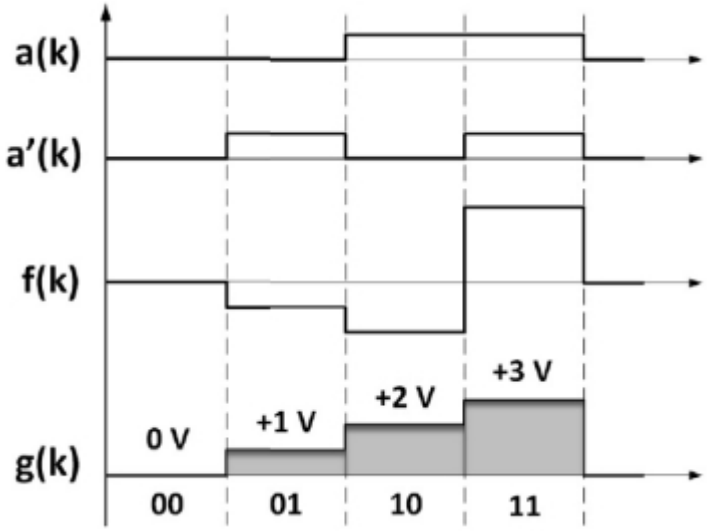

Figure 2.11. Generation of AACC signaling in terms of waveform.[57]

The transmission bandwidth of 4-PAM is a factor of $1/\log_2 M$ less than that of conventional binary modulation formats. For M-ary PAM signal, M refers to the number of levels. As shown in Figure 2.12, the null-to-null bandwidth of AACC measures a spectral width of 2.5 GHz, which is in equivalence to that of 4-PAM. Thus,

the AACC and 4-PAM lead to a spectral efficiency of 4 b/s/Hz. The spectral width of AACC in relation to number of generated levels (L) can be defined as in Eq.(2.20)

$$Spectralwidth = 2 \times \frac{aggregatebitrate}{L-2} \qquad \text{Eq.(2.20)}$$

The bandwidth of the NRZ, however, has a spectral width of 5 GHz, corresponding to a spectral efficiency of 2 b/s/Hz. This is because the AACC is generated based on the partial-response signaling, which makes use of a bit correlation methodology to narrow its spectral width. The spectral width of AACC is half that of NRZ [56].

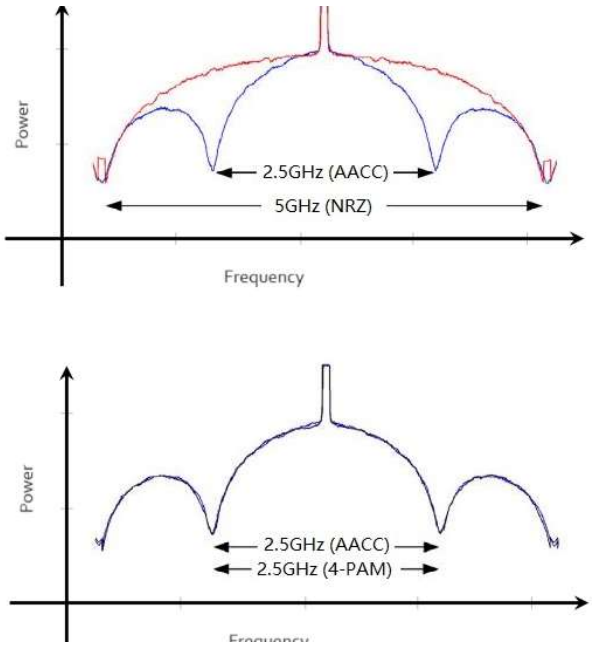

Figure 2.12. Spectral width of AACC in comparison to NRZ and 4-PAM.[56]

2. 4. 3. 6. Orthogonal Frequency Division Multiplexing

OFDM is a spectrally efficient modulation format. In OFDM format, the entire transmission bandwidth is divided into a set of sub-channels, each of which experiences flat fading, when the division is sufficiently dense. OFDM converts a high-rate serial data stream into multiple parallel low-speed data streams, enabling the system to better mitigate ISI caused by channel fading and distortion due to the lower data rate of each channel.

Unlike other frequency division multiplexing (FDM) technologies, OFDM allows overlapping between adjacent subcarrier bands instead of using protection bands.Because OFDM subcarriers are orthogonal to each other, this overlapdoes not

cause interference, thereby avoiding Inter-Carrier Interference (ICI) and enhancing the system's spectrum efficiency.

Another significant advantage of the OFDM format is its ease of implementation. Modulation can be performed using Inverse Fast Fourier transformation (IFFT), and demodulation can be achieved using Fast Fourier transformation (FFT). This simplicity in implementation further solidifies OFDM as a preferred choice for high data rate transmission systems.

2. 4. 3. 7. Colour Shift Keying

Colour Shift Keying (CSK) is an innovative modulation method designed for VLC systems utilizing red, green and blue light sources. At the transmitter, input data is transformed into x, y coordinates based on colour coordinate mapping rules. Figure 2.13illustrates the colour space proposed by the International Commission on Illumination in 1931, along with the colour mapping constellation of 4-CSK.

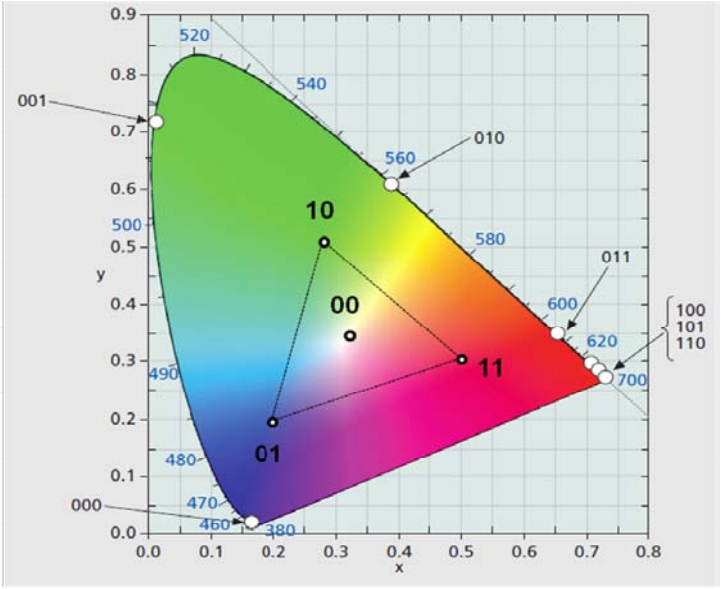

Figure 2.13. ICI colour space.

2. 5. OWC Channel

OWC can generally be divided into outdoor communication and indoor communication, depending on the difference of application scenario. They have different communication channels, which can affect the communication performance of OWC systems.

2. 5. 1. Transmission Windows

When the OWC signal travels through the outdoors atmosphere, the atmosphere exhibits extremely strong absorption for certain wavelengths, making it almost impossible for light waves to pass through. The atmosphere's selective absorption divides electromagnetic bands into zones. These zones with high transmission rates are known as transmission windows. In these windows, atmospheric molecules weakly absorb radiation. It is shown in Figure 2.14. Common OWC wavelengths, typically 850 nm and 1550 nm, fall within these windows. Although the 1550 nm wavelength can cause damage at high power levels, it is preferred under safe conditions for the human eye.

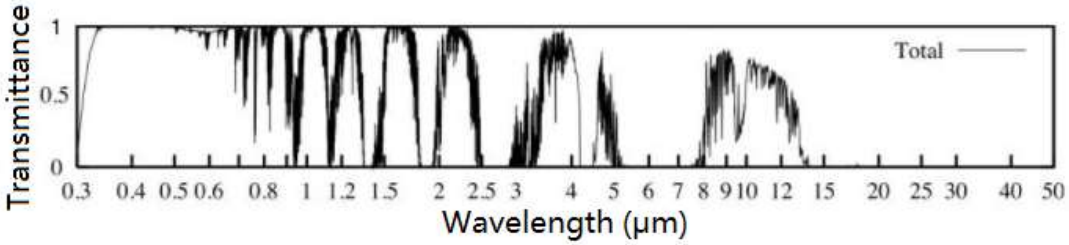

Figure 2.14. Transmission window of OWC.

2. 5. 2. Atmospheric and Weather Effect

When the OWC signal travels through the outdoor channel, the transmission performance of OWC system is seriously affected by the dynamic atmospheric environment and weather conditions. The availability to minimize these effects on signal transmission is the key to the popularity of outdoor OWC technologies. Therefore, it is necessary to examine the performance of outdoor transmission channel and explore the channel models, in order to improve the reliability of optical signal transmission in the atmosphere.

2. 5. 2. 1. Atmospheric losses

Light radiation propagating through the air is influenced by atmospheric absorption and scattering by atmospheric components [58]. When photons interact with atmospheric particles along the transport path, they may beextinguished, converting their energy into heat. Additionally, collisions between photons and particles in the transmission medium can cause the optical beam to deviate from its original path. Both absorption and scattering result in atmospheric losses, commonly referred to as the attenuation effect. These atmospheric losses impact the power transmission curve, as illustrated in Figure 2.15.

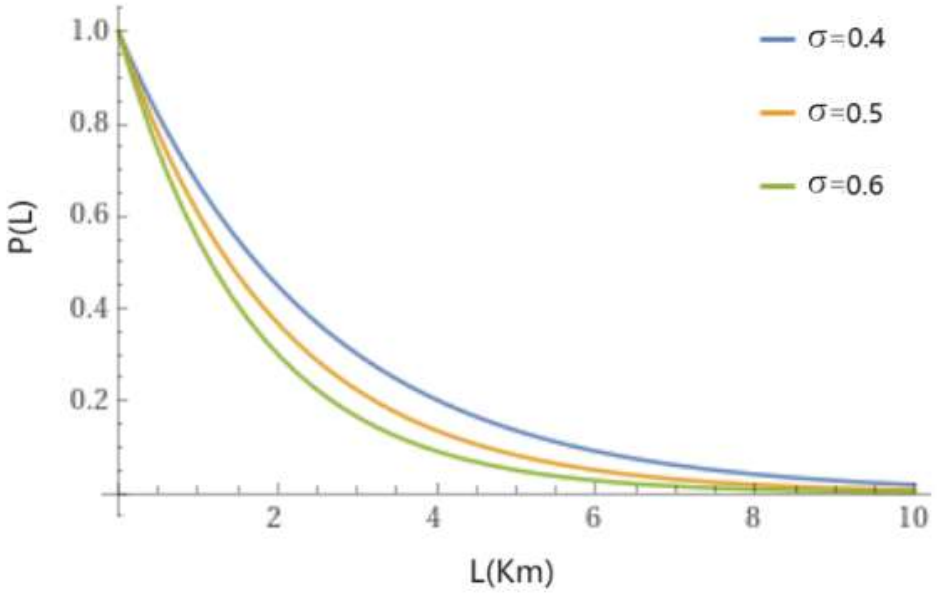

Figure 2.15. Atmospheric attenuation.

It is clear from the above figure that the transmitted optical power decays exponentially with increasing distance when atmospheric attenuation coefficient is constant. As a result, the power of light transmitted in the atmosphere is given in Eq.(2.21)

$$P(L) = P_0 e^{-\sigma L} \qquad \text{Eq.(2.21)}$$

Where P(L) refers to the received optical power after transmission distance L, P_0 denotes the transmitted optical power, σ means atmospheric attenuation coefficient, which is influenced by air composition.

2.5.2.1.1. Absorption

When the optical beam is transmitted in the atmospheric channel, the photons interact with the atmospheric particles in the transmission path, causing strong collisions between other particles in the air. The powerful energy of the particles increases the object's internal energy. It intensifies the heat between objects. Eventually, the light radiation energy decays with particle movement. This demonstrates the absorption effect of the atmosphere.

Atmospheric particles include molecular absorbers and aerosol [59]. Molecular absorption is caused by gases in the air, such as ozone, water vapor and carbon dioxide. Aerosols refer to suspended particles in the transmission medium. These particles can be in liquid and solid forms, with liquids manifesting as fog or mist, and solids appearing as dust or volcanic particles.

2.5.2.1.2. Scattering

The presence of large amounts of dust, smoke and other particles in the atmosphere causes scattering of the optical signal as it travels through the air. The primary scattering processes in the atmosphere are essentially elastic, meaning the optical signal can deviate from its original transmission path without being absorbed and while maintaining the same wavelength [60]. In practical situations, the complex atmospheric environment contains numerous scattering particles of varying sizes and types, which are the main contributors to atmospheric scattering.

Atmospheric scattering can be classified into different categories based on the relationship between the radius of the atmospheric particles and the wavelength of the optical beams. Rayleigh scattering occurs when the radius of the atmospheric particles is much smaller than the wavelength of the optical beams. Mie scattering refers to the scattering process when the size of the scattered particles is comparable to the wavelength of the optical beams. Non-selective scattering occurs when the radius of the atmospheric particles is larger than the wavelength of the optical beams [61].

2. 5. 2. 2. Weather Effect

Weather phenomena, such as haze, fog, clouds, rain and snow can significantly hinder the transmission of light radiation. Atmospheric particles in the transmission channel fluctuate over time, making the optical signal susceptible to scattering and absorption by these randomly distributed particles, including raindrops, fog droplets, haze and snow. In severe weather conditions, the communication quality of OWC systems can deteriorate rapidly, potentially leading to communication interruptions. The composition of atmospheric particles varies across different weather conditions, resulting in distinct effects on optical beam [62].

In rainy weather, the optical beam is particularly sensitive to raindrops, which have a larger radius than the wavelength of the optical beam. Consequently, non-selective scattering is the predominant effect in such conditions. The attenuation coefficient of the optical beam is typically related to the rainfall rate rather than the wavelength. Figure 2.16illustrates the correlation between the attenuation coefficient and the rainfall rate, showing that as the rainfall rate increases, the attenuation coefficient also increases.

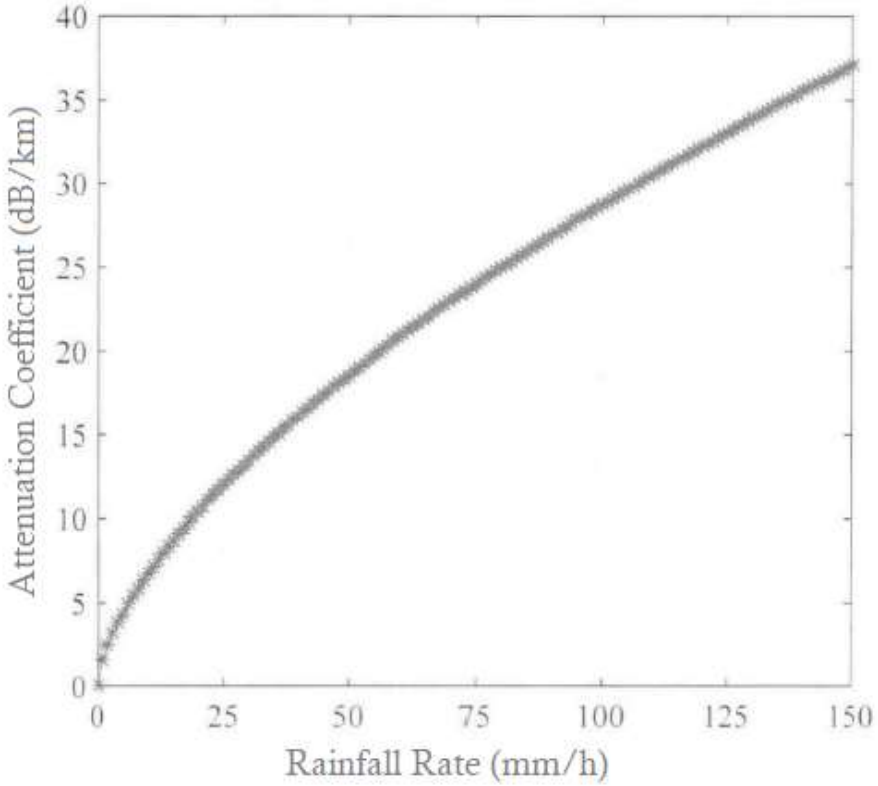

Figure 2.16. Atmospheric attenuation coefficient in rainy weather.[62]

Small water droplets floating in the air can coalesce to form fog droplet. Similar to raindrops, fog droplets significantly impact the transmission performance in the atmospheric channel by causing absorption or scattering of the optical beam. The radius of fog droplets is comparable to the wavelength of an optical beam, resulting in scattering that can be approximated as Mie scattering. The Kruse and Kim models are the most widely used empirical models for determining fog attenuation coefficients. The attenuation coefficient in foggy weather depends on the visibility of the atmosphere and the wavelength of the optical beam. Figure 2.17illustrates the increasing trend in the attenuation coefficient as visibility decreases.

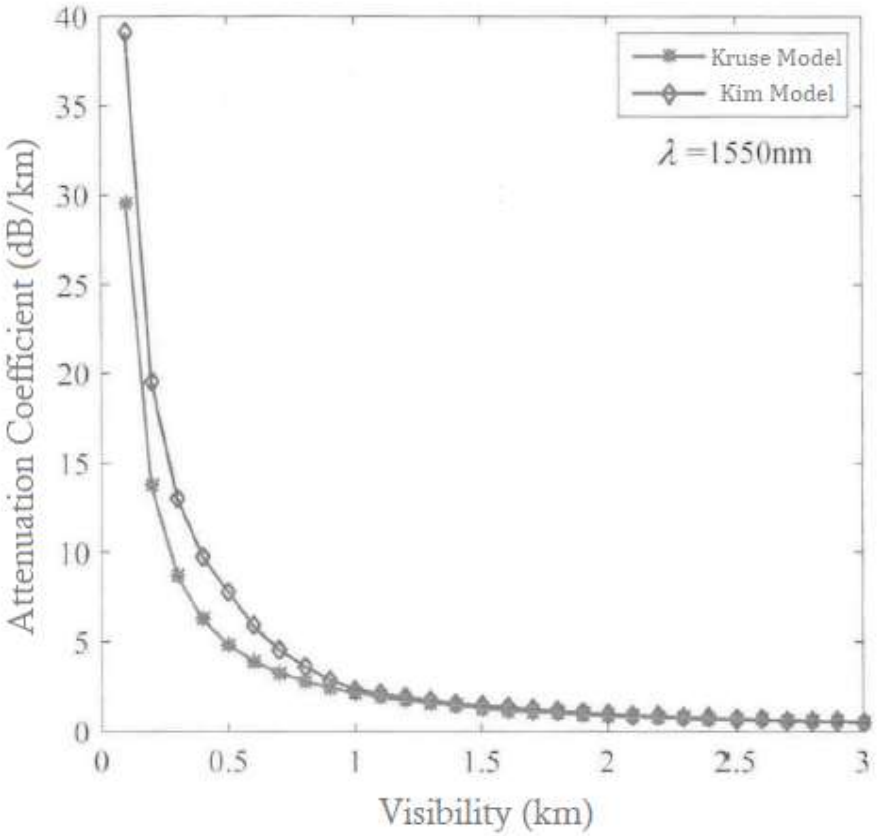

Figure 2.17. Atmospheric attenuation coefficient in foggy weather.[62]

The properties of snow are more complex than those of rain and fog. Generally, for the same water content, the attenuation coefficient in snow falls between that of rain and fog. The particles size in snow is much larger than the wavelength of an optical beam. However, experimental studies have shown that the attenuation coefficient in snowalso depends on the wavelength. Longer wavelengths experience stronger attenuation due to diffraction effects. Additionally, the attenuation coefficient in snow is related to the snowfall rate. Furthermore, the attenuating coefficient of snow on an optical beam varies between wet snow or dry snow. The attenuation caused by dry snow is greater than that caused by wet snow. Figure 2.18illustrates the relationship between the attenuation coefficient and snowfall rate for both wet and dry snow conditions. The attenuation coefficient increases with increasing snowfall rate, and the attenuation effect of dry snow is significantly stronger than that of wet snow.

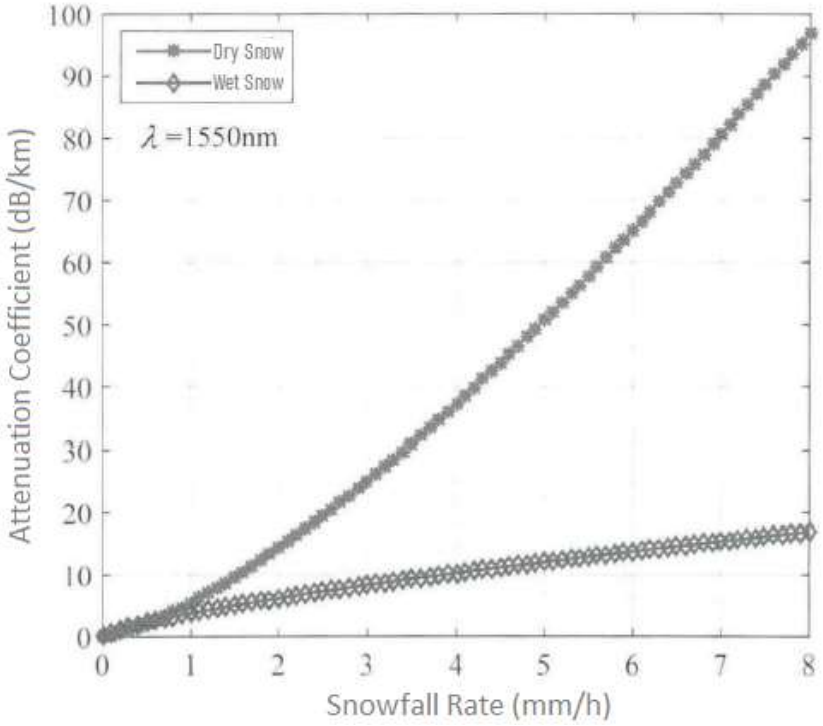

Figure 2.18. Atmospheric attenuation coefficient in snowy weather.[62]

According to the research result of Nazmi A. Mohammed et al., the average power loss and visibility under different weather conditions are shown in Table 2.11[63]. The power loss ranges from 0.155 dB/km to 84.904 dB/km and the visibility ranges from 23 km to 0.2 km correspondingly.

Table 2. 11. Attenuation in different weather conditions. [63]

Weather	Power Loss (dB/km)	Visibility (km)
Clear	0.155	23
	0.441	10
Haze	1.537	4
	4.285	2
	10.115	1
Fog	15.55	0.8
	33.961	0.5
	84.904	0.2

2. 5. 2. 3. Atmospheric Turbulence

Atmospheric turbulence refers to the irregular patterns of air movement in the atmosphere, where physical properties such as pressure, velocity and temperature fluctuate randomly at every point. These fluctuations cause random variations in the

refractive index, which in turn affect the intensity, phase and direction of propagation of light waves passing through the turbulence [64], [65].

Atmospheric turbulence factors can lead to some effects, such as beam spreading, beam wandering and scintillation of optical beam [66]. Generally, these effects may occur simultaneously. However, one of these effects may become dominant according to the relative relationship between the diameter of the optical beam and the scale of the turbulence. When the turbulence scale is much larger than the beam diameter, the main effect of the turbulence is beam spreading. And the optical beam drifts in the receiving plane. When the turbulence scale is close to the beam diameter, the turbulence will cause beam wandering. It is a random deflection of the optical beam, resulting in jitter of the image. When turbulence scale is much smaller than the beam diameter, there are many eddies within the optical beam, causing diffraction and resulting in scintillation. The schematic diagrams of this variation is given in Figure 2.19 and Figure 2.20[67].

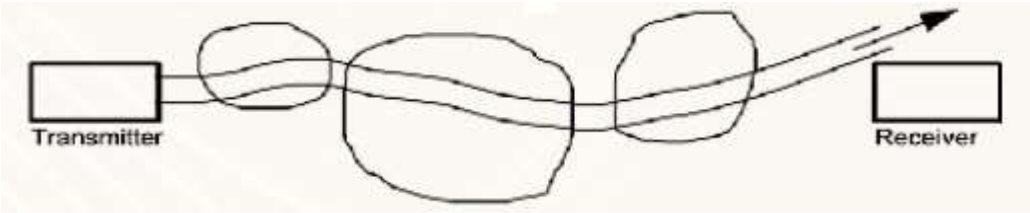

Figure 2.19. Beam spreading.[67]

Figure 2.20. Scintillation.[67]

Refractive index variations in the atmosphere are mainly caused by temperature variations [68]. And turbulent motion derives its energy mainly from solar heating of the ground, thus turbulence shows significant daily variations and varies with geography, weather and season. According to the intensity, turbulence can be divided into strong turbulence ($C_n^2 = 10^{-13}$ $m^{-2/3}$), moderate turbulence ($C_n^2 = 10^{-15}$ $m^{-2/3}$) and weak turbulence ($C_n^2 = 10^{-17}$ $m^{-2/3}$).

2.5.2.4. Ambient Light

Background noise in OWC systems is caused by various ambient light sources, including fluorescent lights, sunlight, and moonlight. These background noises can be modeled as white, Gaussian and signal independent noise, which are programmed into the detector. Poisson random variables may be used for modeling the background noise area.

To mitigate the impact of background radiation, the wavelength of the optical beam should be longer than 1500 nm. Additionally, techniques such as differential mode data detection and double wavelength transmission can be employed to further reduce the effects of background noise. These methods enhance the SNR, thereby improving the overall performance and reliability of the communication system [69].

2.5.2.5. Channel Model

Atmospheric turbulence is hard to describe mathematically, mainly due to the presence of a non-linear mixing of the observed physical quantities. To understand the statistical distribution of received irradiance through atmospheric turbulence, some mathematical models based on measured empirical atmospheric data have been developed. These models are necessary to predict the statistical properties of light intensity and provide an accurate probability density distribution function (PDF). However, no single PDF can accommodate all turbulent states. The most studied channel models for irradiance fluctuations include the log-normal model for weak turbulence, the Gamma-Gamma model for moderate to strong turbulence and the negative-exponential model for saturated turbulence.

2.5.2.5.1. Log-Normal Channel

In general, the intensity of the light field fluctuates randomly as the optical beam appears in the air. The coherence length of such fluctuations is between a few milliseconds and tens of milliseconds. Thus we can assume the progress as a slow decay state. In a weak turbulent environment, the random variation of PDF satisfies a log-normal distribution and can be used to describe accurately the model of light field intensity. Due to the weak irradiance fluctuations, the application of the log-normal

channel model is limited in a short-distance communication system [70]. However, for a small refractive index, it can still be valid for a longer transmission distance. The PDF of the received irradiance under log-normal channel is given in Eq.(2.22) [71]

$$P(I) = \frac{1}{\sqrt{2\pi\sigma_I^2}} \frac{1}{I} exp\left\{ - \frac{\left(\ln(I/I_0) + \sigma_I^2/2\right)^2}{2\sigma_I^2} \right\}, \quad I > 0 \qquad \text{Eq.(2.22)}$$

Where $P(I)$ is the probability density function, σ_I^2 refers to scintillation index, I is the irradiance and I_0 denotes the irradiance in the absence of turbulence.

2. 5. 2. 5. 2. Gamma-Gamma Channel

The Gamma-Gamma distribution model assumes that small-scale and large-scale eddies are generated when the optical beam propagates through the turbulent environment. The two different fluctuations have a corresponding effect on the beam and are independent of each other. The total received irradiance of the system can then be expressed in Eq.(2.23)

$$I = I_{\mathrm{x}} I_{\mathrm{y}} \qquad \text{Eq.(2.23)}$$

Where I means the irradiance and I_x, I_y denote the influence factors of small-scale and large-scale eddies.

The channel model assumes that both small-scale and large-scale irradiance fluctuations follow a gamma distribution. The parameters used in the model are related to atmospheric conditions and are consistent with scintillation theory. The PDFs are given in Eq.(2.24) and Eq.(2.25) [72]

$$P(I_x) = \frac{\alpha(\alpha I_x)^{\alpha-1}}{\Gamma(\alpha)} \mathrm{e}^{-\alpha I_x}, \quad I > 0, \alpha > 0 \qquad \text{Eq.(2.24)}$$

$$\mathrm{P}\left(I_{\mathrm{y}}\right) = \frac{\beta(\beta I_y)^{\beta-1}}{\Gamma(\beta)} \mathrm{e}^{-\beta I_y}, \quad I > 0, \beta > 0 \qquad \text{Eq.(2.25)}$$

According to Eq.(2.23), $I_{\mathrm{y}} = I/I_{\mathrm{x}}$

$$\mathrm{P}\left(I/I_{\mathrm{x}}\right) = \frac{\beta(\beta I/I_{\mathrm{x}})^{\beta-1}}{\Gamma(\beta)} \mathrm{e}^{-\beta I/I_{\mathrm{x}}}, \quad I > 0 \qquad \text{Eq.(2.26)}$$

$$\mathrm{P}(I) = \int_0^{\infty} \mathrm{P}\left(I/I_{\mathrm{x}}\right) P(I_x)\, dI_x \qquad \text{Eq.(2.27)}$$

Statistical averaging of I_{x} gives a PDF for the received irradiance under Gamma-Gamma channel in Eq.(2.28) [72]

$$\mathrm{P}(I) = \frac{2(\alpha\beta)^{(\alpha+\beta)/2}}{\Gamma(\alpha)\Gamma(\beta)} I^{\left(\frac{\alpha+\beta}{2}\right)-1} K_{\alpha-\beta}\left(2\sqrt{\alpha\beta I}\right), \;\; I > 0 \qquad \text{Eq.(2.28)}$$

Where $P(I)$ is the probability density function, $\Gamma(\cdot)$ is gamma function and $\mathrm{K}_{\alpha}(\cdot)$ represents the modified Bessel function of order α. The parameters α and β are given in Eq.(2.29) and Eq.(2.30)

$$\alpha = \left[exp\left(\frac{0.49\sigma_I^2}{\left(1+1.11\sigma_I^{\frac{12}{5}}\right)^{\frac{7}{6}}} \right) - 1 \right]^{-1} \qquad \text{Eq.(2.29)}$$

$$\beta = \left[exp\left(\frac{0.51\sigma_I^2}{\left(1+0.69\ I^{\frac{12}{5}}\right)^{\frac{5}{6}}} \right) - 1 \right]^{-1} \qquad \text{Eq.(2.30)}$$

Where α is the effective number of the small-scale eddies, while β represents the effective number of the large-scale eddies in the scattering process.

The Gamma-Gamma distribution model has a wider scope of application than the log-normal distribution model. It uses two independent parameters to describe the physical properties of turbulence, which can better reflect the fluctuations of the optical signal in moderate and even strong turbulent environments.

2. 5. 2. 5. 3. Negative-Exponential Channel

The negative-exponential model is suitable for strong turbulence, especially when the propagation distance is very large. In this case, the fluctuations in the amplitude of the light waves passing through the atmospheric turbulent channel follow the Rayleigh distribution as shown in Eq.(2.31) [73]

$$\mathrm{P}(I) = \frac{1}{I_0} exp(-I/I_0), \;\; I > 0 \qquad \text{Eq.(2.31)}$$

Where $P(I)$ is the probability density function, I is the irradiance and I_0refers to the mean irradiance.

2. 5. 3. Line-of-sight and Non-line-of-sight Channel

As part of OWC, VLC and IR communication share similar channel characteristics and research methods. So the research method of indoor IR communication channel is an important reference for indoor optical communication channel. The most famous IR channel is the indoor wireless communication system channel model studied by Professor John Barry [74], [75]. They classify the connection of indoor IR communication system channels into six types, directed LOS link, non-directed LOS link, hybrid LOS link, directed NLOS link, non-directed NLOS link and hybrid NLOS link. The channel models are shown in Figure 2.21.

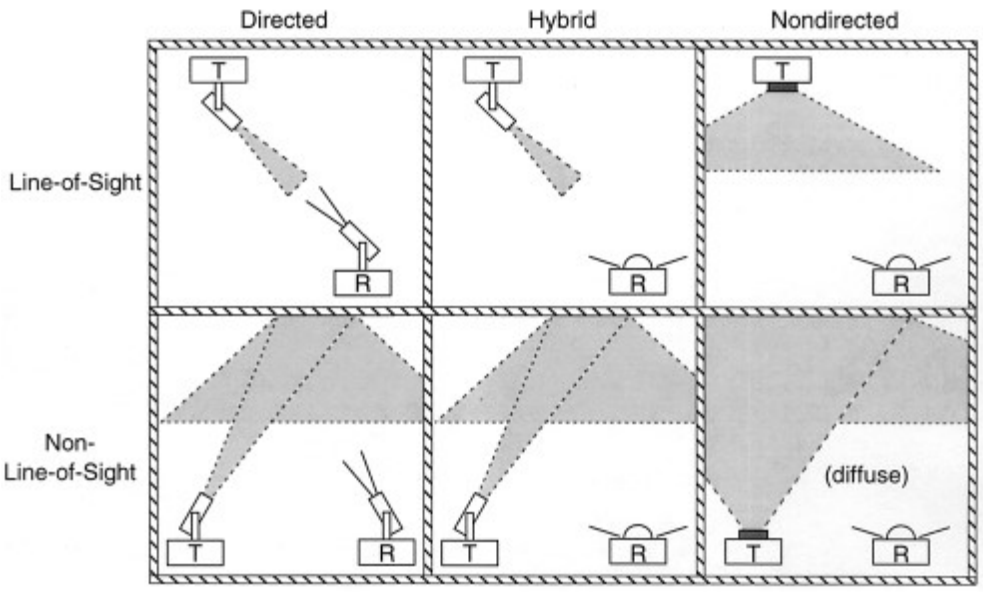

Figure 2.21. IR channel model.[75]

An analysis of these six types of link models shows that the difference lies mainly in whether the transmitter or receiver is directed, and whether the link between transmitter and receiver is a LOS link or a NLOS link. With reference to the above IR channel link models, the above six link models can be grouped into two main types in indoor VLC systems, as the light source emission angle and detector reception angle are both relatively large. They are namely LOS channel and NLOS channel, as shown in Figure 2.22.

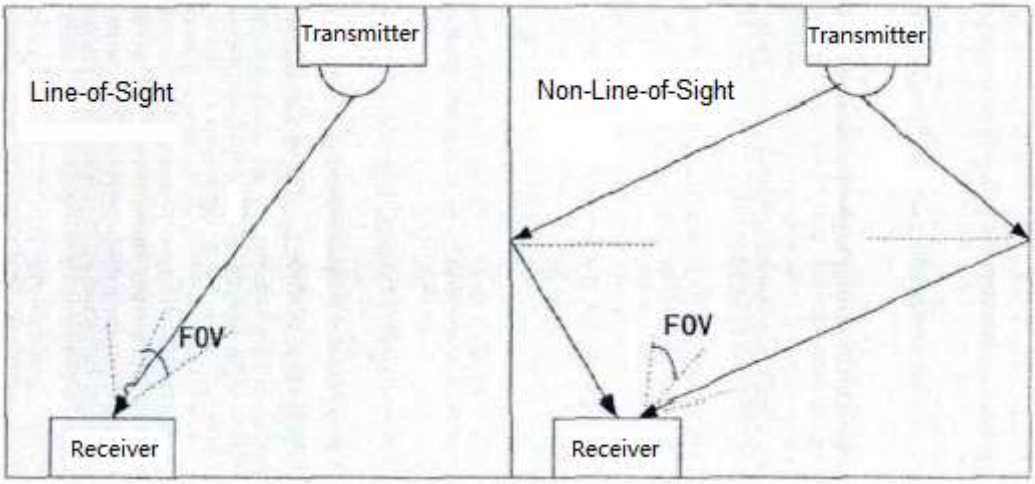

Figure 2.22. VL channel model. [74]

In the LOS channel, the receiver is pointed directly at the light source. Therefore, the attenuation is much less than in the NLOS channel. In addition, the multi-path effect can be ignored due to the directed propagation path. Besides, the high power efficiency makes it convenient to link data at high speed. And it is less affected by background light. However, the LOS channel also has some drawbacks. The LOS channel requires high pointing for the receiver and transmitter, which must always be aligned in the link. Any obstacle in the transmission path could impact the transmission performance. Hence, LOS channel is not very robust and is suitable for point-to-point communication without obstructions. In NLOS channel, light from transmitter is reflected once or more time to reach the receiver. The propagation distance in NLOS channels is usually much longer than that of LOS channel, resulting in much larger attenuation. Moreover, with severe multi-path dispersion, the propagation path is complex and diverse, and the data rate is also limited. However, the NLOS channel has the advantage of a relatively large reception angle. That reduces the requirements of pointing. Besides, the light power can be distributed more evenly in the room, thus greatly reducing the effect of shadowing on the system. The NLOS channel is not easily obscured, so it is very robust. Table 2.12 gives a comparison of some of the communication performance of the two links. In an indoor VLC system, the two channels are often adopted together.

Table 2.12. The difference between LOS link and NLOS link. [74], [75]

Feature	LOS Link	NLOS Link
Data Rate	high	medium
Ponting Requirements	high	low
Resistance to Obstructions	low	high
System Mobility	low	high
System Complexity	low	high
Impact of Ambient Light	low	high
Impact of Multi-path Effects	no	yes
Path Loss	low	high

As a general practice, the LED is assumed to follow the Lambertian radiating pattern, which obeys Lambert's cosine law. The Lambertian radiant intensity of LED array is given in Eq.(2.32)

$$R_0(\phi) = \frac{m+1}{2\pi}\cos^m \phi \qquad \text{Eq.(2.32)}$$

where Lambertian order is given in Eq.(2.33)

$$m = -\frac{\text{lo}}{\log\cos\phi_{1/2}} \qquad \text{Eq.(2.33)}$$

where $\phi_{1/2}$ is transmitter semi-angle at half-power, and its unit is rad

The LOS channel transfer function is given in Eq.(2.34)

$$H_{LOS} = \begin{cases} \frac{(m+1)A_{det}\cos^m\phi T_s(\psi)g(\psi)\cos\psi}{2\pi d^2}, & 0 \le \psi \le \psi_c \\ 0, & \psi > \psi_c \end{cases} \qquad \text{Eq.(2.34)}$$

where $\psi_c$is receiver FOV and its unit is rad, A_{det} is detector area and its unit is cm^2, d isthe distance between transmitter and receiver and its unit is m, T_s is filter transmission gain and concentrator gain $g(\psi)$ is given in Eq.(2.35)

$$g(\psi) = \begin{cases} \frac{n^2}{\sin\psi_c}, & 0 \le \psi \le \psi_c \\ 0, & \psi > \psi_c \end{cases} \qquad \text{Eq.(2.35)}$$

The NLOS channel transfer function is given in Eq.(2.36)

$$H_{NLOS} = \begin{cases} \frac{(m+1)A_{det}\rho\, A_{wall}\cos^m \phi \cos\alpha \cos\beta T_s(\psi) g(\psi) \cos\psi}{2\pi {d_1}^2 {d_2}^2}, & 0 \le \psi \le \psi_c \\ 0, & \psi > \psi_c \end{cases} \quad \text{Eq.(2.36)}$$

where d_1 isthe distance between transmitter and wall and its unit is m, and d_2 isthe distance between wall and receiver and its unit is m

And the total received power in both LOS channel and NLOS channel is given in Eq.(2.37)

$$P_r = \sum\{P_t H_{LOS} + \int P_t \, dH_{NLOS}\} \quad \text{Eq.(2.37)}$$

2. 5. 4. Indoor Illumination

Illumination expresses the brightness of an illuminated surface. When designing an energy efficient indoor VLC system, it is important that the illumination of the room should also be satisfied. According to the International Organization for Standardization (ISO) regarding light and lighting, the illumination requirements for an indoor environment should be within the range of 300 lx to 1500 lx. Besides, for the sake of the human eye, the mean square of the illumination has to be as low as possible, which means that the illumination in the room needs to be uniformly distributed. The luminous intensity at angle θ is given in Eq.(2.38)

$$I(\phi) = I(0)\cos^m \phi \quad \text{Eq.(2.38)}$$

where $I(0)$ is the luminous intensity at center and its unit is cd, m is Lambertian order, and ϕ is the radiation angle with respect to transmitter and its unit is rad

The illumination is given in Eq.(2.39)

$$E = \frac{I(0)\cos^m \phi \cos\psi}{{D_d}^2} \quad \text{Eq.(2.39)}$$

where ψ is the irradiance angle with respect to receiver and its unit is rad, and D_d is the distance between transmitter and receiver and its unit is m

2. 5. 5. Signal-to-Noise Ratio

SNR is defined as the ratio of the power of a signal to the background noise and determines the quality of the transmission performance. By considering the aforesaid optical channel, the SNR is given in Eq.(2.40)

$$SNR = \frac{(\gamma P_r)^2}{\sigma^2{}_{total}} \quad \text{Eq.(2.40)}$$

where γ is photodiode responsivity and total noise variance $\sigma^2{}_{total}$ is given in Eq.(2.41)

$$\sigma^2{}_{total} = \sigma^2{}_{shot} + \sigma^2{}_{therm} \quad \text{Eq.(2.41)}$$

where $\sigma^2{}_{shot}$ is shot noise and $\sigma^2{}_{the}$ is thermal noise.

The $\sigma^2{}_{shot}$ is given in Eq.(2.42)

$$\sigma^2{}_{shot} = 2qiB_e \quad \text{Eq.(2.42)}$$

where q is electronic charge, i is detector current and B_e is equivalent to noise bandwidth.

The $\sigma^2{}_{therm}$ is given in Eq.(2.43)

$$\sigma^2{}_{therm} = \frac{4K_BTB_e}{R_L} \quad \text{Eq.(2.43)}$$

where K_B is Boltzmann constant, T is equivalent temperature and R_L is load resistor.

2. 5. 6. Delay Spread

Delay spread is the diffusion effect of signal waveform caused by multiple paths in the time domain. And it can be used to characterize the multi-path dispersion of communication channel. To put it simply, the signal of wireless communication system propagates in different paths. Because the path length is different, the time of arrival for each path is different. Figure 2.23 shows the maximum delay time spread and RMS delay spread.

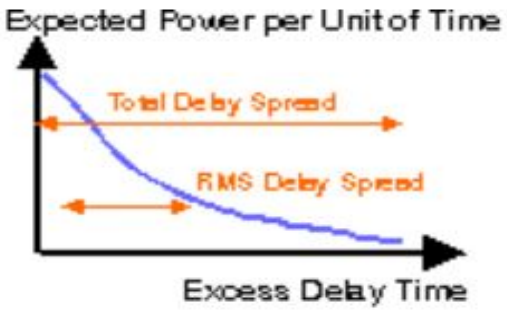

Figure 2.23. Total delay spread and RMS delay spread.

The maximum delay time spread is the total time interval between the earliest arrival signal and the latest arrival signal at the receiver. The RMS delay spread is a standard deviation value of the delay among the multi-path reflection in wireless communication channel. In an indoor VLC system, it is given in Eq.(2.44) to Eq.(2.46)

$$\tau_{RMS} = \sqrt{\bar{\tau}^2 - (\bar{\tau})^2} \qquad \text{Eq.(2.44)}$$

$$\bar{\tau}^2 = \frac{\left(\sum_i^M P_{LOS,i} t_{LOS,i}{}^2 + \sum_j^N P_{NLOS,j} t_{NLOS,j}{}^2\right)}{P_r} \qquad \text{Eq.(2.45)}$$

$$\bar{\tau} = \frac{\left(\sum_i^M P_{LOS,i} t_{LOS,i} + \sum_j^N P_{NLOS,j} t_{NLOS,j}\right)}{P_r} \qquad \text{Eq.(2.46)}$$

where M donates the number of components for LOS channel light and N donates the number of components for NLOS channel light. $P_{LOS,i}$ is the received power of LOS channel at the ith point and $P_{NLOS,j}$ is the received power of NLOS channel at the jth point. $t_{LOS,i}$ is the propagation time of the ith LOS channel light and $t_{NLOS,j}$ is the propagation time of the jth NLOS channel light.

2. 6. Summary

This chapter gives the background of OWC. An overview is given in the first part of this chapter, including literature research, benefits, drawbacks and prospects. Section 2.3 introduces different OWC technologies in detail. The next section is a description of transmit and receive system, including light source, modulator, receiver and filter.

Besides, the modulation formats are introduced in detail. The final section of this chapter describes the OWC channel, including outdoor channel and indoor channel.

3. Research Methodology

3. 1. Introduction

In this chapter, the methodology adopted in this research and the approach engaged to achieve the aim and objectives are described. Simulation softwares, known as OptiSystem and MATLAB, are employed to set up the FSO model and the indoor VLC model. An important aspect of research methodology is to build reliable and accurate simulation models which can be a good representation of the OWC systems under various scenarios. The main purpose of this simulation is to set up the OWC simulation models and to look for the appropriate parameters, so that they can operate at optimum performance when employed on the designed application systems.

3. 2. Simulation Tool

Using simulation software to set up OWC models is not only time-saving and economical, but also can fast predict whether the designed objectives could be achievable. Therefore, the current study applies the simulation software to investigate the transmission performance under different conditions.

3. 2. 1. OptiSystem

OptiSystem is a universal optical communication system simulation software that is used to design, test and optimize optical communication links. The library consisting of active and passive photonic and electrical components is used to set up the FSO model. Besides, this software includes an interface for an integrated module between the OptiSystem and MATLAB programming language. A multi-level signal analyzer tool is set based on this feature. It enables the evaluation of any multi-level modulation formats in accordance with a unique BER model through the MATLAB command [76].

3. 2. 1. 1. **Multi-level signal analyzer tool**

This research utilizes a multi-level signal analyzer tool for analyzing and estimating the BER. However, the built-in BER analyzer of OptiSystem is only able to deal with the conventional binary signals such as RZ and NRZ, but is incapable of estimating the performance of multi-level signals. Therefore, a multi-level signal analyzer tool with built-in MATLAB command of OptiSystem software is utilized to estimate the BER for multi-level modulation formats. The MATLAB for measuring BER is developed by using the Gaussian probability errors approximation method. The developed BER estimation tool simulation can plot the eye diagram and analyze the BER value for 4-PAM and AACC optical communication systems.

The input of this analyzer is the received signal of the FSO model and is attached to the MATLAB command. Figure 3.1 shows the flowchart for designing a multi-level signal analyzer. At first, the simulated test result from OptiSystem is loaded into a workspace in MATLAB. Later the signal is grouped according to the symbol and calculates both the mean and standard deviation. Based on the mean and standard deviation of each symbol, the threshold level is estimated at the same time. According to these, the Q-factor and BER are also calculated. At last, an eye diagram is plotted providing measurement to the model performance [77]. The eye diagram result was based on measured voltage value while BER value needed to refer to several parameters such as mean, standard deviation, threshold level and Q-factor.

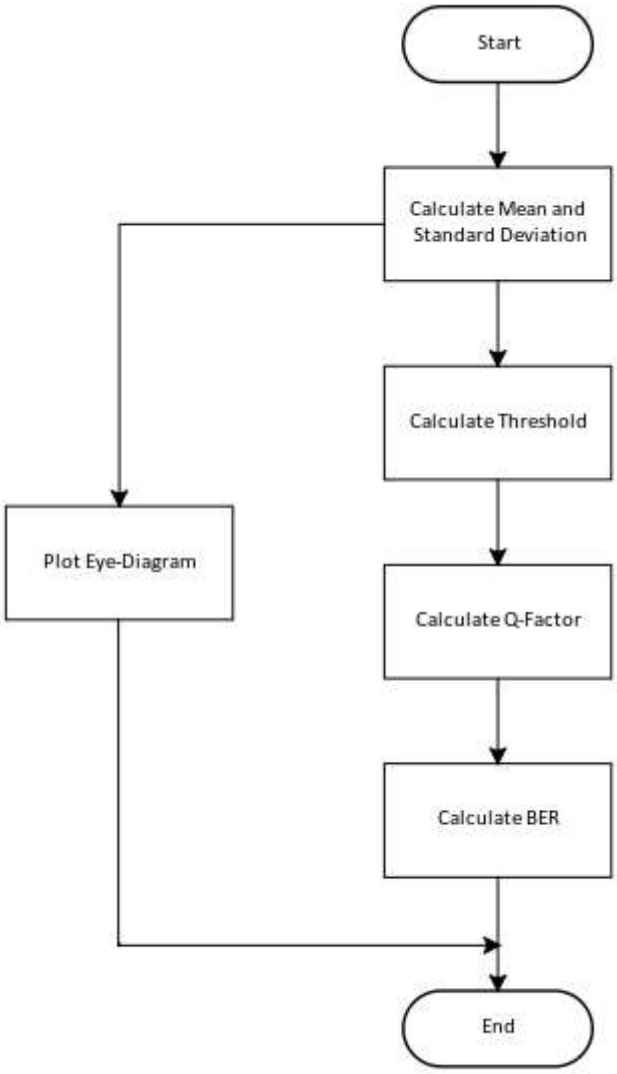

Figure 3.1. Flowchart of multi-level signal analyzer.

3. 2. 2. MATLAB

MATLAB is a computer language designed for technical computing and data visualization. It is built around an interactive programming environment. The MATLAB mathematical function library and graphic processing system are used to set up the indoor VLC model [78].

3. 3. FSO Model

The model of FSO system, which is set up in OptiSystem, is similar to the optical fibre model, but the difference is using air instead of fibre as the channel medium. The simulated FSO model under this study is a point-to-point link that has a transmitter on one end and a receiver on the other. The setup of FSO system is shown in Figure 3.2.

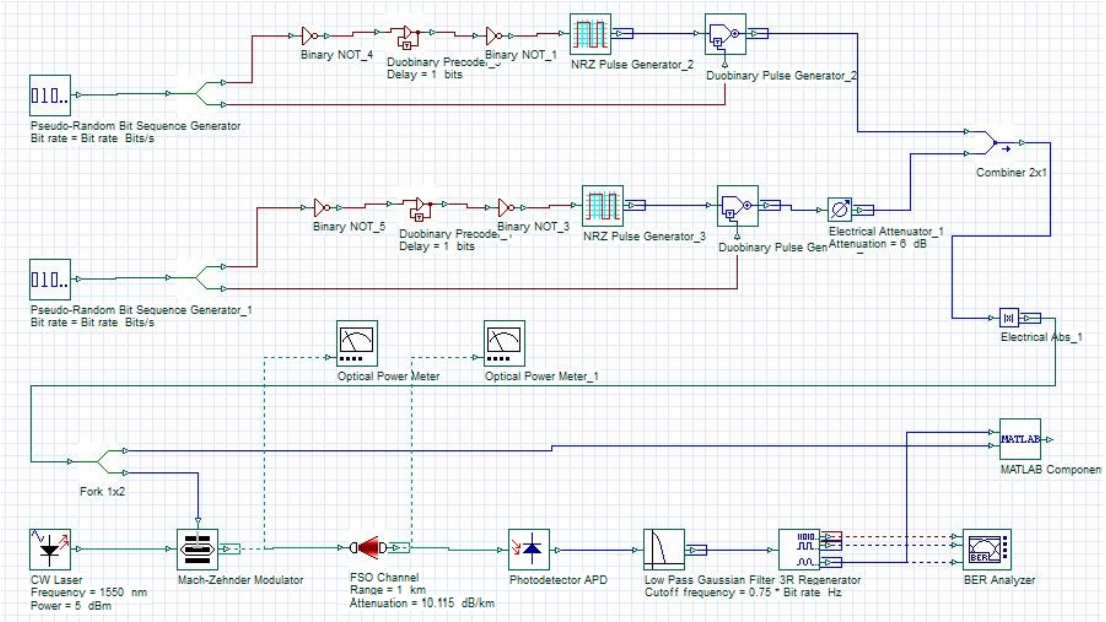

Figure 3.2. Setup of FSO system.

This model transmits information by using AACC modulation which is driven by two Pseudo-Random Bit Sequence Generators at 10 Gbit/s. The information is loaded onto a continuous wave (CW) laser at the wavelength of 1550 nm by a MZM and then transmitted over a FSO channel. The receiver comprises a photodetector that converts the optical signal into an electrical signal. After the high frequency unwanted signal is removed by low pass Gaussian filter, the system performance of the FSO model is evaluated by its BER. A MATLAB command is used to calculate the BER of multi-level signals. The transmitter and receiver can be implemented by using some default components. In this model, the transmitter part includes CW laser and MZM as well as the receiver part includes photodetector APD and low pass Gaussian filter.

3. 3. 1. Simulation Parameter Setting

The parameters of some components in this FSO model are shown in Figure 3.3 to Figure 3.7.

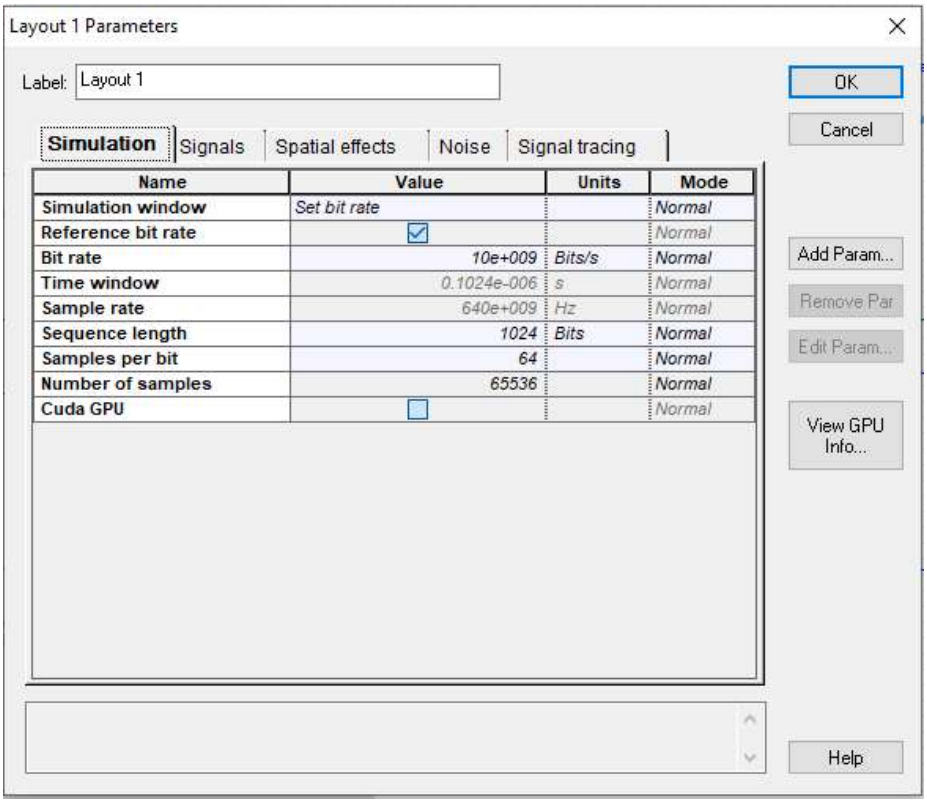

Figure 3.3. Parameters in Layout.

In the Layout Parameters, the simulation window is set by bit rate. The bit rate is set as 10×10^9 bit/s and the sequence length is set as 1024 bits. Every bit contains 64 samples. As a result, the total number of samples is the multiplication of sequence length and samples per bit, namely 65536.

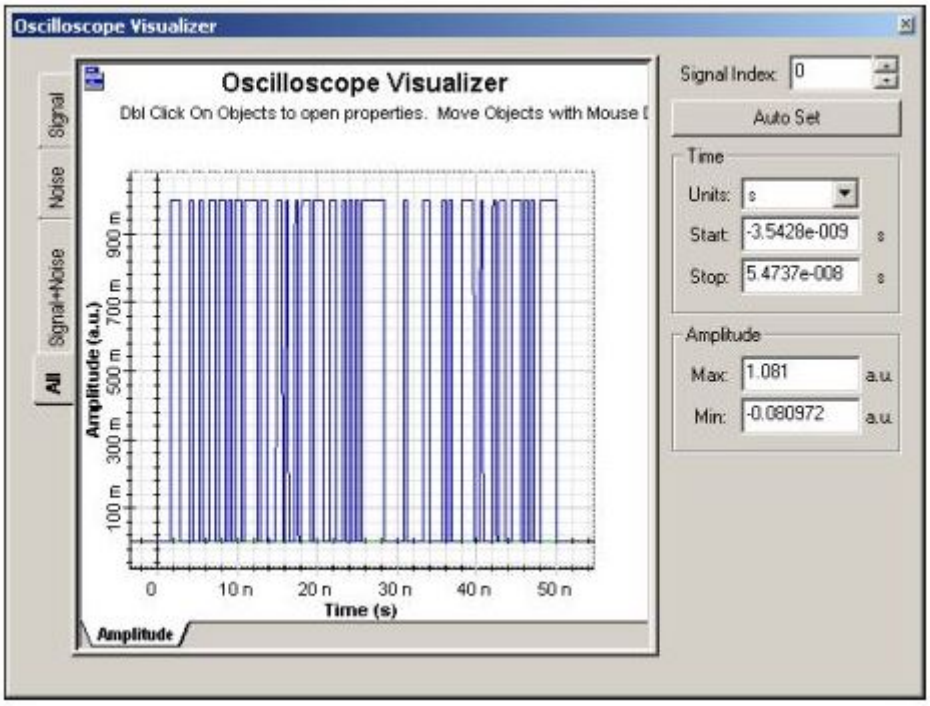

Figure 3.4. Result from Oscilloscope Visualizer.

Figure 3.4 shows the test result from an Oscilloscope Visualizer. It is clear to see that the bit rate refers to how many bits are transmitted in one second. The sequence length refers to how many bits are tested in this Oscilloscope Visualizer. And the sample per bit refers to how many times of these samples are tested in every bit.

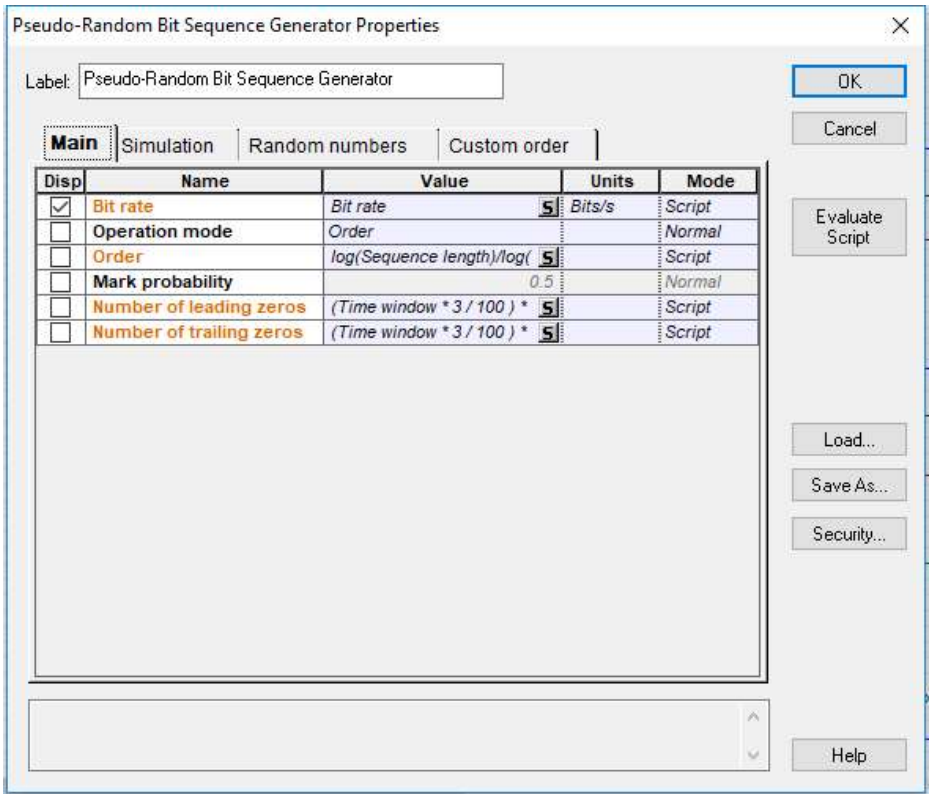

Figure 3.5. Parameters in Pseudo-Random Bit Sequence Generator.

The binary data is generated by the Pseudo-Random Bit Sequence Generator. Parameters Bit rate and Order are used in the setting of internal Pseudo-Random Bit Sequence Generator. The number of bit rate is set in the Layout.

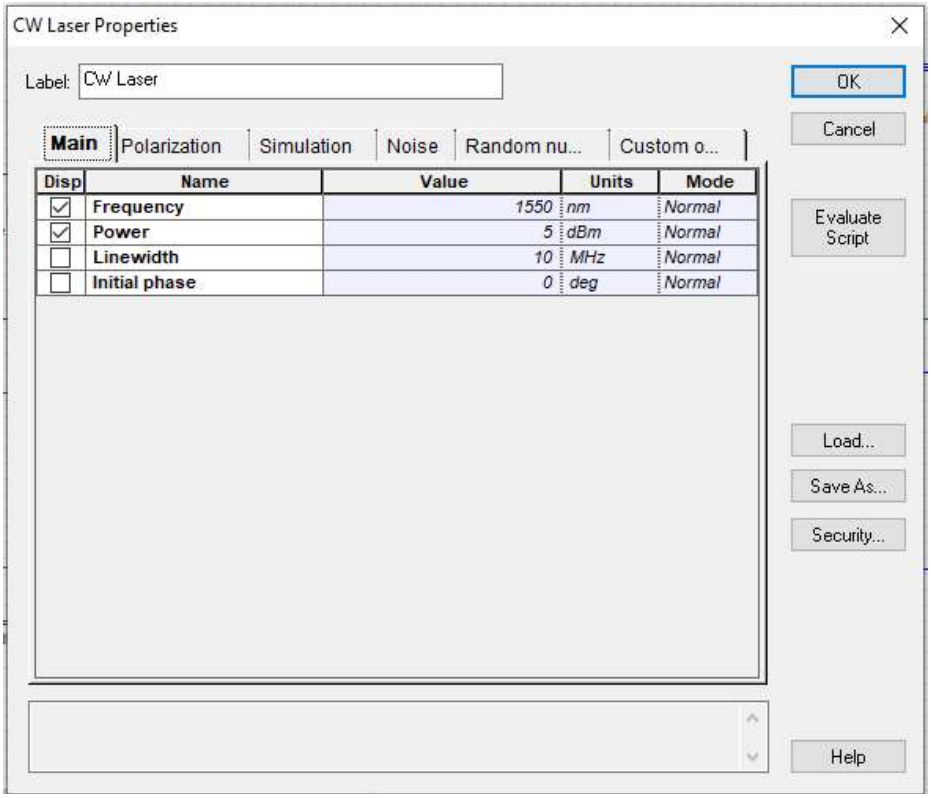

Figure 3.6. Parameters in CW Laser.

Then the data goes through signal processing components and transformed by AACC modulation and transmits to the MZM. A CW laser is used as the light source, of which the frequency is 1550 nm and the power is 5 dBm.

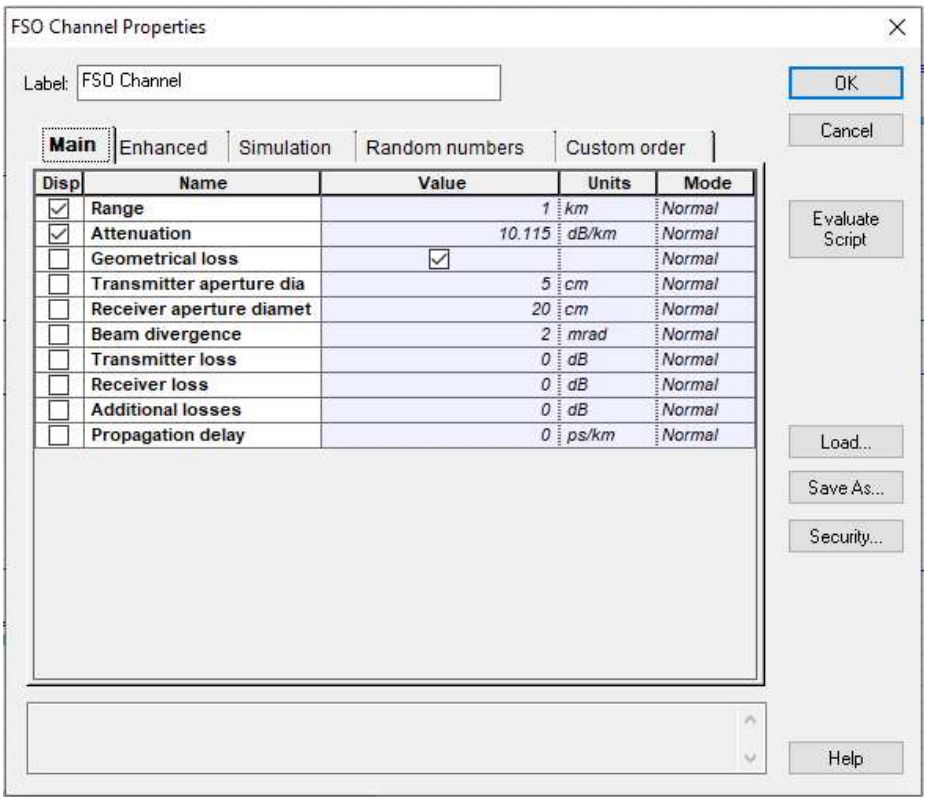

Figure 3.7. Parameters in FSO Channel.

Then the modulated optical signal is launched into the FSO channel. The propagation distance of FSO channel is 1 km. This distance offers a good balance between signal strength and attenuation caused by atmospheric conditions. It also solves the problem of last mile. And it provides a cost-effective deployment of optical equipment and maintains a reasonable communication range. The attenuation is set in heavy haze weather as 10.115 dB/km [63]. Because haze particles scatter light, reducing signal strength and increasing noise. This attenuation affects system performance. Analyse the FSO system adopting this attenuation to mitigate its effects and to ensure reliable communication. Besides, the FSO channel adopts the Gamma-Gamma distribution to model atmospheric fading.

The received optical signal is detected by a photodetector APD with responsivity equal to 0.8 A/W. Followed by is an electrical low-pass filter (LPF) with a cutoff frequency of 0.75*symbol rate, which causes a 3 dB point. The optical carrier is demodulated and returns to the electrical signal. At the end, the error analyzer based upon a MATLAB Command is used to calculate the minimum BER and plot the eye diagram for the designed model.

3. 4. Indoor VLC Model

Figure 3.8 illustrates the arrangement of an indoor VLC model. The model is configured within a room measuring 5 m in length, 5 m in width and 3 m in height. This model is composed of three primary components, the transmitter, the transmission channel and the receiver. In this setup, four LED arrays are mounted on the underside of the ceiling, functioning as the source of optical signals. In optical communication systems, the choice of light source is crucial, as it generates the carrier wave that facilitates information transmission. LED arrays emit optical signals that can be modulated to encode data. The receiver is positioned on the floor and utilizes a photodiode to concert the received optical signal back into an electrical signal for subsequent processing. A PIN photodiode is used as the photodetector due to its high sensitivity and low noise characteristics. ϕ is the radiation angle with respect to transmitter, ψ is the irradiance angle with respect to receiver. θ_1 is the angle from the LED to the wall, θ_2 is the angle from wall to the PD.

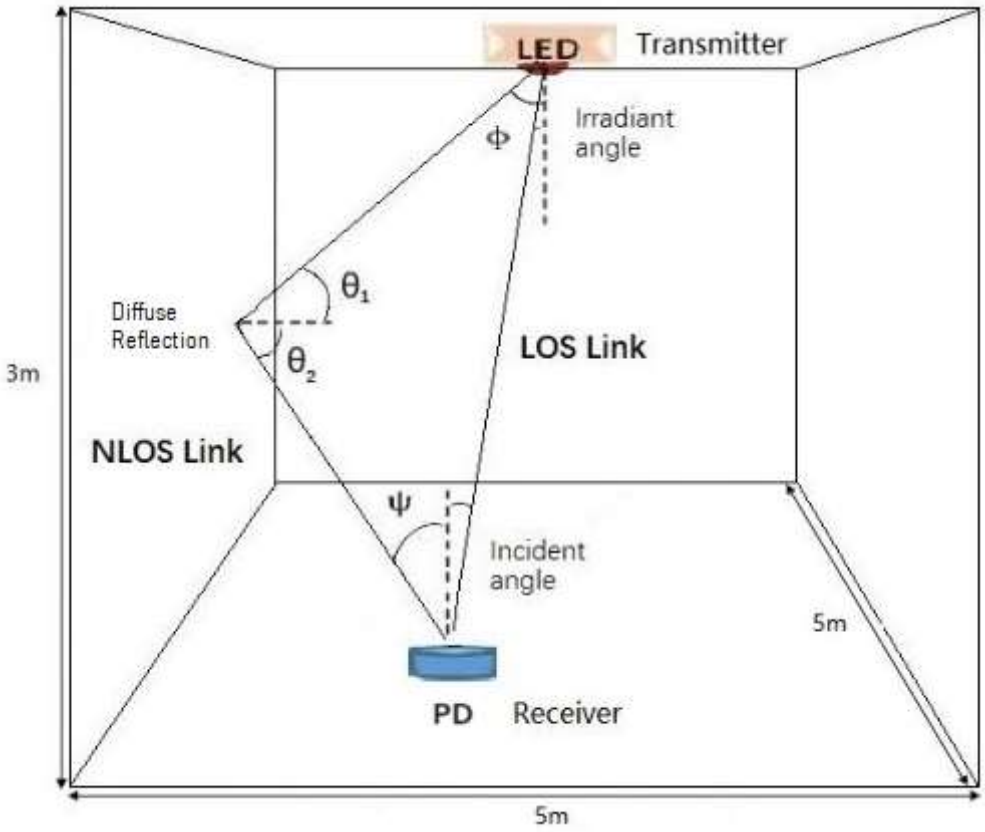

Figure 3.8. Indoor VLC model.

Due to the limitation of current technology, one single LED is difficult to meet the requirement of indoor illumination. In practical engineering applications, the array, which is composed of multiple LEDs, is often used as light source in indoor environment. Figure 3.9 presents the configuration of one LED array and four LED arrays on the underside of the ceiling.

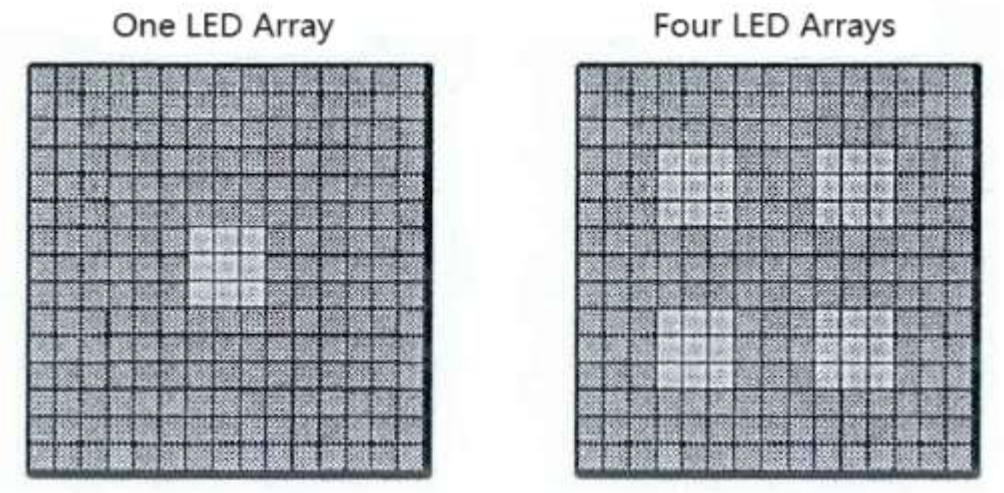

Figure 3.9. Configurations of one LED array and four LED arrays.

The LOS transmission path identifies the direct, unobstructed path that the optical signal follows from the transmitter to the receiver. LOS transmission paths are preferred in optical communication due to their minimal signal attenuation and optimal signal quality. However, practical applications often involve obstacles or constraints that necessitate the consideration of alternative transmission paths. In contrast, the NLOS transmission path denotes scenarios where the optical signal must navigate around obstacles or reach the receiver through reflection or scattering. NLOS transmission paths are more prevalent in practical applications but introduce additional challenges, including increased signal attenuation, multipath effects, and potential interference.

3. 4. 1. Simulation Parameter Setting

The other simulation parameters relevant to the indoor VLC model are shown in the Table 3.1.

Table 3.1. Simulation parameters of indoor VLC model.

Parameter	Value
Room size	5*5*3 m^3

LED array power	30 W[28]
Center luminous intensity	21.5 cd[28]
Semi angle at half power angle of LED	60°[29]
PD responsivity	0.53 A/W[28]
Reflectivity of wall	0.8[28]
FOV of PD	70°[14]
Photosensitive area size of PD	1 cm^2 [9]
Refractive index of lens at PD	1.5[9]
Gain of optical filter	1[29]
Noise bandwidth factor	0.562 [17]
Background noise current	0.62 mA[17]
Load resistance	10 kΩ[17]
Equivalent noise bandwidth	200 MHz[17]

In this simulation model, LED array is used as the transmitter and PD is chosen as the receiver. In terms of commercial single LED, the power ranges from 0.06 W to 0.5 W, the center luminous intensity ranges from 200 ucd to 800 mcd, and half power angle ranges from 20°to 120°. In this simulation model, one LED array consists of 60×60 LEDs. Therefore, the power of one LED array is set as 30 W, the center luminous intensity is set as 21.5 cd and the half power angle is set as 60°. In terms of commercial PD, the FOV ranges from 30° to 150°. In this simulation model, the FOV is set as 70°. The responsivity of PD is set as 0.53 A/W and the photosensitive area size of PD is set as 1 cm^2. Besides, the refractive index of lens at PD is set as 1.5. The transmission channel is LOS and NLOS channel in an indoor environment. The material of the wall is gypsum, and its reflectivity coefficient is 0.8.

3. 5. Summary

This chapter presents the design and setting of the OWC simulation models. The chapter starts with an introduction of simulation tool. Then the setup and parameter setting of the FSO model and the indoor VLC model are separately described in detail.

4. Results and Discussion

4. 1. Introduction

In order to incorporate OWC systems in real world scenarios, the characteristics of each OWC technologies need to be studied in detail. Using simulation softwares, the models of different OWC technologies can be constructed. The simulation softwares then analyze the OWC systems' results and optimize their system parameters, in order to achieve highly reliable OWC links. This chapter presents the simulation results obtained from various OWC technologies, including the FSO model, the Li-Fi model and the IPS.

4. 2. Performance Investigation

4. 2. 1. Results of FSO Model

In an FSO communication model, the performance comparison between two multi-level modulation formats, AACC and 4-PAM are studied. AACC is a recent established multi-level modulation format which was proposed in a 40 Gbit/s light wave system. It is a modulation format with memory that has been presented as a replacement to the 4-PAM format and is applicable to optical interconnects applications and OWC systems [79]. Although there are many studies focusing on AACC, most of them, however, are based on fibre communication systems. Hence, there is a lack of results on a direct comparison in FSO communication systems. This gap is addressed by conducting a numerical analysis on direct-detection FSO communication systems with AACC and 4-PAM.

4. 2. 1. 1. Transmission Distance

Figure 4.1 illustrates the BER performance against distance for AACC and 4-PAM transmission for FSO channel operating at 10 Gbit/sunder different weather conditions. It is shown that under clear weather condition, the attenuation at 0.441 dB/km, AACC is observed to support a longer link distance of 3.8 km than the 4-PAM, which supports 3.7 km, at a BER of 10^{-9}. In a foggy environment, the attenuation at 33.961 dB/km, however, both signals travel the shortest distance of 0.5 km.

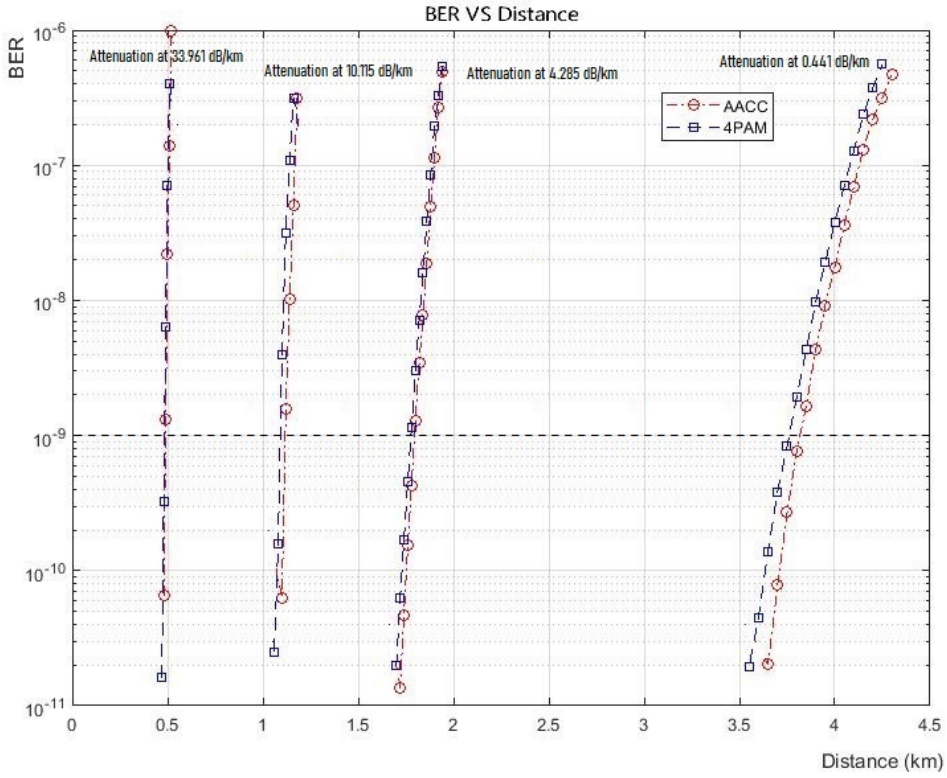

Figure 4.1. BER versus Distance under different weather conditions.

Figure 4.2 illustrates the BER performance of the AACC and 4-PAM for an FSO channel operating at 10 Gbit/sin heavy haze weather, the attenuation at 10.115 dB/km, more distinctly than Figure 4.2. For a fair comparison between these two multi-level signaling formats, the bitrate and BER estimation technique were kept the same as in the simulation. It is shown that the transmission distance of AACC is 1.12 km, and the transmission distance of 4-PAM is 1.09 km at BER of 10^{-9}. Because AACC has a better dispersion tolerance, reduce signal distortion during the transmission.

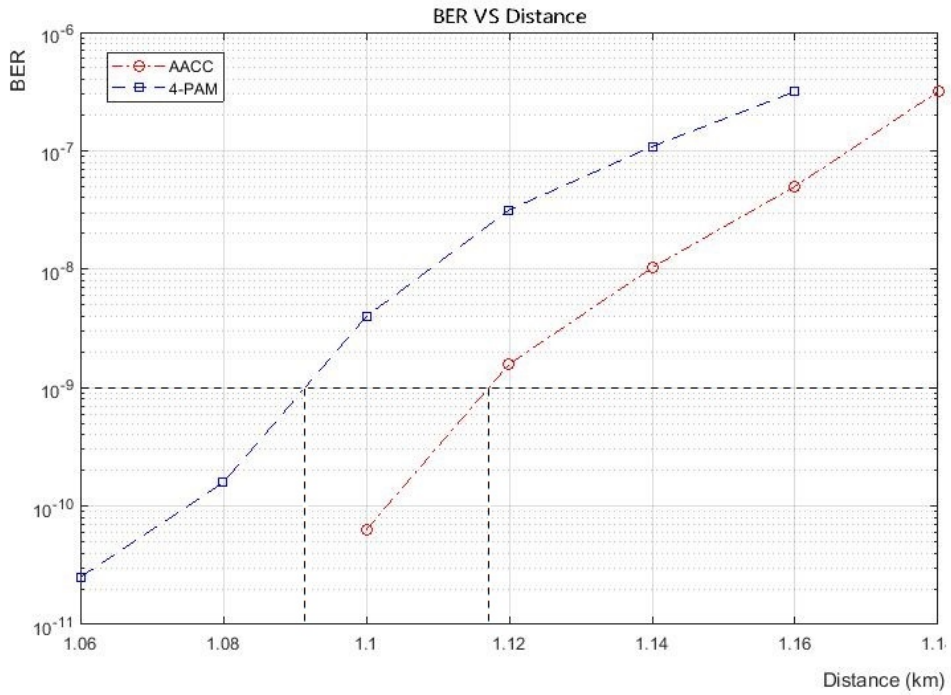

Figure 4.2. Comparison of BER versus Distance in FSO model.

4. 2. 1. 2. Eye Diagram

Figure 4.3 shows the eye diagrams of the modulated FSO systems that are extracted using a BER analyzer for different weather conditions. The eye diagrams under clear weather condition have the clearest lines, indicating a low noise impact. The eye opening is the widest and straightest, as a result of an almost distortion-free signal transmission. On the contrary, the lines of the eye diagrams under heavy haze condition are blurred bands. The small eye opening with jitter shows the noise impact due to the attenuation. The distinction between clear weather condition, moderate haze, and heavy haze underscores the need for accurate channel characterization under different weather conditions. The haze conditions alter the propagation characteristics of optical waves used in FSO and significantly impact signal quality and reliability. Besides, the colour of the AACC signal is lighter than that of the 4-PAM signal. It implies that AACC offers a more reliable communication under heavy haze condition.

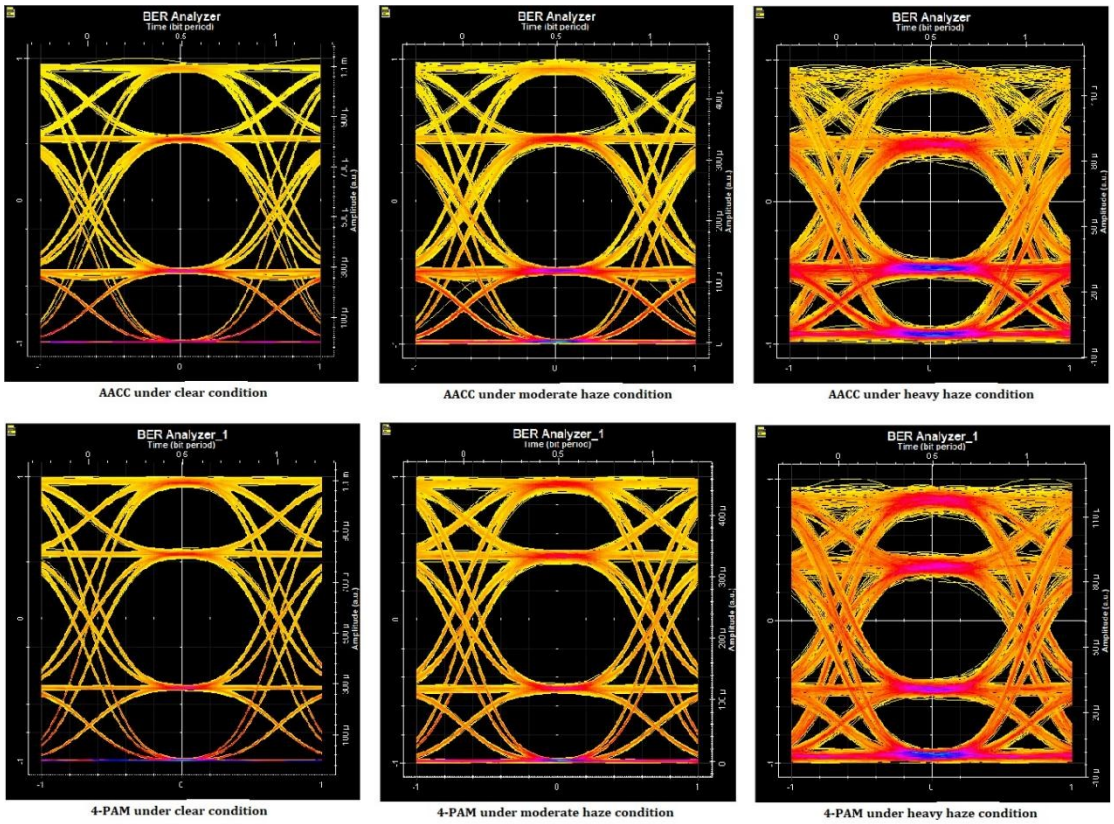

Figure 4.3. Eye diagrams under different weather conditions.

4. 2. 1. 3. **Bitrate**

Figure 4.4 illustrates the comparison of the BER value for AACC and 4-PAM at different bitrate in heavy haze weather, the attenuation at 10.115 dB/km. From the figures, the amount of BER increases with the bitrate. It is evident that AACC can transmit signal at a higher bitrate than 4-PAM at the same BER value. When the BER reaches at 10^{-9}, the bitrate of AACC is 18.7 Gbit/s, while the bitrate of 4-PAM is 16.7 Gbit/s. In general, the FSO system using the AACC modulation format, transmits at a higher bitrate than the FSO system using the 4-PAM format. Because AACC adopt advanced error correction coding, can correct errors generated during the transmission.

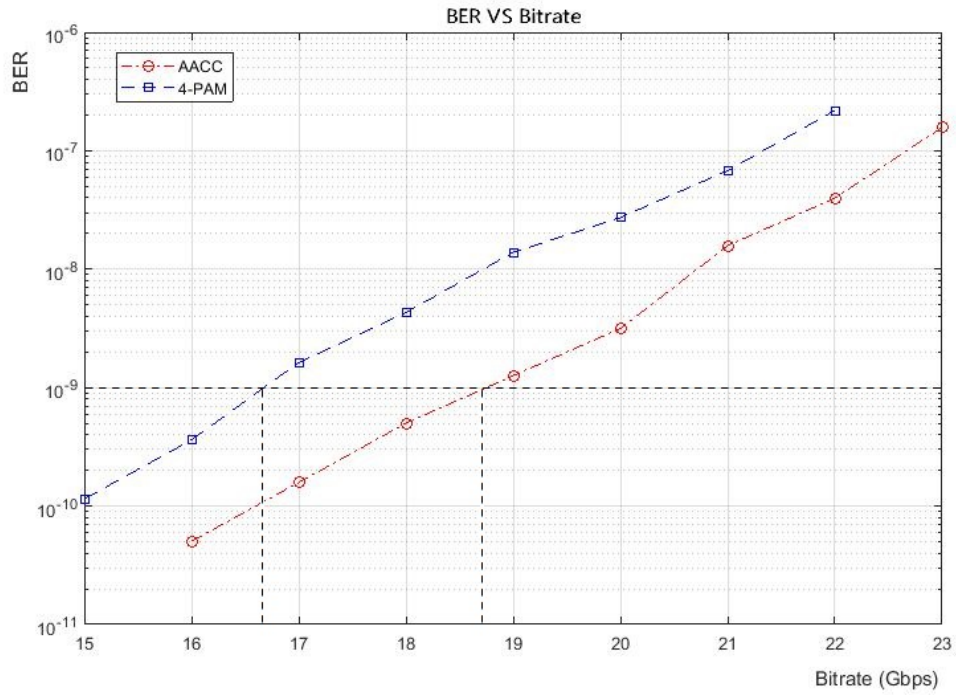

Figure 4.4. Comparison of BER versus Bitrate in FSO model.

4. 2. 2. Results of Li-Fi Model

The Li-Fi system research results are built on an indoor VLC model. First some key factors, which can affect the illumination and communication performance are studied. These simulation parameters include semi-angle, LED power, FOV. Then the illumination distribution with different LED layout and the received power with different transmission channels are evaluated. The SNR value and RMS delay are also measured and discussed.

4. 2. 2. 1. Semi Angle at Half Power

Figure 4.5 and Figure 4.6 illustrate the received power curve and SNR value curve with different semi angle at half power. From the figures, the received power and SNR value initially increase fast with the increment of the semi angle at half power. After reaching the maximum value, the received power and SNR value decrease. The received power is observed to decrease at a larger rate than the SNR value.

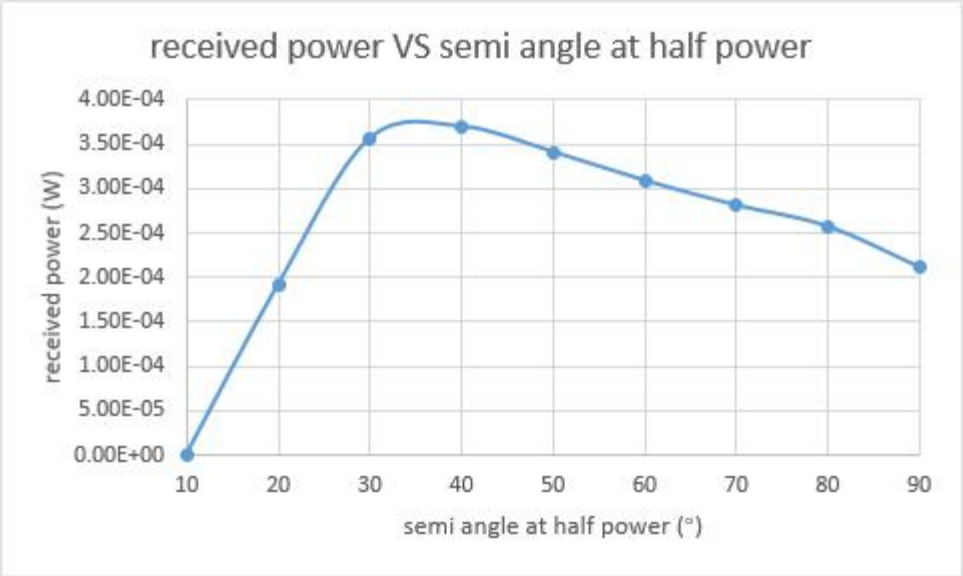

Figure 4.5. Received power versus Semi angle at half power in Li-Fi model.

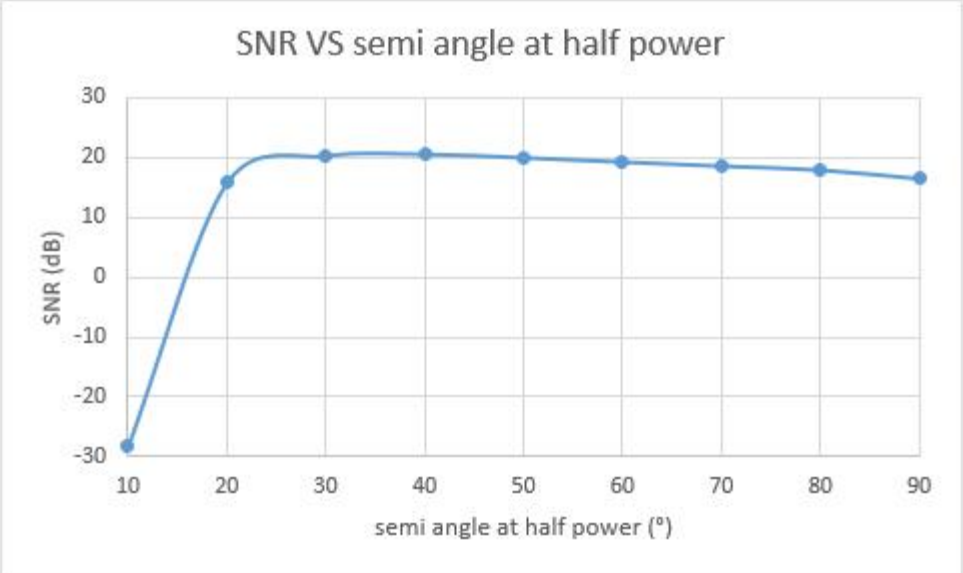

Figure 4.6. SNR versus Semi angle at half power in Li-Fi model.

4. 2. 2. 2. LED Power

Figure 4.7 and Figure 4.8 illustrate the received power curve and SNR value curve with the changing LED power. The tested LED power variates from 10 W to 50 W. From the figures, the received power is linear with the LED power and the SNR value also increases with the LED power. A higher LED power causes stronger optical signal, therefore the received power increases in linear. In term of SNR, noise is usually relatively stable in an indoor environment. When LED power increases, the signal

power increases. Therefore, as the signal power increases while noise remains relatively stable, the SNR value will also increases.

Figure 4.7. Received power versus LED power in Li-Fi model.

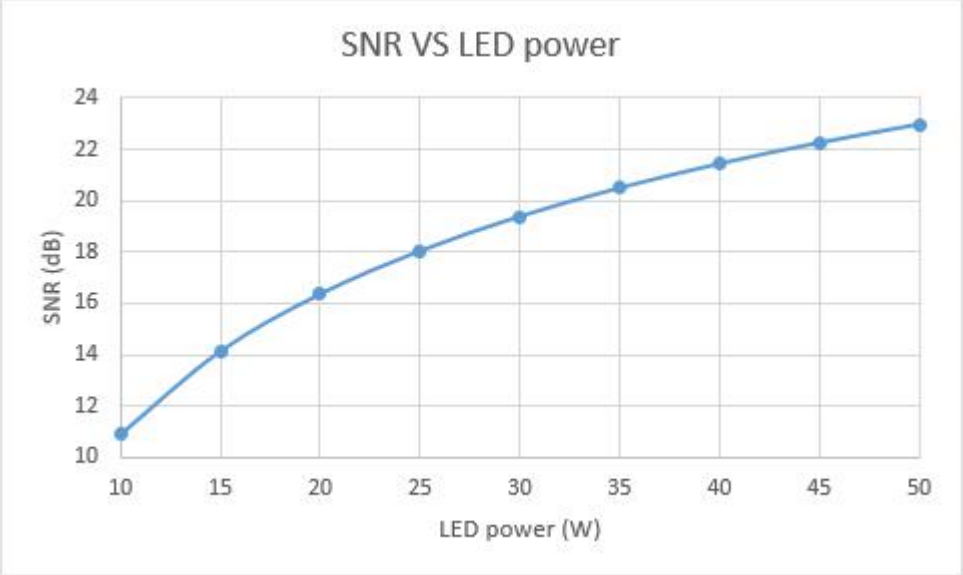

Figure 4.8. SNR versus LED power in Li-Fi model.

4. 2. 2. 3. Field of View

Figure 4.9 and Figure 4.10 illustrate the received power curve and SNR value curve for different FOV of PD. The tested FOV value changes from 50°to 80°. From the figures, it is evident that the larger the FOV, the larger the received power and the SNR value. A larger FOV means that the receiver can capture more light, therefore increases the

received power. In terms of SNR, as the received power increases while noise remains relatively stable, the SNR value will also increases.

Figure 4.9. Received power versus FOV in Li-Fi model.

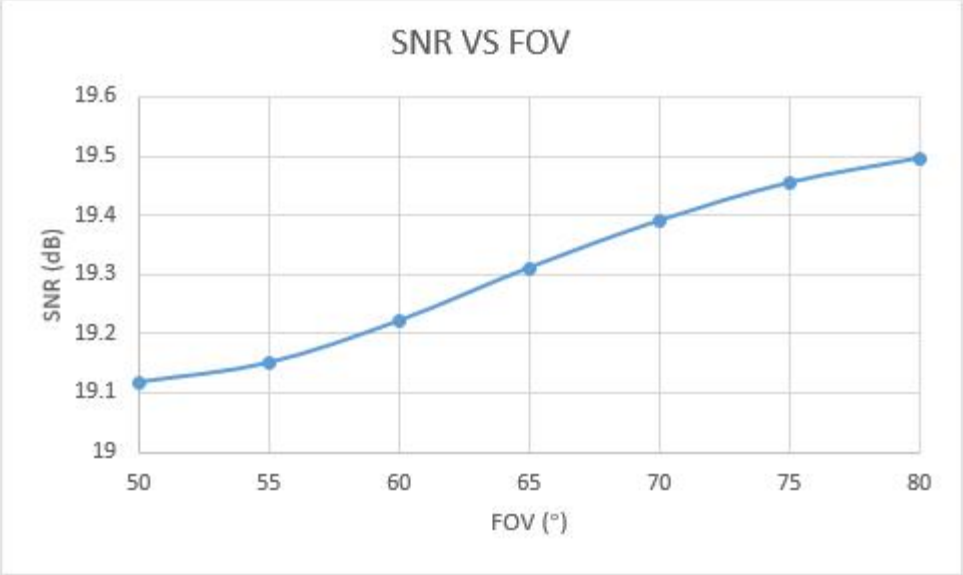

Figure 4.10. SNR versus FOV in Li-Fi model.

4. 2. 2. 4. Refractive Index

Figure 4.11 and Figure 4.12 illustrate the received power curve and SNR value curve with different refractive index of PD. From the following figures, the larger the refractive index, the larger the received power and the SNR value. The refractive index will affect the transmission of light in indoor environment. A higher refractive index

causes more obvious refraction and reflection, and leads to more optical power received by PD. In terms of SNR, the noise increases less than the signal power increases. This leads to an increasing SNR value.

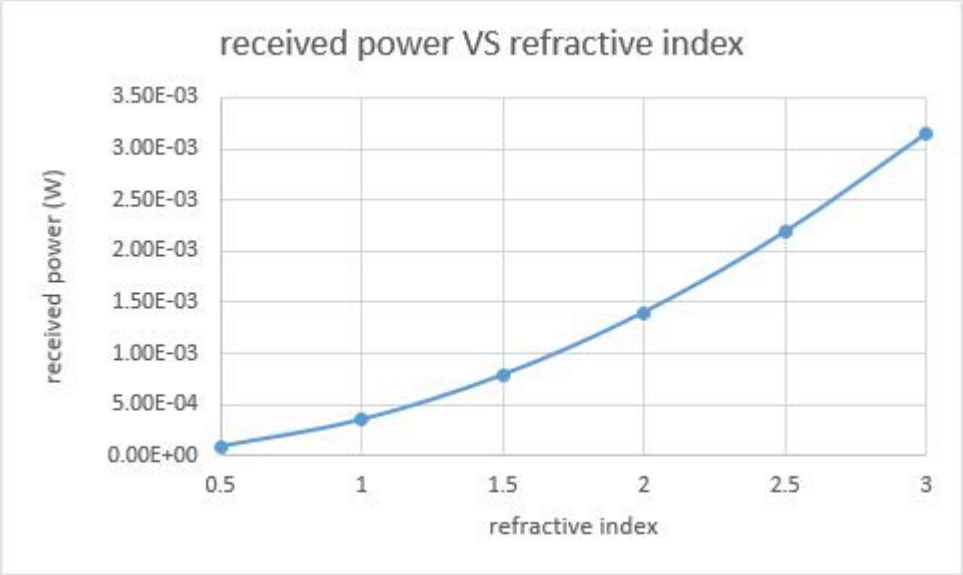

Figure 4.11. Received power versus Refractive index in Li-Fi model.

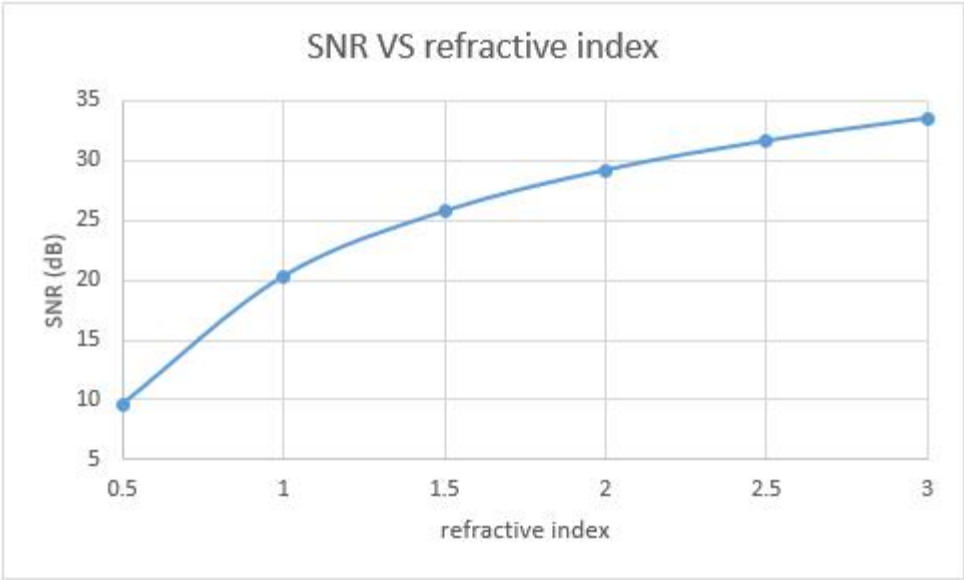

Figure 4.12. SNR versus Refractive index in Li-Fi model.

4. 2. 2. 5. Gain of Optical Filter

Figure 4.13 and Figure 4.14 illustrate the received power curve and SNR value curve for different gain of optical filter. From the figures, the received power is linear to the gain of optical filter. And the larger the gain of optical filter, the larger the SNR value.

When the gain of optical filter increases, it can more effectively filter and receive optical signals, therefore the received power increases in linear. In terms of SNR, the noise increases less than the signal power increases. This leads to an increasing SNR value.

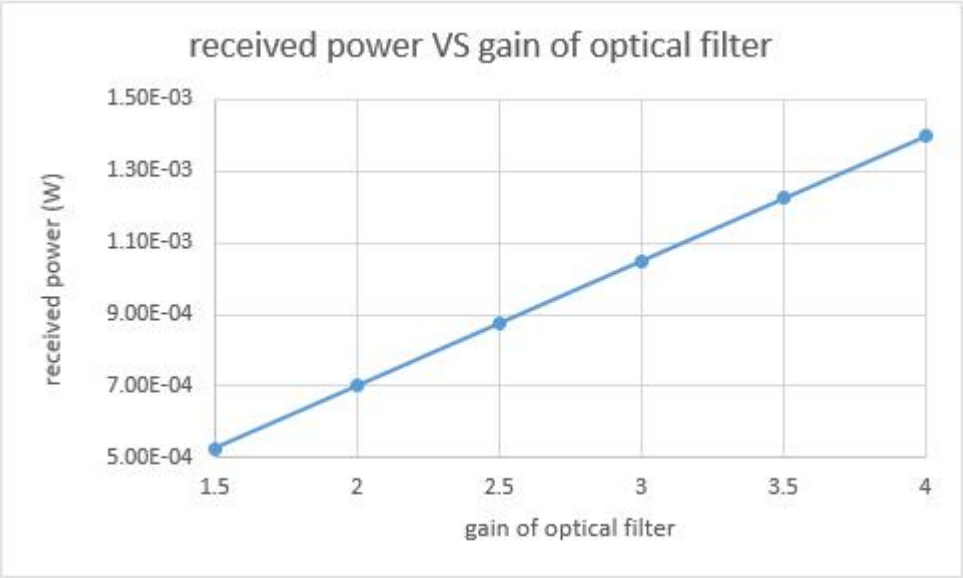

Figure 4.13. Received power versus Gain of optical filter in Li-Fi model.

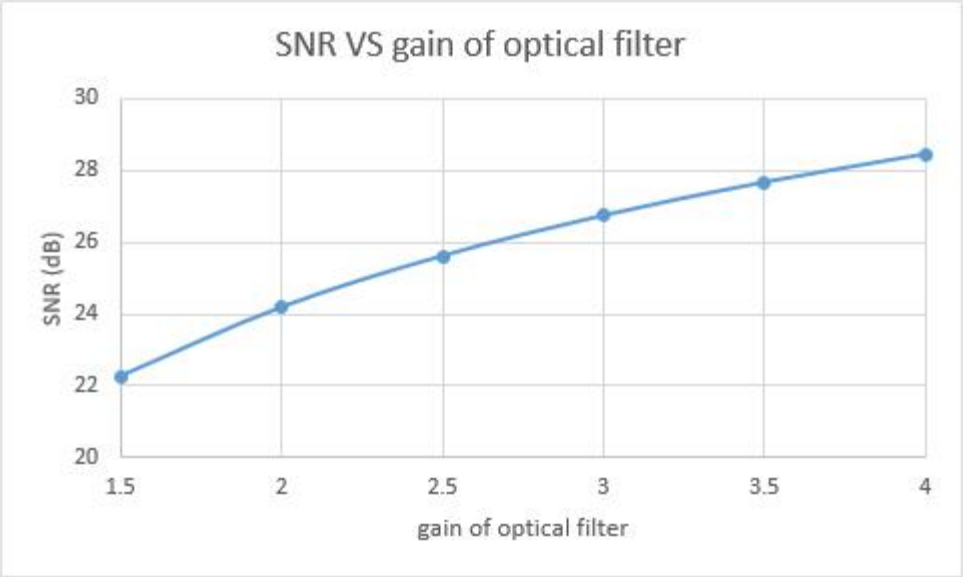

Figure 4.14. SNR versus Gain of optical filter in Li-Fi model.

4. 2. 2. 6. Illumination Distribution

In order to analyse the illumination distribution at different locations in the room, 51×51 receivers are evenly distributed on the floor of the simulation model, 10

receivers per meter. Figure 4.15 and Figure 4.16 present the illumination distribution using one LED array and four LED arrays. The layout of four LED arrays provides a more uniform illumination than the layout of one LED array.

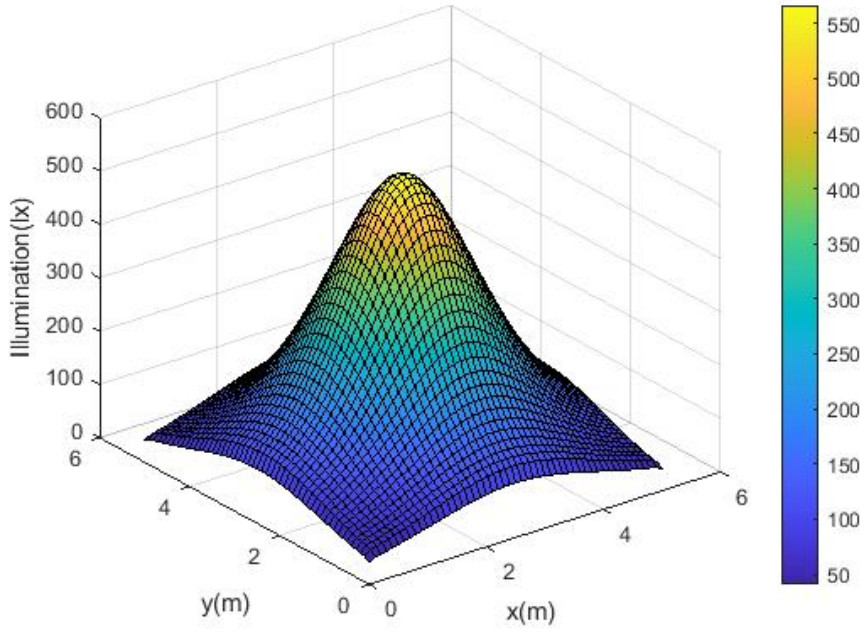

Figure 4.15. Illumination with one LED array.

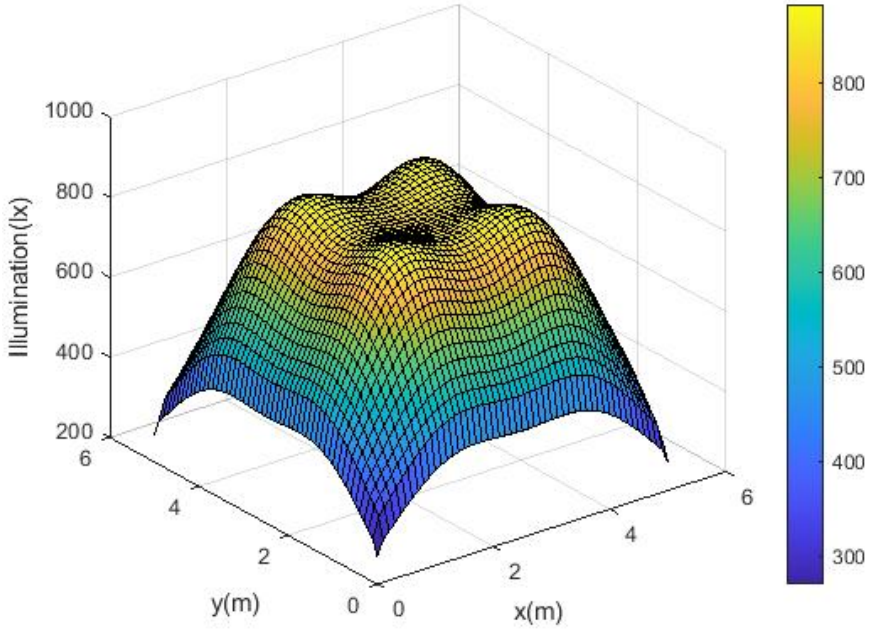

Figure 4.16. Illumination with four LED arrays.

4. 2. 2. 7. Received Power

Figure 4.17 and Figure 4.18 present the received power in LOS channel and NLOS channel. It is obvious that the contribution of the LOS channel, as opposed to the NLOS channel, is decisive for the received power. In LOS channel, optical signals transmit in a straight line without blocking, and the signal loss is little. In NLOS channel, optical signals will go through multiple propagation, and lead to a significant attenuation of signal strength. Therefore, the LOS channel has more contribution than NLOS in received power. The contribution of NLOS channel is concentrated in the area near the walls because they will cause refraction and reflection. When the distance between the receiver and the wall increases, the intensity of refracted and reflected signal weakens, the received power decreases rapidly.

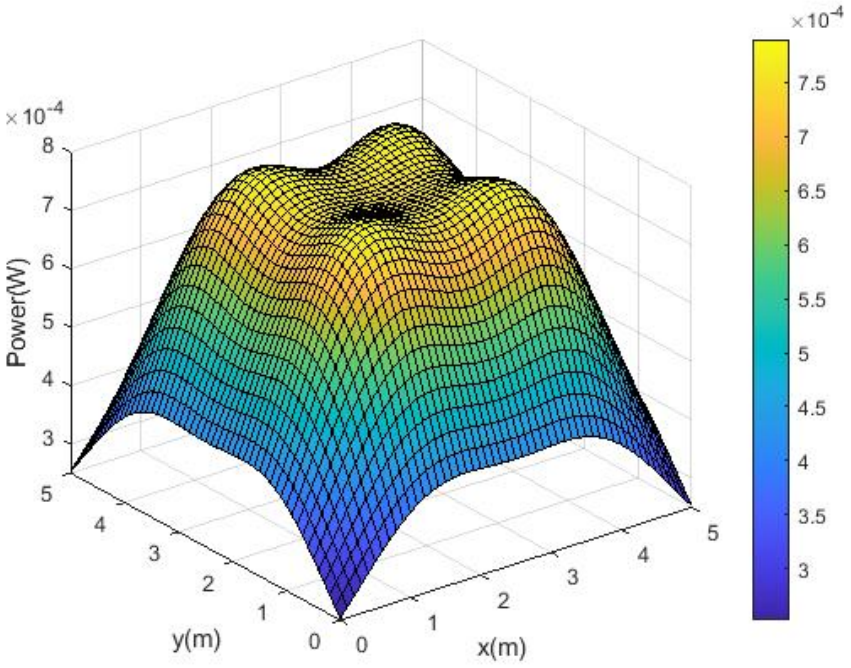

Figure 4.17. Received power in LOS channel.

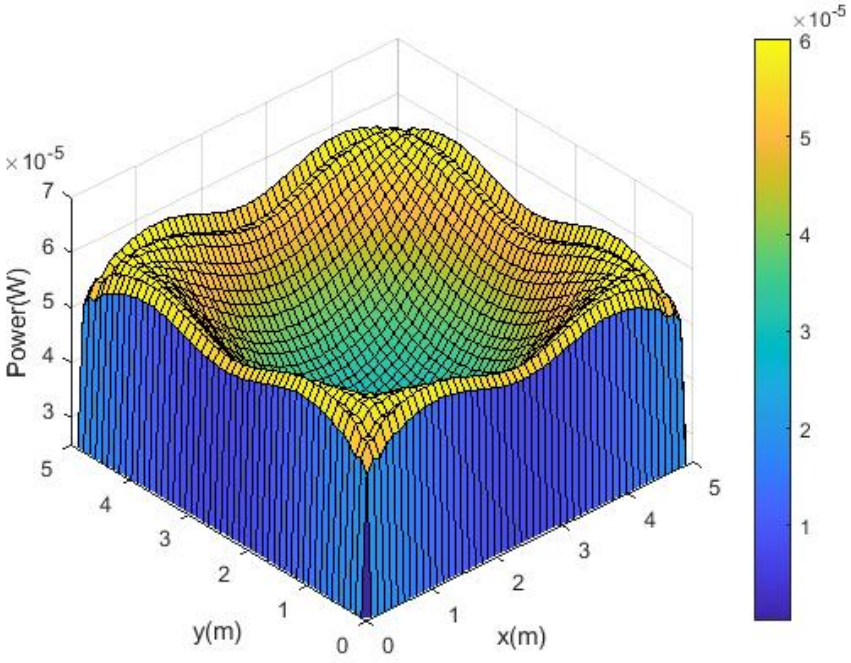

Figure 4.18. Received power in NLOS channel.

4. 2. 2. 8. SNR

Figure 4.19 shows the noise at each receiver in the simulation model. This noise includes shot noise and thermal noise. The maximum noise is 5.148×10^{-10} and the average noise is 4.544×10^{-10}.

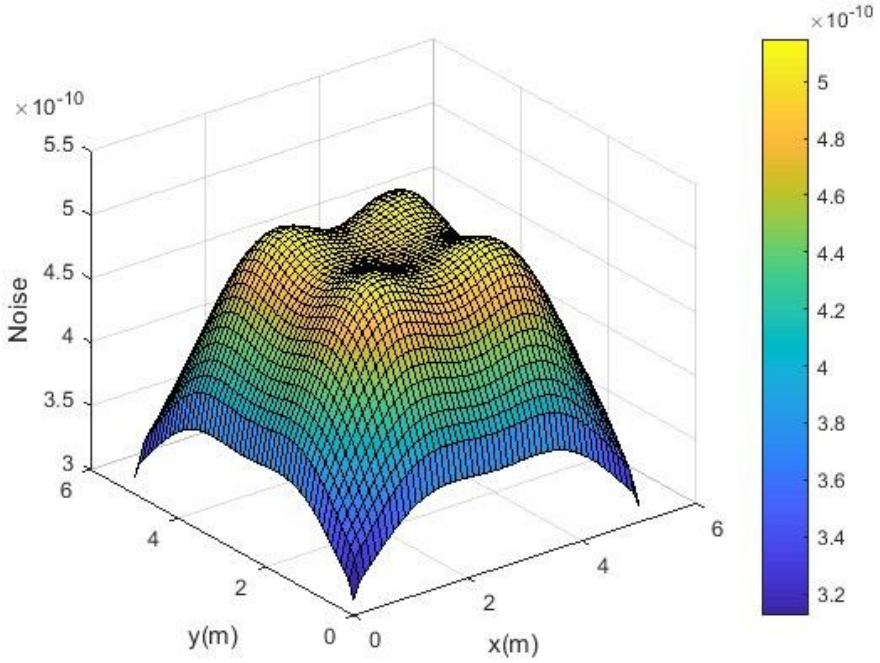

Figure 4.19. Noise of indoor VLC.

A consistent SNR at all receivers in the indoor environment will ensure a consistent communication performance. Figure 4.20 illustrates the SNR at each receiver in the simulation model. The maximum SNR is 26 dB and the average SNR is 24.4 dB.

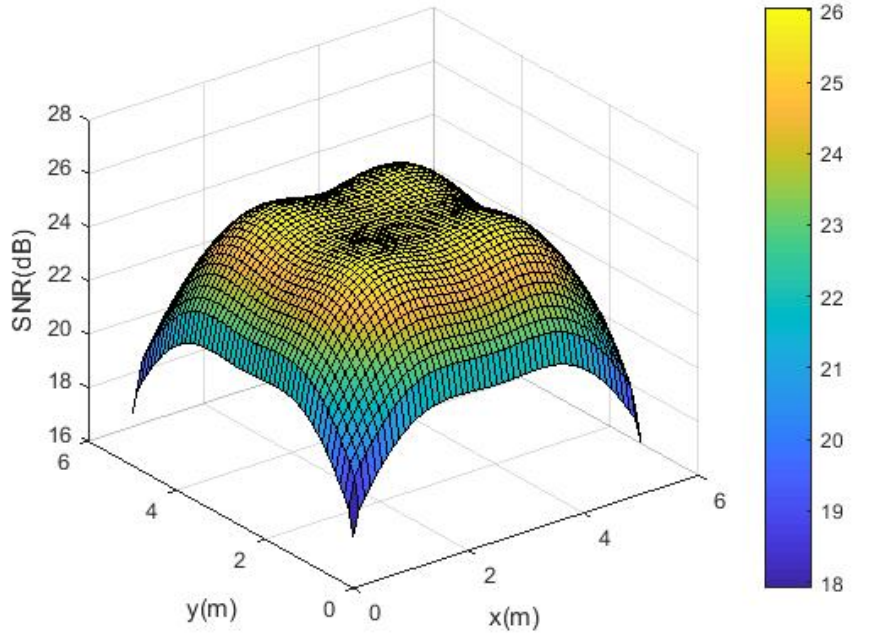

Figure 4.20. SNR of indoor VLC.

4. 2. 2. 9. RMS Delay

Figure 4.21 illustrates the RMS delay at each receiver in the simulation model. The maximum RMS delay is 3×10^{-9} s and the average RMS delay is 2.38×10^{-9} s.

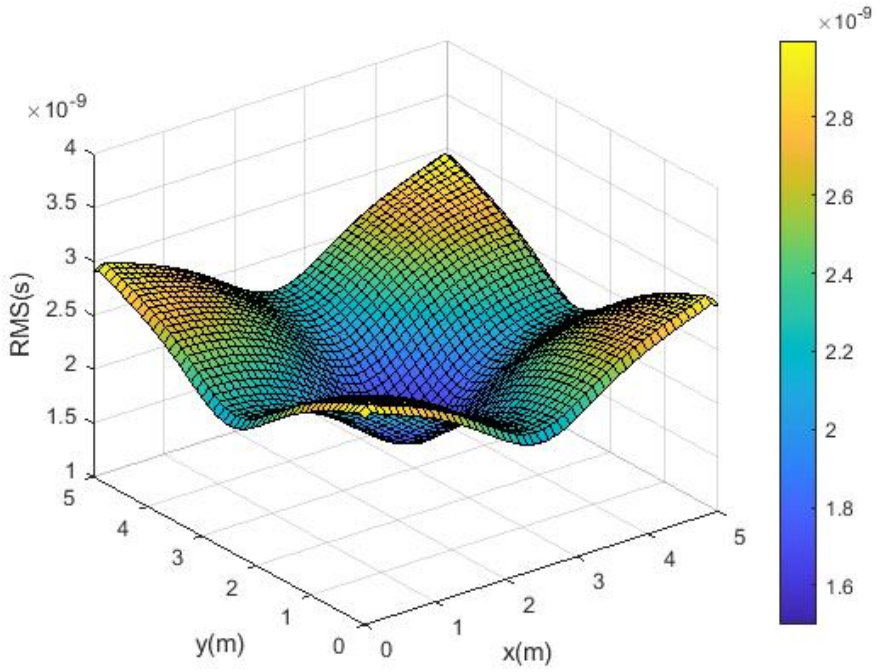

Figure 4.21. RMS delay of indoor VLC.

The maximum data rate that can be transmitted through the indoor VLC channel without an equalizer can be given in Eq.(4.1)

$$R_b \leq \frac{1}{10\times\tau_{RMS}} \qquad \text{Eq.(4.1)}$$

According to Eq.(4.1), when the maximum RMS delay is 3×10^{-9} s, the data rate of this Li-Fi model can be transmitted at least 33 Mbps.

4. 2. 3. Results of IPS

This thesis investigates the IPS by using the model of an indoor VLC system. It is an off-line fingerprinting database which adopts MATLAB simulation results.

At the off-line survey stage, the specific information of the indoor VLC model, such as the received power and SNR value of the signal, is collected, processed and recorded in

the database. Figure 4.22 and Figure 4.23 present the database of received power and SNR value from the MATLAB simulation results of the indoor VLC system. At the on-line positioning stage, the target is estimated by matching the measured data with that previously collected in the off-line database.

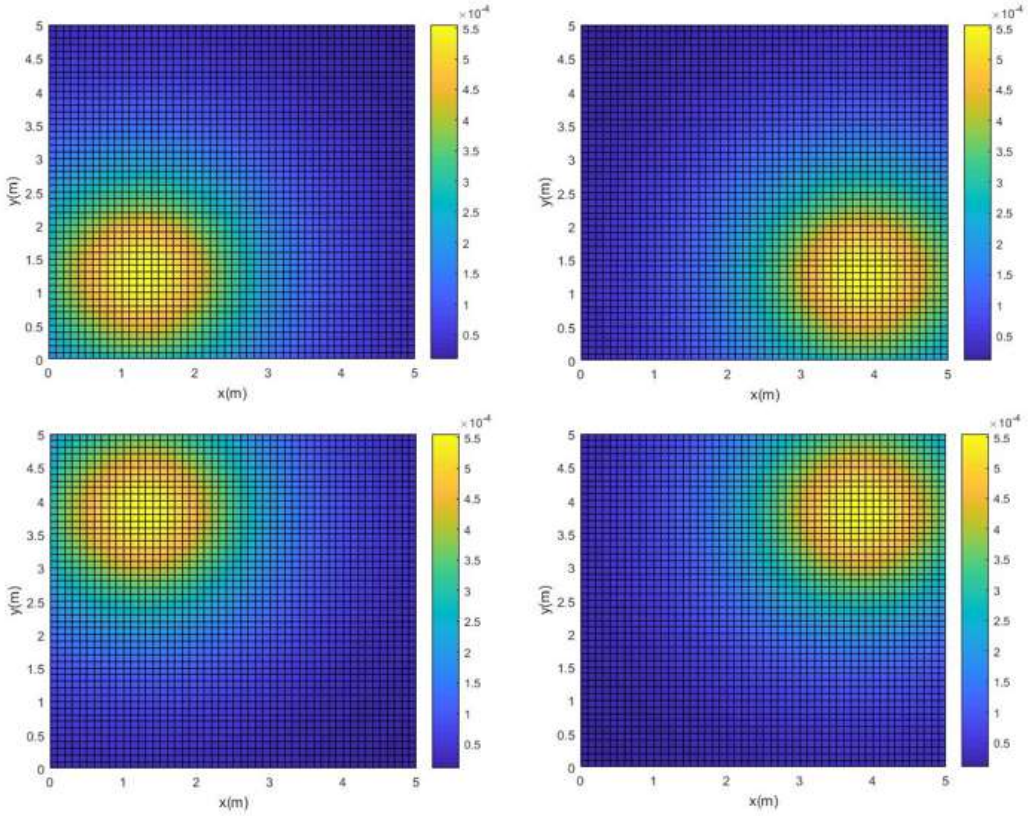

Figure 4.22. Fingerprint database of received power.

Figure 4.22 presents the database of received power distribution in the IPS. The four charts represent the simulation results of the received power at the receiver. These results are calculated by an indoor optical channel using the MATLAB program, and each chart corresponds to a different LED array respectively. From these results, the received power value at every point can be got, that is represented by the colour at the location in the grid. Moreover, the database can be used to match the on-line measured data to find the location of the target.

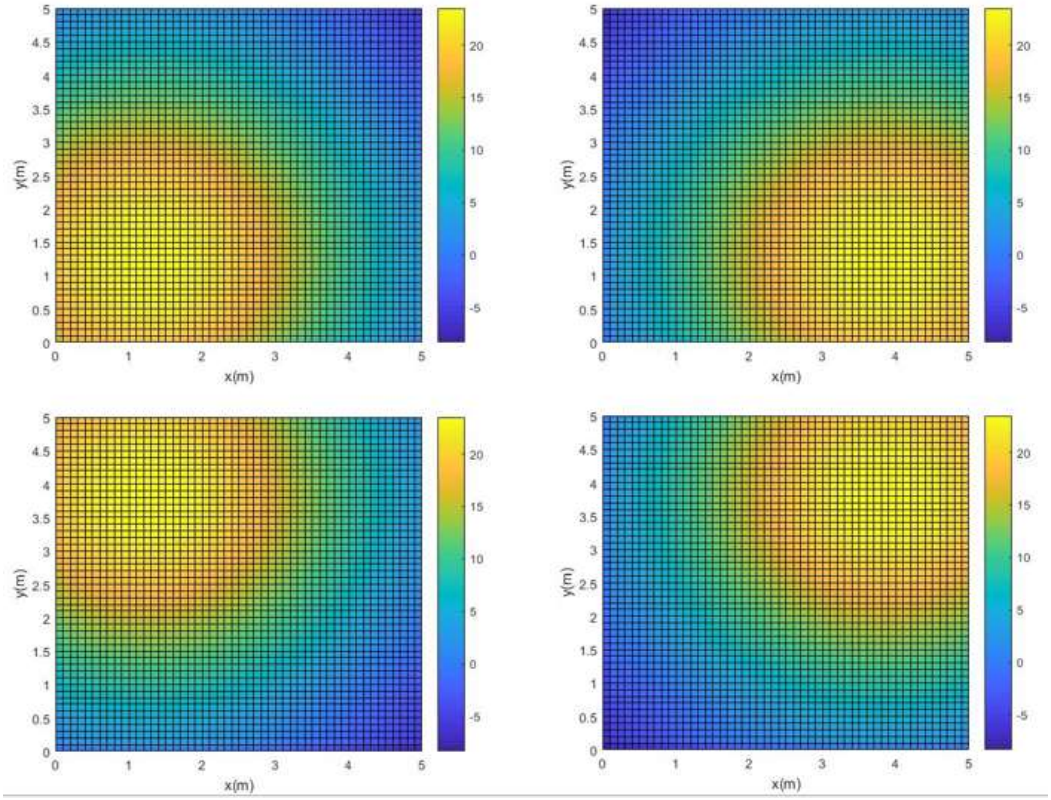

Figure 4.23. Fingerprint database of SNR.

Similarly, Figure 4.23 shows the database of the SNR distribution in the IPS. The four charts are also the simulation results of the SNR value from the MATLAB program, and each chart corresponds to a different LED array respectively. Both received power and SNR value databases can be used to find the location of target.

5. Conclusion and Prospect

5. 1. Conclusion

OWC technologies provide a potential solution to release the problems in RF communication technologies. With the rapidly increasing requirement, OWC technologies have a great scope in future applications. This research gives light on analyzing the OWC technologies, by using simulation models and mathematical techniques.

The FSO system model is built in OptiSystem software and simulated by using AACC and 4-PAM format. By comparing these two modulation formats, it can be seen that AACC format has an advantage over the 4-PAM format. It is revealed that at 10 Gbit/s and BER of 10^{-9}, AACC signal can be transmitted over 1.12 km of FSO whereas 4-PAM just reaches to 1.09 km in moderate haze weather condition. Besides, at the distance of 1 km, the bitrate of AACC can reach to 18.7 Gbit/s, while the bitrate of 4-PAM reaches to 16.7 Gbit/s. Because AACC format has a better dispersion tolerance and adopt advanced error correction coding. It offers promise that AACC will be essential and become a replacement for 4-PAM in the future of high-speed OWC.

The indoor VLC system model, which is simulated by MATLAB software, is used to research the performance of Li-Fi system and IPS. In the Li-Fi system, some key factors which can affect the illumination and communication performance are studied. Then the simulation results of illumination distribution and received power are evaluated under different conditions. Besides, SNR and RMS delay are also discussed. These results offer a theoretical support for the construction of a robust and high data rate Li-Fi system. In terms of IPS, a new approach of collecting data in fingerprinting is studied. The traditional way of fingerprinting consumes a long time and is laborious to collect a large number of samples as off-line database in advance. The new approach can shorten the time by using MATLAB program to generate an off-line database which is used to match the on-line measured data to find the location of the target.

5. 2. Future Research Directions

This thesis focuses on the key technologies in high data rate OWC systems based on IM/DD, and achieves some research results through simulation models. However, due to time and capacity constraints, there are still some issues that need to be further investigated.

Firstly, a live testing of the transmission performance of OWC systems will help in improving the performance. And a live testing will identify any performance issues from the simulation results.

Presently, the simulation work so far has not considered the vary of the ambient effect in FSO system. The full test performance of the FSO system can be improved by accumulating even more factors to compare and generate more precise results.

Furthermore, the effect of random orientation and the shadowing in indoor VLC system has not been considered. The stability of the connection will be improved by analysis these effects.

Nevertheless, the outlay of LED array in Li-Fi is more complicated in practical application. Expect the square alignment, the round alignment or elliptical alignment is used according to the room arrangement.

Finally, the measurement of IPS to determine the accuracy and performance, in term of the positioning estimation error and computation time will also be studied in the future.

References

[1] T. Cisco and A. Internet, “Cisco: 2020 CISO Benchmark Report,” *Comput. Fraud Secur.*, vol. 2020, no. 3, p. 4, 2020, doi: 10.1016/s1361-3723(20)30026-9.

[2] ITU-R, “IMT Vision – Framework and overall objectives of the future development of IMT for 2020 and beyond,” *Recomm. Itu-R M.2083-0*, vol. 0, pp. 1–21, 2015, [Online]. Available: https://www.itu.int/dms_pubrec/itu-r/rec/m/R-REC-M

[3] D. Karunatilaka, F. Zafar, V. Kalavally, and R. Parthiban, “LED based indoor visible light communications: State of the art,” *IEEE Commun. Surv. Tutorials*, vol. 17, no. 3, pp. 1649–1678, 2015, doi: 10.1109/COMST.2015.2417576.

[4] T. Tolker-Nielsen and G. Oppenhauser, “In-orbit test result of an operational optical intersatellite link between ARTEMIS and SPOT4, SILEX,” in *Free-Space Laser Communication Technologies XIV*, 2002, vol. 4635, pp. 1–15.

[5] NASA, “NASA Laser Communication System Sets Record with Data Transmissions to and from Moon,” 2017. https://esc.gsfc.nasa.gov/news/NASA_Laser_Communication_System_Sets_Record_with_Data_Transmissions_to_and_from_Moon_

[6] T. Rokkas, T. Kamalakis, D. Katsianis, D. Varoutas, and T. Sphicopoulos, “Business prospects of wide-scale deployment of free space optical technology as a last-mile solution: a techno-economic evaluation,” *J. Opt. Netw.*, vol. 6, no. 7, pp. 860–870, 2007.

[7] M. Uysal and H. Nouri, “Optical wireless communications - An emerging technology,” *Int. Conf. Transparent Opt. Networks*, pp. 1–7, 2014, doi: 10.1109/ICTON.2014.6876267.

[8] pureLiFi, “Legacy Products,” 2018. http://purelifi.com/legacy-products/

[9] E. W. Lam and T. D. C. Little, “Indoor 3D Localization with Low-Cost LiFi Components,” *2019 Glob. LIFI Congr. GLC 2019*, pp. 7–12, 2019, doi: 10.1109/GLC.2019.8864119.

[10] B. Aly, M. Elamassie, H. B. Eldeeb, and M. Uysal, “Experimental Investigation of Lens Combinations on the Performance of Vehicular VLC,” pp. 5–9, 2020.

[11] A. S. Hamza, J. S. Deogun, and D. R. Alexander, “Classification Framework for Free Space Optical Communication Links and Systems,” *IEEE Commun. Surv. Tutorials*, vol. 21, no. 2, pp. 1346–1382, 2019, doi: 10.1109/COMST.2018.2876805.

[12] Al-Gailani, S.A., Salleh, M.F.M., Salem, A.A., Shaddad, R.Q., Sheikh, U.U., Algeelani, N.A. and Almohamad, T.A, “A survey of free space optics (FSO) communication systems, links, and networks,”*IEEE Access,* 9, pp.7353-7373, 2020.

[13] H. Kaushal and G. Kaddoum, “Optical Communication in Space: Challenges and Mitigation Techniques,” *IEEE Commun. Surv. Tutorials*, vol. 19, no. 1, pp. 57–96, 2017, doi: 10.1109/COMST.2016.2603518.

[14] Jahid, A., Alsharif, M. H., & Hall, T. J, “A contemporary survey on free space optical communication: Potentials, technical challenges, recent advances and research direction,” *Journal of network and computer applications,* 200, 103311. https://doi.org/10.1016/j.jnca.2021.103311

[15] N. D. Chatzidiamantis, A. S. Lioumpas, G. K. Karagiannidis, and S. Arnon, “Adaptive subcarrier PSK intensity modulation in free space optical systems,” *IEEE Trans. Commun.*, vol. 59, no. 5, pp. 1368–1377, 2011, doi: 10.1109/TCOMM.2011.022811.100078.

[16] Levidala, B.K., Ramavath, P.N. and Krishnan, P, “Performance enhancement using multiple input multiple output in dual-hop convergent underwater wireless optical communication–free-space optical communication system under strong turbulence with pointing errors,” *Optical Engineering,* 60(10), pp.106106-106106, 2021. https://doi.org/10.1117/1.OE.60.10.106106.

[17] Magidi, S., & Jabeena, A, " Free space optics, channel models and hybrid modulation schemes: A review," *Wireless Personal Communications,* 119(4), 2951-2974, 2021.

[18] Naveenkumar, M., Vaddadi, V.C.S. and Shivaleela, E.S, "Experimental Demonstration of Optical PAM-4 Generation for Short-Reach Optical Communications,"*In 2022 IEEE Microwaves, Antennas, and Propagation Conference (MAPCON)* (pp. 547-551). IEEE. https://doi.org/10.1109/MAPCON56011.2022.10046730.

[19] K. Szczerba *et al.*, "4-PAM for High-Speed Short-Range Optical Communications," vol. 4, no. 11, pp. 885–894, 2012.

[20] Chowdhury, R. and Choyon, "Design of novel hybrid CPDM-CO-OFDM FSO communication system and its performance analysis under diverse weather conditions," *arXiv preprint arXiv:*2103.15751, A.K.M., 2021. https://doi.org/10.48550/arXiv.2103.15751

[21] Siddique, I., Awan, M.Z., Khan, M.Y. and Mazhar, A, "Li-Fi the next generation of wireless communication through visible light communication (VLC) technology," *International Journal of Scientific Research in Computer Science, Engineering and Information Technology,* 5(1), pp.30-37, 2019. https://doi.org/10.32628/CSEIT1838108.

[22] Jenila, C. and Jeyachitra, R.K, "Green indoor optical wireless communication systems: Pathway towards pervasive deployment," *Digital Communications and Networks,* 7(3), pp.410-444, 2021. https://doi.org/10.1016/j.dcan.2020.09.004.

[23] Wu, H.W., Lu, H.H., Tsai, W.S., Huang, Y.C., Xie, J.Y., Huang, Q.P. and Tu, S.C., "A 448-Gb/s PAM4 FSO communication with polarization-multiplexing injection-locked VCSELs through 600 m free-space link," *IEEE Access,* 8, pp.28859-28866, 2020. https://doi.org/10.1109/ACCESS.2020.2972943.

[24] Rahman, M.T., Bakibillah, A.S.M., Parthiban, R. and Bakaul, M., "Review of advanced techniques for multi-gigabit visible light communication," *IET*

optoelectronics, 14(6), pp.359-373, 2020. https://doi.org/10.1049/iet-opt.2019.0120.

[25] Wang, L., Wei, Z., Chen, C.J., Wang, L., Fu, H.Y., Zhang, L., Chen, K.C., Wu, M.C., Dong, Y., Hao, Z. and Luo, Y., "1.3 GHz EO bandwidth GaN-based micro-LED for multi-gigabit visible light communication," *Photonics Research*, 9(5), pp.792-802, 2021. https://doi.org/10.1364/PRJ.411863.

[26] Lian, J. and Brandt-Pearce, M., " Multiuser visible light communication systems using OFDMA," *Journal of Lightwave Technology*, 38(21), pp.6015-6023, 2020.

[27] Hu, J., Hu, F., Jia, J., Li, G., Shi, J., Zhang, J., Li, Z., Chi, N., Yu, S. and Shen, C., "46.4 Gbps visible light communication system utilizing a compact tricolor laser transmitter," *Optics Express*, 30(3), pp.4365-4373, 2022.

[28] Geng, Z., Khan, F.N., Guan, X. and Dong, Y., "Advances in visible light communication technologies and applications,"*In Photonics* (Vol. 9, No. 12, p. 893). MDPI, 2022, November. https://doi.org/10.3390/photonics9120893.

[29] Loureiro, P.A., Guiomar, F.P. and Monteiro, P.P., "Visible light communications: a survey on recent high-capacity demonstrations and digital modulation techniques," *In Photonics* (Vol. 10, No. 9, p. 993). MDPI, 2023, August. https://doi.org/10.3390/photonics10090993.

[30] Miramirkhani, F. and Uysal, M., "Channel modelling for indoor visible light communications," *Philosophical Transactions of the Royal Society* A, 378(2169), p.20190187, 2020.

[31] T. H. Do and M. Yoo, "An in-depth survey of visible light communication based positioning systems," *Sensors (Switzerland)*, vol. 16, no. 5, 2016, doi: 10.3390/s16050678.

[32] Sheikh, S.M., Asif, H.M., Raahemifar, K. and Al-Turjman, F., "Time difference of arrival based indoor positioning system using visible light communication," *IEEE Access*, 9, pp.52113-52124, 2021. https://doi.org/10.1109/ACCESS.2021.3069793.

[33] A. B. M. M. Rahman, T. Li, and Y. Wang, "Recent advances in indoor localization via visible lights: A survey," *Sensors (Switzerland)*, vol. 20, no. 5, 2020, doi: 10.3390/s20051382.

[34] Yang, S., Sun, C. and Kim, Y., "Indoor 3D localization scheme based on BLE signal fingerprinting and 1D convolutional neural network," *Electronics,* 10(15), p.1758, 2021. https://doi.org/10.3390/electronics10151758.

[35] Maheepala, M., Kouzani, A.Z. and Joordens, M.A., "Light-based indoor positioning systems: A review," *IEEE Sensors Journal,* 20(8), pp.3971-3995, 2020. https://doi.org/10.1109/JSEN.2020.2964380.

[36] El-Ganiny, M.Y., Khalaf, A.A., Hussein, A.I. and Hamed, H.F., "A proposed preamble channel estimation scheme for flip FBMC-based indoor VLC systems," *Opto-Electronics Review,* 30, 2022. http://dx.doi.org/10.24425/opelre.2022.140859.

[37] Zhu, Z., Yang, Y., Guo, C., Feng, C. and Jia, B., "Visible light communication assisted perspective circle and arc algorithm for indoor positioning," *In ICC 2022-IEEE International Conference on Communications* (pp. 3832-3837), 2022, May. IEEE. https://doi.org/10.1109/ICC45855.2022.9838938.

[38] Dawood, M.A., Saleh, S.S., El-Badawy, E.S.A. and Aly, M.H., "A comparative analysis of localization algorithms for visible light communication," *Optical and Quantum Electronics,* 53, pp.1-25, 2021.

[39] Hosseini, K.S., Azaddel, M.H., Nourian, M.A. and Azirani, A.A., "Improving Multi-floor WiFi-based Indoor positioning systems by Fingerprint grouping,"*In 2021 5th International Conference on Internet of Things and Applications (IoT)* (pp. 1-6), 2021, May. IEEE. https://doi.org/10.1109/IoT52625.2021.9469602.

[40] Tiku, S. and Pasricha, S., "An overview of indoor localization techniques," *Machine Learning for Indoor Localization and Navigation,* pp.3-25, 2023.

[41] M. Z. Chowdhury, M. T. Hossan, A. Islam, and Y. M. Jang, "A Comparative Survey of Optical Wireless Technologies: Architectures and Applications,"

IEEE Access, vol. 6, pp. 9819–9840, 2018, doi: 10.1109/ACCESS.2018.2792419.

[42] KATHRYN ZICKUHR, "Location-Based Services." PEW RESEARCH CENTER.

[43] Z. Ghassemlooy, P. Luo, and S. Zvanovec, "Optical camera communications," in *Optical Wireless Communications*, Springer, 2016, pp. 547–568.

[44] M. Schöberl, "Photometric limits for digital camera systems," *J. Electron. Imaging*, vol. 21, no. 2, p. 020501, 2012, doi: 10.1117/1.jei.21.2.020501.

[45] Y. Qin, T. T. Vu, and Y. Ban, "Toward an optimal algorithm for LiDAR waveform decomposition," *IEEE Geosci. Remote Sens. Lett.*, vol. 9, no. 3, pp. 482–486, 2012, doi: 10.1109/LGRS.2011.2172676.

[46] A. P. Cracknell, *Introduction to remote sensing*. CRC press, 2007.

[47] J. Carter *et al.*, "An introduction to LiDAR technology, data, and applications," *NOAA Coast. Serv. Cent.*, p. 2, 2012.

[48] K. Zhang and H. C. Frey, "Road grade estimation for on-road vehicle emissions modeling using light detection and ranging data," *J. Air Waste Manag. Assoc.*, vol. 56, no. 6, pp. 777–788, 2006, doi: 10.1080/10473289.2006.10464500.

[49] S. K. Kwon, E. Hyun, J.-H. Lee, J. Lee, and S. H. Son, "Detection scheme for a partially occluded pedestrian based on occluded depth in lidar–radar sensor fusion," *Opt. Eng.*, vol. 56, no. 11, p. 1, 2017, doi: 10.1117/1.oe.56.11.113112.

[50] G. Gigli and N. Casagli, "Semi-automatic extraction of rock mass structural data from high resolution LIDAR point clouds," *Int. J. Rock Mech. Min. Sci.*, vol. 48, no. 2, pp. 187–198, 2011, doi: 10.1016/j.ijrmms.2010.11.009.

[51] K. D. Langer and J. Grubor, "Recent developments in optical wireless communications using infrared and visible light," *Proc. 2007 9th Int. Conf. Transparent Opt. Networks, Ict. 2007*, vol. 3, pp. 146–151, 2007, doi: 10.1109/ICTON.2007.4296267.

[52] R. Henderson, "Understanding optical fiber communications," *Opt. Lasers Eng.*, vol. 38, no. 6, pp. 606–607, 2002, doi: 10.1016/s0143-8166(01)00181-6.

[53] M. S. Islim and H. Haas, “Modulation Techniques for Li-Fi,” 2019.

[54] Y. Li, M. Li, Y. Poo, J. Ding, M. Tang, and Y. Lu, “Performance analysis of OOK, BPSK, QPSK modulation schemes in uplink of ground-to-satellite laser communication system under atmospheric fluctuation,” *Opt. Commun.*, vol. 317, pp. 57–61, 2014, doi: 10.1016/j.optcom.2013.12.032.

[55] N. Dong-Nhat, L. Nguyen, and A. Malekmohammadi, “75 Gbit/s transmission over single mode fibre links using 8-PAM and 8-AACC modulations,” *Electron. Lett.*, vol. 53, no. 5, pp. 326–328, 2017, doi: 10.1049/el.2016.3619.

[56] N. Dong-Nhat, M. A. Elsherif, and A. Malekmohammadi, “Investigations of high-speed optical transmission systems employing Absolute Added Correlative Coding (AACC),” *Opt. Fiber Technol.*, vol. 30, pp. 23–31, 2016, doi: 10.1016/j.yofte.2016.01.013.

[57] N. Dong-Nhat and A. Malekmohammadi, “Absolute added correlative coding: An enhanced M-PAM modulation format,” *Electron. Lett.*, vol. 51, no. 20, pp. 1593–1595, 2015, doi: 10.1049/el.2015.1937.

[58] X. Wang, L. Guo, Y. Liu, and L. Zhang, “Analysis of atmosphere channel for space-to-ground optical communications,” *Opt. Commun.*, vol. 306, pp. 42–48, 2013, doi: 10.1016/j.optcom.2013.05.033.

[59] H. Kaushal and G. Kaddoum, “Free Space Optical Communication: Challenges and Mitigation Techniques,” *IEEE Commun. Surv. Tutorials*, vol. 19, no. 1, pp. 57–96, 2017, doi: 10.1109/COMST.2016.2603518.

[60] M. Hulea, Z. Ghassemlooy, S. Rajbhandari, and X. Tang, “Compensating for optical beam scattering and wandering in FSO communications,” *J. Light. Technol.*, vol. 32, no. 7, pp. 1323–1328, 2014, doi: 10.1109/JLT.2014.2304182.

[61] E. J. McCartney, “Optics of the atmosphere: scattering by molecules and particles,” *New York, John Wiley Sons, Inc., 1976. 421 p.*, 1976.

[62] I. I. Kim, B. Mcarthur, E. Korevaar, R. Street, and S. Diego, “Comparison of laser beam propagation at 785 nm and 1550 nm in fog and haze for optical wireless communications”.

[63] N. a Mohammed, A. S. El-wakeel, and M. H. Aly, “Pointing Error in FSO Link under Different Weather Conditions,” *Int. J. Video Image Process. Netw. Secur.*, vol. 12, no. 1, pp. 6–9, 2012.

[64] A. García-Zambrana, C. Castillo-Vázquez, and B. Castillo-Vázquez, “Space-time trellis coding with transmit laser selection for FSO links over strong atmospheric turbulence channels,” *Opt. Express*, vol. 18, no. 6, p. 5356, 2010, doi: 10.1364/oe.18.005356.

[65] A. Touati, S. J. Hussain, F. Touati, and A. Bouallegue, “Atmospheric turbulence effect on hybrid FSO/RF systems,” *IFIP Int. Conf. Wirel. Opt. Commun. Networks, WOCN*, vol. 4, no. 1, pp. 1–7, 2017, doi: 10.1109/WOCN.2015.8064516.

[66] M. Born and E. Wolf, *Principles of optics*. Elsevier, 2013.

[67] S. M. Rytov, *Principles of statistical radiophysics: wave propagation through random media*. Springer, 2011.

[68] Z. Wang, W. De Zhong, S. Fu, and C. Lin, “Performance comparison of different modulation formats Over free-space optical (FSO) turbulence links with space diversity reception technique,” *IEEE Photonics J.*, vol. 1, no. 6, pp. 277–285, 2009, doi: 10.1109/JPHOT.2009.2039015.

[69] E. Leitgeb *et al.*, “Analysis and evaluation of optimum wavelengths for free-space optical transceivers,” *2010 12th Int. Conf. Transparent Opt. Networks, Ict. 2010*, pp. 1–7, 2010, doi: 10.1109/ICTON.2010.5549009.

[70] P. K. Jha, N. Kachare, K. Kalyani, and D. S. Kumar, “Performance analysis of FSO using relays and spatial diversity under log-normal fading channel,” *Proc. 4th Int. Conf. Electr. Energy Syst. ICEES 2018*, pp. 121–125, 2018, doi: 10.1109/ICEES.2018.8442405.

[71] K. Anbarasi, C. Hemanth, and R. G. Sangeetha, “A review on channel models in free space optical communication systems,” *Opt. Laser Technol.*, vol. 97, pp. 161–171, 2017, doi: 10.1016/j.optlastec.2017.06.018.

[72] R. K. Giri and B. Patnaik, “BER analysis and capacity evaluation of FSO system using hybrid subcarrier intensity modulation with receiver spatial diversity over log-normal and gamma–gamma channel model,” *Opt. Quantum Electron.*, vol. 50, no. 6, pp. 1–20, 2018, doi: 10.1007/s11082-018-1499-8.

[73] A. García-Zambrana, “Error rate performance for STBC in free-space optical communications through strong atmospheric turbulence,” *IEEE Commun. Lett.*, vol. 11, no. 5, pp. 390–392, 2007, doi: 10.1109/LCOMM.2007.061980.

[74] J. R. Barry, J. M. Kahn, W. J. Krause, E. A. Lee, and D. G. Messerschmitt, “Simulation of Multipath Impulse Response for Indoor Wireless Optical Channels,” *IEEE J. Sel. Areas Commun.*, vol. 11, no. 3, pp. 367–379, 1993, doi: 10.1109/49.219552.

[75] J. R. Barry, “Wireless Infrared Communications,” *Wirel. Infrared Commun.*, vol. 9219, no. 97, 1994, doi: 10.1007/978-1-4615-2700-8.

[76] Optiwave, “OptiSystem Getting Started Optical Communication System Design Software,” *OptiSystem*, p. 68, 2013.

[77] M. F. . Abdullah and R. Talib, “Multilevel Signal Analyzer Tool for Optical Communication System,” *Int. J. Electr. Comput. Eng.*, vol. 2, no. 4, pp. 529–537, 2012, doi: 10.11591/ijece.v2i4.1464.

[78] The MathWorks Inc., “Getting Started with MATLAB Version 7,” *Manual*, vol. 7, no. 1, p. 1995, 1984, [Online]. Available: http://dx.doi.org/10.1016/j.mechatronics.2012.10.002%0Awww.mathworks.com%0Ahttp://www.mathworks.de/products/matlab/%0Awww.mathworks.com

[79] N. Dong-Nhat, M. A. Elsherif, H. Le Minh, and A. Malekmohammadi, “NRZ versus RZ over Absolute Added Correlative coding in optical metro-access networks,” *Opt. Commun.*, vol. 387, no. November 2016, pp. 30–36, 2017, doi: 10.1016/j.optcom.2016.11.017.

Appendices

Appendix A

MATLAB Codes of LOS channel in VLC model

```
function
[H_LOS,RMS_delay_LOS,RMS_delay_square_LOS]=RMS_delay_LOS(LED_positi
on,receiver_X,receiver_Y,room_height)


c0 = 3e8;
psi_hf = 60;                                        %semi angle of LED
m = -log10(2)/log10(cosd(psi_hf));                  %lambertian order of emission
Adet = 1e-4;                                        %detector physical area of PD
Ts = 1;                          %gain of an optical filter; ignore if no filter is used
index = 1.5              %refractive index of lens at a PD; ignore if no lens is used
FOV = 70;            %Field of View at receiver
%G_Con = 1;                                         %when no optical concentrator is used
G_Con = (index^2)/(sind(FOV)^2);                    %gain of an optical concentrator;
ignore if no lens is used


LED_positionx = LED_position(1);
LED_positiony = LED_position(2);
LED_positionz = LED_position(3);
```

```
D1 =
sqrt((LED_positionx-receiver_X).^2+(LED_positiony-receiver_Y).^2+(LED_positio
nz-receiver_height).^2);                                    %distance vector
from source 1
cos_phi = (LED_positionz-receiver_height)./D1;              %angle vector
receiver_angle = acosd(cos_phi);

H_LOS=(m+1)*cos_phi.^(m+1).*Adet./(2*pi*D1.^2)*Ts*G_Con;    %channel DC
      gain for source 1
H_LOS(abs(receiver_angle)>FOV) = 0;

RMS_delay_LOS = D1/c0.*H_LOS;
RMS_delay_square_LOS = (D1/c0).^2.*H_LOS;
```

Appendix B

MATLAB Codes of NLOS channel in VLC model

```
function
[H_NLOS,RMS_delay_NLOS,RMS_delay_square_NLOS]=RMS_delay_NLOS(LE
D_position,receiver_X,receiver_Y,n_grid,room_x,room_y,room_height)


c0 = 3e8;
psi_hf = 60;                %semi angle of LED
m = -log10(2)/log10(cosd(psi_hf));                  %lambertian order of emission
Adet = 1e-4;                                        %detector physical area of PD
Ts = 1;                             %gain of an optical filter; ignore if no filter is used
index = 1.5                 %refractive index of lens at a PD; ignore if no lens is used
FOV = 70;           %Field of View at receiver
%G_Con = 1;                                         %when no optical concentrator is used
G_Con = (index^2)/(sind(FOV)^2);                    %gain of an optical concentrator;
ignore if no lens is used
n_wall = 0.8;                       %reflectivity of wall


LED_positionx = LED_position(1);
LED_positiony = LED_position(2);
LED_positionz = LED_position(3);


H1_NLOS = zeros(n_grid,n_grid);                     %gain contribution from wall 1
H2_NLOS = zeros(n_grid,n_grid);
```

```
H3_NLOS = zeros(n_grid,n_grid);
H4_NLOS = zeros(n_grid,n_grid);

t1_NLOS = zeros(n_grid,n_grid);                    %travel time of light × gain
t2_NLOS = zeros(n_grid,n_grid);
t3_NLOS = zeros(n_grid,n_grid);
t4_NLOS = zeros(n_grid,n_grid);

t1_square_NLOS = zeros(n_grid,n_grid);          %(travel time of light)^2 × gain
t2_square_NLOS = zeros(n_grid,n_grid);
t3_square_NLOS = zeros(n_grid,n_grid);
t4_square_NLOS = zeros(n_grid,n_grid);

%% wall1
dx = 0.1;                                                %grid size of wall 1
dz = 0.1;
x1 = -room_x/2:dx:room_x/2;                              %wall 1 plane grid
y1 = room_y/2;
z1 = receiver_height:dz:room_height;
[X1,Z1] = meshgrid(x1,z1);
D11 =
sqrt((X1-LED_positionx).^2+(y1-LED_positiony).^2+(Z1-LED_positionz).^2);
cos_phi = (LED_positionz-Z1)./D11;
cos_alpha = (y1-LED_positiony)./D11;
```

```
for i=1:n_grid
    for j=1:n_grid
        D12 =
sqrt((X1-receiver_X(i,j)).^2+(y1-receiver_Y(i,j)).^2+(Z1-receiver_height).^2);
cos_psai = (Z1-receiver_height)./D12;
receiver_angle = acosd(cos_psai);
cos_beta = (y1-receiver_Y(i,j))./D12;
        dH1_NLOS =
(m+1)*Adet/2/pi./(D11.*D12).^2.*n_wall*dx*dz.*cos_phi.^m.*cos_alpha.*cos_beta.
*Ts.*G_Con.*cos_psai;
        dH1_NLOS(abs(receiver_angle)>FOV) = 0;
        dH1_NLOS(isnan(dH1_NLOS)) = 0;
        H1_NLOS(i,j) = 1/8*sum(sum(dH1_NLOS));

        dt1_NLOS = (D11+D12)/c0.*dH1_NLOS;
        t1_NLOS(i,j) = 1/8*sum(sum(dt1_NLOS));

        dt1_square_NLOS = ((D11+D12)/c0).^2.*dH1_NLOS;
        t1_square_NLOS(i,j) = 1/8*sum(sum(dt1_square_NLOS));
    end
end

%% wall2
dx = 0.1;
dz = 0.1;
x2 = -room_x/2:dx:room_x/2;
```

```
y2 = -room_y/2;
z2 = receiver_height:dz:room_height;
[X2,Z2] = meshgrid(x2,z2);
D21 =
sqrt((X2-LED_positionx).^2+(y2-LED_positiony).^2+(Z2-LED_positionz).^2);
cos_phi = (LED_positionz-Z2)./D21;
cos_alpha = (LED_positiony-y2)./D21;

for i=1:n_grid
    for j=1:n_grid
        D22 =
sqrt((X2-receiver_X(i,j)).^2+(y2-receiver_Y(i,j)).^2+(Z2-receiver_height).^2);
cos_psai = (Z2-receiver_height)./D22;
receiver_angle = acosd(cos_psai);
cos_beta = (receiver_Y(i,j)-y2)./D22;
        dH2_NLOS =
(m+1)*Adet/2/pi./(D21.*D22).^2.*n_wall*dx*dz.*cos_phi.^m.*cos_alpha.*cos_beta.
*Ts.*G_Con.*cos_psai;
        dH2_NLOS(abs(receiver_angle)>FOV) = 0;
        dH2_NLOS(isnan(dH2_NLOS)) = 0;
        H2_NLOS(i,j) = 1/8*sum(sum(dH2_NLOS));

        dt2_NLOS = (D21+D22)/c0.*dH2_NLOS;
        t2_NLOS(i,j) = 1/8*sum(sum(dt2_NLOS));

        dt2_square_NLOS = ((D21+D22)/c0).^2.*dH2_NLOS;
```

```
        t2_square_NLOS(i,j) = 1/8*sum(sum(dt2_square_NLOS));
    end
end

%% wall3
dy = 0.1;
dz = 0.1;
x3 = -room_x/2;
y3 = -room_y/2:dy:room_y/2;
z3 = receiver_height:dz:room_height;
[Y3,Z3] = meshgrid(y3,z3);
D31 =
sqrt((x3-LED_positionx).^2+(Y3-LED_positiony).^2+(Z3-LED_positionz).^2);
cos_phi = (LED_positionz-Z3)./D31;
cos_alpha = (LED_positionx-x3)./D31;

for i=1:n_grid
    for j=1:n_grid
        D32 =
sqrt((x3-receiver_X(i,j)).^2+(Y3-receiver_Y(i,j)).^2+(Z3-receiver_height).^2);
cos_psai = (Z3-receiver_height)./D32;
receiver_angle = acosd(cos_psai);
cos_beta = (receiver_X(i,j)-x3)./D32;
        dH3_NLOS =
(m+1)*Adet/2/pi./(D31.*D32).^2.*n_wall*dy*dz.*cos_phi.^m.*cos_alpha.*cos_beta.
*Ts.*G_Con.*cos_psai;
```

```
        dH3_NLOS(abs(receiver_angle)>FOV) = 0;
        dH3_NLOS(isnan(dH3_NLOS)) = 0;
        H3_NLOS(i,j) = 1/8*sum(sum(dH3_NLOS));

        dt3_NLOS = (D31+D32)/c0.*dH3_NLOS;
        t3_NLOS(i,j) = 1/8*sum(sum(dt3_NLOS));

        dt3_square_NLOS = ((D31+D32)/c0).^2.*dH3_NLOS;
        t3_square_NLOS(i,j) = 1/8*sum(sum(dt3_square_NLOS));
    end
end

%% wall4
dy = 0.1;
dz = 0.1;
x4 = room_x/2;
y4 = -room_y/2:dy:room_y/2;
z4 = receiver_height:dz:room_height;
[Y4,Z4] = meshgrid(y4,z4);
D41 =
sqrt((x4-LED_positionx).^2+(Y4-LED_positiony).^2+(Z4-LED_positionz).^2);
cos_phi = (LED_positionz-Z4)./D41;
cos_alpha = (x4-LED_positionx)./D41;

for i=1:n_grid
```

```
    for j=1:n_grid
        D42 =
sqrt((x4-receiver_X(i,j)).^2+(Y4-receiver_Y(i,j)).^2+(Z4-receiver_height).^2);
cos_psai = (Z4-receiver_height)./D42;
receiver_angle = acosd(cos_psai);
cos_beta = (x4-receiver_X(i,j))./D42;
        dH4_NLOS =
(m+1)*Adet/2/pi./(D41.*D42).^2.*n_wall*dy*dz.*cos_phi.^m.*cos_alpha.*cos_beta.
*Ts.*G_Con.*cos_psai;
        dH4_NLOS(abs(receiver_angle)>FOV) = 0;
        dH4_NLOS(isnan(dH4_NLOS)) = 0;
        H4_NLOS(i,j) = 1/8*sum(sum(dH4_NLOS));

        dt4_NLOS = (D41+D42)/c0.*dH4_NLOS;
        t4_NLOS(i,j) = 1/8*sum(sum(dt4_NLOS));

        dt4_square_NLOS = ((D41+D42)/c0).^2.*dH4_NLOS;
        t4_square_NLOS(i,j) = 1/8*sum(sum(dt4_square_NLOS));
    end
end

H_NLOS = H1_NLOS+H2_NLOS+H3_NLOS+H4_NLOS;
RMS_delay_NLOS = t1_NLOS+t2_NLOS+t3_NLOS+t4_NLOS;
RMS_delay_square_NLOS =
t1_square_NLOS+t2_square_NLOS+t3_square_NLOS+t4_square_NLOS;
```